CONTROL AND SIMULATION OF RELATIVE MOTION FOR AERIAL REFUELING IN RACETRACK MANEUVER

by

EUNYOUNG KIM

Presented to the Faculty of the Graduate School of

The University of Texas at Arlington in Partial Fulfillment

of the Requirements

for the Degree of

MASTER OF SCIENCE IN AEROSPACE ENGINEERING

THE UNIVERSITY OF TEXAS AT ARLINGTON

May 2007

To my parents for their support and determination

in getting me to where I am.

ACKNOWLEDGEMENTS

I would like to thank the University of Texas at Arlington for giving me the opportunity to develop my research and further my knowledge in the field of Aerospace Engineering.

I would like to express both my gratitude and admiration to my supervising professor Dr. Atilla Dogan who took me under his wing and supported me with his guidance, patience, and insight.

I am grateful to Dr. Donald Wilson and Dr. Kamesh Subbarao for agreeing to serve on my thesis defense committee. Dr. Doanld Wilson taught me propulsion and guided me through my pursuit of a master's degree as an advisor. Dr. Subbarao gave me encouragement and inspiration about nonlinear controls.

I would like to express special thanks to my family and friends who have supported me in pursuing my dreams.

April 19, 2007

ABSTRACT

CONTROL AND SIMULATION OF RELATIVE
MOTION FOR AERIAL REFUELING IN
RACETRACK MANEUVER

Publication No. _____

Eunyoung Kim, M.S.

The University of Texas at Arlington, 2007

Supervising Professor: Atilla Dogan

This thesis addresses the problem of controlling the receiver aircraft to achieve a successful aerial refueling. For the performance verification of the controller, a new set of nonlinear, 6-DOF, rigid body equations of motion for the receiver aircraft has been used. The equations are written in terms of state variables that are relative to the reference frame that is attached to, translates and rotates with the tanker aircraft. Furthermore, the nonlinear equations contain the wind effect terms and their time derivatives to represent the aerodynamic coupling involved between the two aircraft. These wind terms are obtained using an averaging technique that computes the effective induced wind components and wind gradients in the receiver aircraft's body frame. Dynamics of the engine and the actuators are also included in the study. A position-tracking controller has been designed using "gain scheduling" technique based on a combination of integral control and optimal LQR design. The scheduling is utilized to satisfy the performance requirement of the controller during the whole "racetrack" maneuver of the tanker in a standard

aerial refueling operation. The nominal flight conditions that are used for the linearization of the nonlinear equations of motion are (i) straight wing-level flight and (ii) steady turn. The position tracking controller can be used for (i) flying from observation position to the refueling position, (ii) station keeping for the actual fuel transfer during the whole racetrack maneuver of the tanker and (iii) flying away from the refueling position once the fuel transfer is completed. The performance of the controller is evaluated in a high fidelity simulation environment, which, employing the new sets of equations of motion, includes the relative motion of the receiver and the tanker and the aerodynamic coupling due to the trailing vortex of the tanker. The simulation and control design are applied to a tailless fighter aircraft with innovative control effectors and thrust vectoring capability.

TABLE OF CONTENTS

LIST OF FIGURES

LIST OF TABLES

CHAPTER 1

INTRODUCTION

1.1 Background on Aerial Refueling Related Research

The effectiveness of aircraft is increased with the capability of aerial refueling, which extends the range, endurance and payload capacity [1]. There has recently been several research efforts in this area, especially for the purpose of enabling unmanned aerial vehicles with this critical capability. There are two different aerial refueling procedures, probe-and-drogue method, and boom-receptacle method. Probe and drogue refueling (PDR) is the standard aerial refueling procedure for both the US Navy and North Atlantic Treaty Organization (NATO) nations. PDR method has two significant drawbacks. First, this method depends on the receiver aircraft to make the refueling connection. Second, this fuel transfer rates are slower than the boom receptacle refueling [1]. Boom-receptacle refueling (BRR) is employed by the US Air Force (USAF). The disadvantage of BRR is that it requires the use of special tankers with booms and human operator in the tanker. However the receiver's workload is slightly lower, compared to PDR method, especially during night or bad weather flight condition, since the boom operator will actually carry out the connection [1]. While it is potentially applicable to PDR method, this paper focuses on the development of an integrated simulation environment and control algorithms for a receiver aircraft in BRR operation while the tanker flies in a racetrack maneuver. Racetrack maneuver is the standard pattern flown by tanker aircraft with straight legs and bank turns [1].

There has been some recent work such as those reported in References [2, 3, 4, 5, 6, 7, 8, 9] demonstrating the benefits of and issues with the control system development

for aerial refueling. Ref. [2] designs a PID control law for each of the three separate position error channels. The first channel is from x-component of the position error vector to the throttle; the second channel is from y-component to the ailerons; and the third one is from z-component to the elevator. The controller performance is analyzed in a simulation environment in station keeping and in maneuvering between contact, pre-contact and observation positions while the tanker flies straight-level and turns. The simulation has the 6-DOF models of the two aircraft; both are with respect to an inertial frame and the relative motion is determined by utilizing kinematic relations. The effect of the trailing wake-vortex is not modeled in the simulation, but the effect of a Von-Karman type turbulence model angle-of-attack and side slip angle is included. The controllers are also evaluated in actual flight tests. Ref. [3] addresses the tanker-boom interactions, and how to model them for simulation purposes. Ref. [4] investigates the applicability of proportional navigation guidance, developed for missile guidance, and line-of-sight angle control, developed for instrument landing systems, in the area of aerial refueling. In [4], the longitudinal and lateral relative motions are separately controlled. The controllers are evaluated in a simulation environment employing the linear model of a jet trainer as the receiver. This reference also uses a turbulence model to represent the wind effect and ignores the modeling of the vortex induced wind field. Ref. [5] developed "a reference-observer-based tracking controller" using a cooperative vision based sensor for docking in PDR operations. In controller performance evaluation, Ref. [5] uses a linearized aircraft model with a simplified wake-vortex model and a turbulence model. Ref. [6] describes the implementation of a modeling and simulation environment for evaluating a refueling control scheme based on sensor fusion between GPS-based and machine vision-based measurements. In this reference also, the tanker and the receiver are separately modeled while the wake-vortex effect is modeled through the interpolation of experimental data as perturbation to the aerodynamic coefficients. In Ref. [7], an approach for simulating

a PDR maneuver based on optical sensors is presented. Ref. [7] also uses a nonlinear model of the receiver aircraft without considering the wake-vortex effect. Ref. [8] develops an autopilot using techniques from differential games and adaptive control for PDR. It considers only longitudinal dynamics, uses a simplified longitudinal model of the receiver and assumes that the tanker is in steady-level flight. Ref. [9] presents a lateral autopilot design for aerial refueling using root-locus method. A simple roll disturbance model is created as a function of downwash amplitude and frequency.

1.2 Contribution

This research work applies the earlier work on mathematical modeling of relative motion [10, 11, 12] and aerodynamic coupling [13] to the simulation of aerial refueling, and develops control laws for the motion of the receiver relative to the tanker that flies in racetrack maneuvers. An integrated simulation environment is developed to take into account tanker maneuvers, motion of the receiver relative to the tanker and the aerodynamic coupling due to the trailing wake-vortex of the tanker. The simulation employs a full 6-DOF nonlinear mathematical model of the tanker aircraft. Additionally, the receiver dynamics is modeled utilizing the new set of equations derived to explicitly formulate the translational and rotational motion of the receiver relative to the tanker. Further, the equations have explicit terms that incorporate the vortex-induced wind effects in the translational and rotational dynamics and kinematics. The separate dynamic model of the tanker, including its own controller, allows the simulation of the standard racetrack maneuvers of the tanker in aerial refueling operations. The mathematical model of the receiver expressed in terms of the relative position and orientation with respect to the tanker's body frame facilitates the formulation, in a single frame work, of maneuvers of the receiver to move to the contact position and the station-keeping at the contact position while the tanker flies in racetrack pattern. For the racetrack maneuvers

of the tanker, an LQR-based MIMO state-feedback and integral control is developed to track commanded speed, altitude and yaw rate. Similarly, for the relative motion of the receiver, an LQR-based MIMO state-feedback and integral control is designed to track commanded trajectory expressed in the body frame of the tanker. Both controllers schedule their corresponding feedback and integral gains based on the commanded speed and yaw rate of the tanker. The tanker aircraft model represents KC-135R while the receiver aircraft model is for a tailless fighter aircraft with innovative control effectors (ICE) and thrust vectoring capability. Thus, the receiver aircraft has six control variables (three control effectors, throttle setting and two thrust vectoring angles) while the tanker has four standard control variables (three control surfaces and throttle setting). Since the receiver has redundant control variables, various control allocation schemes are investigated for trajectory-tracking and station-keeping while the tanker flies in various racetrack maneuvers with different commanded turn rates.

1.3 Thesis Summary

The remainder of the thesis is organized as follows. Chapter 2 gives the equations of motion of the tanker and the modeling of the trailing wake-vortex and its effect on the receiver dynamics are briefly discussed while Chapter 3 presents the modeling of the receiver aircraft. Chapter 4 starts with the requirements for the trajectory tracking controller for the tanker and receiver aircraft and presents later on the design procedure and the structure of the control law. Chapter 5 describes various simulation cases based on tanker maneuvers and receiver control-allocation schemes as well as some special cases to quantify the effects of gain scheduling and trailing wake-vortex. Finally, Section 6 presents the conclusion and discusses topics for future work.

CHAPTER 2

MODELING OF THE TANKER DYNAMICS RELATIVE TO THE INERTIAL FRAME

2.1 Introduction

The performance of an aerial refueling operation depends on the motion of the tanker as much as the motion of the receiver. Thus, for the evaluation of aerial refueling controllers, the simulation environments should include the full dynamic model of the tanker. In standard aerial refueling operation, the tanker flies in a pre-specified race-track maneuver relative to an inertial frame while the receiver moves and stays at the contact position defined relative to the tanker. Further, for a true representation of the aerodynamic coupling due to the trailing wake vortex, the motion of the tanker should be modeled accurately. In the following sections, the scalar forms of the equations of motion of the tanker are presented as they are used in the simulation and in the control design.

2.2 Translational Kinematics Equations

The translational kinematics equation is written in terms of the position vector of the tanker with respect to an inertial frame. In matrix form, the translational kinematics equation is

$$\dot{r}_{B_T} = \mathbf{R}^{\mathbf{T}}_{\mathbf{B_T I}} \mathbf{R}_{\mathbf{B_T w_T}} V_{w_T} \tag{2.1}$$

where r_{B_T} is the position of the tanker relative to the inertial frame expressed in the inertial frame, $\mathbf{R_{B_T I}}$ is the rotation matrix from the inertial frame to the body frame of the tanker, $\mathbf{R_{B_T w_T}}$ is the rotation matrix from the tanker wind frame to body frame,

V_{w_T} is the velocity of the tanker relative to the surrounding air expressed in the tanker wind frame. The followings are the scalar forms of translational kinematics equations:

$$\begin{aligned}\dot{x}_T =& V_T\big[\cos\beta_T\cos\alpha_T\cos\theta_T\cos\psi_T + \sin\beta_T\left(-\cos\phi_T\sin\psi_T + \sin\phi_T\sin\theta_T\cos\psi_T\right)\\ &+\cos\beta_T\sin\alpha_T\left(\sin\phi_T\sin\psi_T + \cos\phi_T\sin\theta_T\cos\psi_T\right)\big]\end{aligned} \tag{2.2}$$

$$\begin{aligned}\dot{y}_T =& V_T\big[\cos\beta_T\cos\alpha_T\cos\theta_T\sin\psi_T + \sin\beta_T\left(\cos\phi_T\cos\psi_T + \sin\phi_T\sin\theta_T\cos\psi_T\right)\\ &+\cos\beta_T\sin\alpha_T\left(-\sin\phi_T\cos\psi_T + \cos\phi_T\sin\theta_T\sin\psi_T\right)\big]\end{aligned} \tag{2.3}$$

$$\dot{z}_T = V_T\big[-\cos\beta_T\cos\alpha_T\sin\theta_T + \sin\beta_T\sin\phi_T\cos\theta_T + \cos\beta_T\sin\alpha_T\cos\phi_T\cos\theta_T\big] \tag{2.4}$$

where (x_T, y_T, z_T) is the position of the tanker aircraft relative the inertial frame, $(\psi_T, \theta_T, \phi_T)$ is the orientation of the tanker relative to the inertial frame in terms of the Euler angles, (V_T, β_T, α_T) are the airspeed, side slip angle and angle-of-attack of the tanker.

2.3 Translational Dynamics Equations

Translational dynamics equation of the tanker aircraft in matrix form is

$$\begin{bmatrix}\dot{V}_T\\ \dot{\beta}_T\\ \dot{\alpha}_T\end{bmatrix} = \mathcal{E}_{\mathbf{T}}^{-\mathbf{1}}\mathbf{S}(\omega_{\mathbf{B_T}})\mathbf{R}_{\mathbf{B_T w_T}}V_{w_T} + \frac{1}{m_T}\mathcal{E}_{\mathbf{T}}^{-\mathbf{1}}\left(\mathbf{R}_{\mathbf{B_R I}}M_T\mathbf{R}_{\mathbf{B_T w_T}}A_T + P_T\right) \tag{2.5}$$

where

$$\mathcal{E}_{\mathbf{T}}^{-\mathbf{1}} = \begin{bmatrix}\cos\alpha_T\cos\beta_T & \sin\beta_T & \cos\beta_T\sin\alpha_T\\ -\frac{1}{V_T}\cos\alpha_T\sin\beta_T & \frac{1}{V_T}\cos\beta_T & -\frac{1}{V_T}\sin\alpha_T\sin\beta_T\\ -\frac{1}{V_T}\sec\beta_T\sin\alpha_T & 0 & \frac{1}{V_T}\cos\alpha_T\sec\beta_T\end{bmatrix} \tag{2.6}$$

The external forces acting on the tanker are the gravitational force M_T (expressed in the inertial frame), the aerodynamic force A_T (expressed in the wind frame of the

tanker) and propulsive force P_T (expressed in the body frame of the tanker). In general, the representations of the forces are

$$M_T = \begin{bmatrix} 0 \\ 0 \\ m_T\ g \end{bmatrix} \quad A_T = \begin{bmatrix} -D_T \\ -S_T \\ -L_T \end{bmatrix} \quad P_T = \begin{bmatrix} T_T \cos\delta_T \\ 0 \\ -T_T \sin\delta_T \end{bmatrix} \tag{2.7}$$

where g is the gravitational acceleration, m_T is the mass of the tanker, (D_T, S_T, L_T) are the drag, side force and lift on the tanker, respectively, T_T is the thrust magnitude, and δ_T is the thrust inclination angle. Also, note that $\mathbf{S}(\cdot)$ is the skew-symmetric matrix operation on the representation of a vector and defined as

$$\mathbf{S}(x) = \begin{bmatrix} 0 & x_3 & -x_2 \\ -x_3 & 0 & x_1 \\ x_2 & -x_1 & 0 \end{bmatrix}, \tag{2.8}$$

for an arbitrary vector $\underline{x}$ with the representation $[x_1\ x_2\ x_3]^T$.

The scalar forms of the translational dynamics equation are given as:

$$\begin{aligned} \dot{V}_T &= g\left[\cos\theta_T \sin\beta_T \sin\phi_T + \cos\beta_T \left(\cos\phi_T \cos\theta_T \sin\alpha_T - \cos\alpha_T \sin\theta_T\right)\right] \\ &\quad + \frac{1}{m_T}\left[-D_T + T_T \cos\left(\alpha_T + \delta_T\right)\cos\beta_T\right] \qquad (2.9) \\ \dot{\beta}_T &= -r_T \cos\alpha_T + p_T \sin\alpha_T \\ &\quad + \frac{g}{V_T}\left[-\cos\phi_T \cos\theta_T \sin\alpha_T \sin\beta_T + \cos\beta_T \cos\theta_T \sin\phi_T + \cos\alpha_T \sin\beta_T \sin\theta_T\right] \\ &\quad - \frac{1}{m_T\ V_T}\left[S_T + T_T \cos\left(\alpha_T + \delta_T\right)\sin\beta_T\right] \qquad (2.10) \\ \dot{\alpha}_T &= q_T - \left(p_T \cos\alpha_T + r_T \sin\alpha_T\right)\tan\beta_T \\ &\quad + \frac{g\ \sec\beta_T}{V_T}\left[\cos\alpha_T \cos\phi_T \cos\theta_T + \sin\alpha_T \sin\theta_T\right] \\ &\quad - \frac{\sec\beta_T}{m_T\ V_T}\left[L_T + T_T \sin\left(\alpha_T + \delta_T\right)\right] \qquad (2.11) \end{aligned}$$

where (p_T, q_T, r_T) is the angular velocity of the tanker expressed in the tanker's body frame. The aerodynamic forces are given by the following standard expressions

$$D_T = \frac{1}{2}\rho V_T^2 \mathcal{S}_T C_{D_T} , \tag{2.12}$$

$$S_T = \frac{1}{2}\rho V_T^2 \mathcal{S}_T C_{S_T} , \tag{2.13}$$

$$L_T = \frac{1}{2}\rho V_T^2 \mathcal{S}_T C_{L_T} , \tag{2.14}$$

where $\mathcal{S}_T$ is the reference area of the tanker and ρ is the ambient air density. The aerodynamic coefficients are

$$C_{D_T} = C_{D0} + C_{D\alpha^2}\ \alpha_T^2 \tag{2.15}$$

$$C_{S_T} = C_{S0} + C_{S\beta}\beta_T + C_{S\delta_r}\delta_{r_T} \tag{2.16}$$

$$C_{L_{wing}} = C_{L0} + C_{L\alpha}\alpha_T + C_{L\alpha 2}\ (\alpha_T - \alpha_{ref})^2 + C_{Lq}\frac{c_T}{2V_T}q_T \tag{2.17}$$

$$C_{L_{tail}} = C_{L\delta_e}\delta_{e_T} \tag{2.18}$$

$$C_{L_T} = C_{L_{wing}} + C_{L_{tail}} \tag{2.19}$$

where $(\delta_{a_T}, \delta_{e_T}, \delta_{r_T})$ are the deflections of the control surfaces (aileron, elevator, rudder, respectively) and c_T is the chord length for the tanker. As it will be seen in the next section, the notation for the tanker's stability derivatives is the same as that for the receiver. However, it is should be obvious to the reader that their values for the tanker and the receiver are different as they are different aircraft. Note also that the lift coefficients for the wing and the horizontal tail are defined separately. This is needed for the modeling of the aerodynamic coupling as explained in Chapter 3.

2.4 Rotational Kinematics Equations

The rotational kinematics equation in matrix form is the well known standard equation:

$$\mathbf{R_{B_TI}}\dot{\mathbf{R}}_{\mathbf{B_TI}} = -\mathbf{S}(\omega_{\mathbf{B_T}}) \tag{2.20}$$

where $\omega_{\mathbf{B_T}}$ is the representation of the angular velocity vector of the tanker relative to the inertial frame expressed in its own body frame as

$$\omega_{\mathbf{B_T}} = \begin{bmatrix} p_T \\ q_T \\ r_T \end{bmatrix} \tag{2.21}$$

The rotational motion of the tanker aircraft in terms of Euler angles is, in scalar form,

$$\dot{\phi}_T = p_T + q_T \sin\phi_T \tan\theta_T + r\cos\phi_T \tan\theta_T \tag{2.22}$$

$$\dot{\theta}_T = q_T \cos\phi_T - r\sin\phi_T \tag{2.23}$$

$$\dot{\psi}_T = (q_T \sin\phi_T + r_T \cos\phi_T)\sec\theta_T \tag{2.24}$$

where note that both the orientation in terms of $(\psi_T, \theta_T, \phi_T)$, and the angular velocity, (p_T, q_T, r_T), of the tanker are relative to the inertial frame.

2.5 Rotational Dynamics Equations

The matrix form of the rotational dynamics of the tanker is modeled with the standard rotational dynamics equation.

$$\dot{\omega}_{B_T} = \underline{\underline{\mathbf{I}}}_{\mathbf{T}}^{-\mathbf{1}} M_{B_T} + \underline{\underline{\mathbf{I}}}_{\mathbf{T}}^{-\mathbf{1}} \mathbf{S}(\omega_{\mathbf{B_T}}) \underline{\underline{\mathbf{I}}}_{\mathbf{T}} \omega_{B_T} \tag{2.25}$$

where $\underline{\underline{\mathbf{I}}}_{\mathbf{T}}$ is the inertia matrix of the tanker aircraft, M_{B_T} is the moment of the external forces around the origin of tanker body frame and expressed in the tanker body frame as

$$M_{B_T} = \begin{bmatrix} \mathcal{L}_{\mathcal{T}} \\ \mathcal{M}_{\mathcal{T}} \\ \mathcal{N}_{\mathcal{T}} \end{bmatrix} \tag{2.26}$$

The scalar forms of the rotational dynamics equation are given as:

$$\dot{p}_T = \frac{1}{(I_{xx}I_{zz} - I_{xz}^2)}\big[\,(I_{xx} - I_{yy} + I_{zz})\,I_{xz}p_Tq_T + \left(I_{yy} - I_{zz} + I_{zz}^2 - I_{xz}^2\right)q_Tr_T + I_{zz}\mathcal{L}_T + I_{xz}\mathcal{N}_T\big] \tag{2.27}$$

$$\dot{q}_T = \frac{1}{I_{yy}}\big[\,(I_{zz} - I_{xx})\,p_Tr_T + \left(r_T^2 - p_T^2\right)I_{xz} + \mathcal{M}_T\big] \tag{2.28}$$

$$\dot{r}_T = \frac{1}{(I_{xx}I_{zz} - I_{xz}^2)}\big[\,\left(I_{xx}^2 - I_{xx}I_{yy} + I_{xz}^2\right)p_Tq_T + (-I_{xx} + I_{yy} - I_{zz})\,I_{xz}q_Tr_T + I_{xz}\mathcal{L}_T + I_{xx}\mathcal{N}_T\big] \tag{2.29}$$

where $I_{(\cdot)(\cdot)}$ is the moment or product of inertia of the tanker relative to the corresponding axis of the tanker's body frame. Note here also that the notation for $I_{(\cdot)(\cdot)}$ is the same for both tanker and the receiver while their values are obviously different. $(\mathcal{L}_T, \mathcal{M}_T, \mathcal{N}_T)$ are the rolling, pitching and yawing moments, respectively.

$$\mathcal{L}_T = \frac{1}{2}\rho V_T^2 \mathcal{S}_T b_T C_{\mathcal{L}_T} \tag{2.30}$$

$$\mathcal{M}_T = \frac{1}{2}\rho V_T^2 \mathcal{S}_T c_T C_{\mathcal{M}_T} + \Delta_{z_T} T_T \tag{2.31}$$

$$\mathcal{N}_T = \frac{1}{2}\rho V_T^2 \mathcal{S}_T b_T C_{\mathcal{N}_T} \tag{2.32}$$

where b_T is the wingspan of the tanker aircraft and Δ_{z_T} is the moment arms of the thrust in the tanker's body frame. The aerodynamic moment coefficients are

$$C_{\mathcal{L}_T} = C_{\mathcal{L}0} + C_{\mathcal{L}\delta_a}\delta_{a_T} + C_{\mathcal{L}\delta_r}\delta_{r_T} + C_{\mathcal{L}\beta}\beta_T + C_{\mathcal{L}p}\frac{b_T}{2V_T}p_T + C_{\mathcal{L}r}\frac{b_T}{2V_T}r_T \tag{2.33}$$

$$C_{\mathcal{M}_T} = C_{\mathcal{L}\alpha}\alpha_T + C_{\mathcal{L}\delta_e}\delta_{e_T} + C_{\mathcal{M}q}\frac{c_T}{2V_T}q_T \tag{2.34}$$

$$C_{\mathcal{N}_T} = C_{\mathcal{N}0} + C_{\mathcal{N}\delta_a}\delta_{a_T} + C_{\mathcal{N}\delta_r}\delta_{r_T} + C_{\mathcal{N}\beta}\beta_T + C_{\mathcal{N}p}\frac{b_T}{2V_T}p_T + C_{\mathcal{N}r}\frac{b_T}{2V_T}r_T \tag{2.35}$$

2.6 Engine Dynamics

The thrust generated by the engine (T_T) is

$$T_T = \xi_T\, T_{max_T} \tag{2.36}$$

where ξ_T denotes the instantaneous throttle setting and T_{max_T} is the maximum available thrust of the tanker and assumed to be constant in this paper. The engine dynamics is modeled as that of a first order system with time constant τ_T. Therefore, we have

$$\dot{\xi}_T = \frac{\xi_T - \xi_{t_T}}{\tau_T} \ , \tag{2.37}$$

where ξ_{t_T} is the commanded throttle setting ($0 \leq \xi_t \leq 1$).

2.7 Actuator Dynamics

For the present study, only the actuator saturation are considered. The deflection range attainable from each control surface is (-20 deg, 20 deg).

CHAPTER 3

MODELING OF THE RECEIVER DYNAMICS RELATIVE TO THE TANKER

3.1 Introduction

In an efficient aerial refueling operation, the receiver aircraft needs to be controlled with respect to the tanker's position and orientation rather than with respect to the inertial reference. Moreover, the receiver aircraft will be exposed to a nonuniform wind field during the whole refueling operation when it is in the proximity of the tanker due to the trailing vortex of the tanker. To address these challenges, a new set of nonlinear equations was derived earlier [10] and used herein to represent the position and orientation of the receiver relative to the tanker and at the same time to explicitly represent the vortex effect on the dynamics of the receiver aircraft. In the following sections, the matrix forms of the equations are given as they are used in the simulation of the closed loop system. In their scalar forms, however, the wind terms are not included as the controller is designed without the assumption of the availability of the wind terms.

3.2 Translational Kinematics Equations

The translational kinematics equation is written in terms of the position vector of the receiver with respect to the tanker, not its absolute position vector with respect to the inertial frame. In matrix form, the translational kinematics equation is [10].

$$\dot{\xi} = \mathbf{R}^{\mathbf{T}}_{\mathbf{B_R B_T}} \mathbf{R}_{\mathbf{B_R w_R}} \, V_w + \mathbf{R}^{\mathbf{T}}_{\mathbf{B_R B_T}} \, W - \mathbf{R}_{\mathbf{B_T I}} \, \dot{r}_{B_T} + \mathbf{S}(\omega_{\mathbf{B_T}})\xi \tag{3.1}$$

where ξ is the position of the receiver relative to the tanker expressed in the body frame of the tanker, $\mathbf{R_{B_R w_R}}$ is the rotation matrix from the receiver wind frame to body frame, V_w is the velocity of the receiver relative to the surrounding air expressed in the receiver wind frame, W is the velocity of the surrounding air relative to the ground expressed in the receiver body frame, $\mathbf{R_{B_R B_T}}$ is the rotation matrix from tanker body frame to receiver body frame, and $\dot{r}_{B_T}$ is the velocity of the tanker relative to the inertial frame.

The followings are the scalar forms of Eq. (3.1) without the wind terms:

$$\begin{aligned}
\dot{x} = \; & V\big[\cos\beta\cos\alpha\cos\theta\cos\psi + \sin\beta\,(-\cos\phi\sin\psi + \sin\phi\sin\theta\cos\psi) \\
& + \cos\beta\sin\alpha\,(\sin\phi\sin\psi + \cos\phi\sin\theta\cos\psi)\big] \\
& - \cos\theta_T\cos\psi_T\;V_{xT} - \cos\theta_T\sin\psi_T\;V_{yT} + \sin\theta_T\;V_{zT} \\
& + r_T\;y - q_T\;z
\end{aligned} \tag{3.2}$$

$$\begin{aligned}
\dot{y} = \; & V\big[\cos\beta\cos\alpha\cos\theta\sin\psi + \sin\beta\,(\cos\phi\cos\psi + \sin\phi\sin\theta\cos\psi) \\
& + \cos\beta\sin\alpha\,(-\sin\phi\cos\psi + \cos\phi\sin\theta\sin\psi)\big] \\
& - (-\cos\phi_T\sin\psi_T + \sin\phi_T\sin\theta_T\cos\psi_T)\,V_{xT} \\
& - (\cos\phi_T\cos\psi_T + \sin\phi_T\sin\theta_T\sin\psi_T)\,V_{yT} + \sin\phi_T\cos\theta_T\;V_{zT} \\
& - r_T\;x + p_T\;z
\end{aligned} \tag{3.3}$$

$$\begin{aligned}
\dot{z} = \; & V\big[-\cos\beta\cos\alpha\sin\theta + \sin\beta\sin\phi\cos\theta + \cos\beta\sin\alpha\cos\phi\cos\theta\big] \\
& - (\sin\phi_T\sin\psi_T + \cos\phi_T\sin\theta_T\cos\psi_T)\,V_{xT} \\
& - (-\sin\phi_T\cos\psi_T + \cos\phi_T\sin\theta_T\sin\psi_T)\,V_{yT} - \cos\phi_T\cos\theta_T\;V_{zT} \\
& + q_T\;x - p_T\;y
\end{aligned} \tag{3.4}$$

where (x, y, z) is the position of the receiver aircraft relative to the tanker, (ψ, θ, ϕ) is the orientation of the receiver relative to the tanker in terms of the Euler angles, (V, β, α) are the airspeed, side slip angle and angle-of-attack of the receiver, $(\psi_T, \theta_T, \phi_T)$

is the orientation of the tanker relative to the inertial frame. Recall that (p_T, q_T, r_T) are the components of the angular velocity of the tanker relative to the inertial frame, and (V_{xT}, V_{yT}, V_{zT}) are the components of the velocity of the tanker relative to the inertial frame. Note that $V_{xT} = \dot{x}_T$ in Eq. (2.2), $V_{yT} = \dot{y}_T$ in Eq. (2.3), and $V_{zT} = \dot{z}_T$ in Eq. (2.4).

3.3 Translational Dynamics Equations

The translational dynamics equation of the receiver aircraft including the wind effect in matrix form is [10]

$$\begin{aligned}\begin{bmatrix} \dot{V}_R \\ \dot{\beta}_R \\ \dot{\alpha}_R \end{bmatrix} &= \mathcal{E}_{\mathbf{R}}^{-\mathbf{1}}\left[\mathbf{S}(\omega_{\mathbf{B_R B_T}}) + \mathbf{R}_{\mathbf{B_R B_T}}\mathbf{S}(\omega_{\mathbf{B_T}})\mathbf{R}_{\mathbf{B_R B_T}}^{\mathbf{T}}\right]\left(\mathbf{R}_{\mathbf{B_R w_R}}\, V_w + W\right) \\ &\quad -\mathcal{E}_{\mathbf{R}}^{-\mathbf{1}}\dot{W} + \frac{1}{m_R}\mathcal{E}_{\mathbf{R}}^{-\mathbf{1}}\left(\mathbf{R}_{\mathbf{B_R B_T}}\mathbf{R}_{\mathbf{B_T I}}M_R + \mathbf{R}_{\mathbf{B_R w_R}}\, A_R + P_R\right) \end{aligned} \tag{3.5}$$

where

$$\mathcal{E}_{\mathbf{R}}^{-\mathbf{1}} = \begin{bmatrix} \cos\alpha\cos\beta & \sin\beta & \cos\beta\sin\alpha \\ -\frac{1}{V_R}\cos\alpha\sin\beta & \frac{1}{V_R}\cos\beta & -\frac{1}{V_R}\sin\alpha\sin\beta \\ -\frac{1}{V_R}\sec\beta\sin\alpha & 0 & \frac{1}{V_R}\cos\alpha\sec\beta \end{bmatrix} \tag{3.6}$$

The external forces acting on the receiver are the gravitational force M_R (expressed in the inertial frame), the aerodynamic force A_R (expressed in the wind frame of the receiver) and the propulsive force P_R (expressed in the body frame of the receiver). In general, the representations of the forces M_R, A_R and P_R are

$$M_R = \begin{bmatrix} 0 \\ 0 \\ m_R\, g \end{bmatrix} \quad A_R = \begin{bmatrix} -D \\ -S \\ -L \end{bmatrix} \quad P_R = \begin{bmatrix} T_x \\ T_y \\ T_z \end{bmatrix} \tag{3.7}$$

where m_R is the mass of the receiver, (D, S, L) are the drag, side force and lift on the receiver, respectively, and (T_x, T_y, T_z) are the components of the thrust vector in the body frame of the receiver.

The propulsion force P_R has three components, which are functions of thrust magnitude T_R and the direction of the thrust vector. The thrust vectoring is parameterized by the angles of the thrust vector with the receiver's body xy– and xz– planes. Thus, as seen in Fig. 3.1, the components of the thrust are

$$\begin{aligned} T_x &= T_R \cos\delta_z \cos\delta_y \\ T_y &= T_R \sin\delta_z \\ T_z &= T_R \cos\delta_z \sin\delta_y \end{aligned} \tag{3.8}$$

Note that a positive δ_y rotation of the thrust generates a positive thrust component in the positive z–direction while inducing a positive pitching moment (moment around y-axis). Similarly, a positive δ_z rotation of the thrust generates a positive thrust component in the positive y–direction while inducing a negative yawing moment (moment around z-axis).

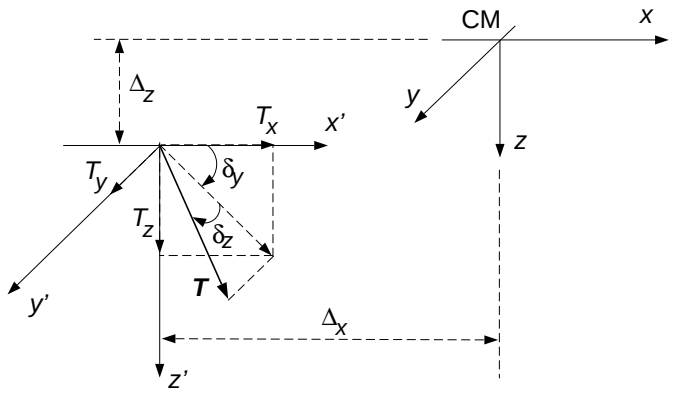

Figure 3.1. Thrust vectoring angles and moment arms.

The aerodynamic forces are given by

$$D = \frac{1}{2}\rho V_R^2 \mathcal{S}_R C_D \ , \tag{3.9}$$

$$S = \frac{1}{2}\rho V_R^2 \mathcal{S}_R C_S \ , \tag{3.10}$$

$$L = \frac{1}{2}\rho V_R^2 \mathcal{S}_R C_L \ , \tag{3.11}$$

where $\mathcal{S}_R$ is the reference area of the receiver. The aerodynamic coefficients are

$$C_D = C_{D0} + C_{D\alpha}\alpha + C_{D\alpha 2}\alpha^2 + C_{D\delta_e}\delta_e + C_{D\delta_e 2}\delta_e^2 \tag{3.12}$$

$$C_S = C_{S0} + C_{S\beta}\beta + C_{S\delta_a}\delta_a + C_{S\delta_r}\delta_r \tag{3.13}$$

$$C_L = C_{L0} + C_{L\alpha}\alpha + C_{L\alpha 2}(\alpha - \alpha_{ref})^2 + C_{Lq}\frac{c}{2V_R}q_{rel} + C_{L\delta_e}\delta_e \tag{3.14}$$

where (δ_a,δ_e,δ_r) are the deflections of the control effectors (aileron, elevator, rudder) as the conventional control surfaces or (elevon, pitch flap, clamshell) as in the ICE (Innovative Control Effectors) aircraft, respectively. Note that, in Eq. (3.14), q_{rel} is the angular velocity of the receiver relative to the surrounding air around the body–y axis. However, in control design, $q_{rel} = q$ since the wind is not considered.

The scalar forms of the translational dynamics equation, without the wind terms, are given as:

$$\begin{aligned}
\dot{V} = g \Big\{ & \cos\alpha\cos\beta\,(-\cos\theta\cos\psi\cos\theta_T + \cos\theta\sin\psi\sin\phi_T\cos\theta_T - \sin\theta\cos\phi_T\cos\theta_T) \\
& + \sin\beta\big[-(-\cos\phi\sin\psi + \sin\phi\sin\theta\cos\psi)\sin\theta_T \\
& \qquad + (\cos\phi\cos\psi + \sin\phi\sin\theta\sin\psi)\sin\phi_T\cos\theta_T \\
& \qquad + \sin\phi\cos\theta\cos\phi_T\cos\theta_T\big] \\
& + \cos\beta\sin\alpha\big[-(\sin\phi\sin\psi + \cos\phi\sin\theta\cos\psi)\sin\theta_T \\
& \qquad + (-\sin\phi\cos\psi + \cos\phi\sin\theta\sin\psi)\sin\phi_T\cos\theta_T \\
& \qquad + \cos\phi\cos\theta\cos\phi_T\cos\theta_T\big]\Big\} \\
& + \frac{1}{m_R}\left(-D + T_x\cos\alpha\cos\beta + T_y\sin\beta + T_z\cos\beta\sin\alpha\right)
\end{aligned} \tag{3.15}$$

$$
\begin{aligned}
\dot{\beta} = {} & \sin\alpha\,(p + p_T\cos\psi\cos\theta + q_T\sin\psi\cos\theta - r_T\sin\theta) \\
& - \cos\alpha\big[r + p_T\,(\sin\phi\sin\psi + \cos\phi\cos\psi\sin\theta) + q_T\,(\sin\theta\cos\phi\sin\psi - \sin\phi\cos\psi) \\
& \qquad + r_T\cos\phi\cos\theta\big] \\
& + \frac{g}{V}\Big\{ - \cos\alpha\sin\beta\,(-\cos\theta\cos\psi\sin\theta_T + \cos\theta\sin\psi\sin\phi_T\cos\theta_T - \sin\theta\cos\phi_T\cos\theta_T) \\
& \quad + \cos\beta\big[- (-\cos\phi\sin\psi + \sin\phi\sin\theta\cos\psi)\sin\theta_T \\
& \qquad + (\cos\phi\cos\psi + \sin\phi\sin\theta\sin\psi)\sin\phi_T\cos\theta_T + \sin\phi\cos\theta\cos\phi_T\cos\theta_T\big] \\
& \quad - \sin\alpha\sin\beta\big[- (\sin\phi\sin\psi + \cos\phi\sin\theta\cos\psi)\sin\theta_T \\
& \qquad + (-\sin\phi\cos\psi + \cos\phi\sin\theta\sin\psi)\sin\phi_T\cos\theta_T \\
& \qquad + \cos\phi\cos\theta\cos\phi_T\cos\theta_T\big]\Big\} \\
& + \frac{1}{m_R\,V}\,(-S - T_x\cos\alpha\sin\beta + T_y\cos\beta - T_z\sin\alpha\sin\beta)
\end{aligned}
\tag{3.16}
$$

$$
\begin{aligned}
\dot{\alpha} = {} & q - p_T\,(\cos\phi\sin\psi - \sin\theta\sin\phi\cos\psi) + q_T\,(\cos\phi\cos\psi + \sin\theta\sin\phi\sin\psi) \\
& + r_T\sin\phi\cos\theta \\
& - \sin\alpha\tan\beta\big[r + p_T\,(\sin\psi\sin\phi + \cos\psi\sin\theta\cos\phi) + q_T\,(\sin\psi\sin\theta\cos\phi - \sin\psi\sin\phi) \\
& \qquad + r_T\cos\phi\cos\theta\big] \\
& + \cos\alpha\tan\beta\,(-p - p_T\cos\psi\cos\theta - q_T\sin\psi\cos\theta + r_T\sin\theta) \\
& + \frac{g}{V}\Big\{ - \sec\beta\sin\alpha\,(-\cos\theta\cos\psi\sin\theta_T + \cos\theta\sin\psi\sin\phi_T\cos\theta_T - \sin\theta\cos\phi_T\cos\theta_T) \\
& \quad + \cos\alpha\sec\beta\big[- (\sin\phi\sin\psi + \cos\phi\sin\theta\cos\psi)\sin\theta_T \\
& \qquad + (-\sin\phi\cos\psi + \cos\phi\sin\theta\sin\psi)\sin\phi_T\cos\theta_T \\
& \qquad + \cos\phi\cos\theta\cos\phi_T\cos\theta_T\big]\Big\} \\
& + \frac{\sec\beta}{m_R\,V}\,(-L - T_x\sin\alpha + T_z\cos\alpha)
\end{aligned}
\tag{3.17}
$$

Note that the motion of the tanker aircraft –both translational and rotational– is represented as exogenous inputs in the translational equations of motion of the receiver

aircraft. The variables included in this category are translational velocity (V_{xT}, V_{yT}, V_{zT}), orientation in terms of Euler angles $(\psi_T, \theta_T, \phi_T)$ and angular velocity (p_T, q_T, r_T), all relative to the inertial frame.

3.4 Rotational Kinematics Equations

The rotational motion of the receiver aircraft, similar to its translational motion, is also analyzed with reference to the tanker body frame. Even though the standard rotational kinematics and dynamics equations are used, their interpretations are different because both angular position and angular velocity of the receiver aircraft are relative to the tanker body frame, an accelerating and rotating reference frame.

The rotational kinematics equation of the receiver aircraft in matrix form is also the well known standard equation:

$$\mathbf{R_{B_R B_T}} \dot{\mathbf{R}}^{\mathbf{T}}_{\mathbf{B_R B_T}} = -\mathbf{S}(\omega_{\mathbf{B_R B_T}}) \tag{3.18}$$

where $\omega_{B_R B_T}$ is the representation of the angular velocity vector of the receiver aircraft relative to the tanker body frame expressed in its own body frame as

$$\omega_{B_R B_T} = \begin{bmatrix} p_{R_T} \\ q_{R_T} \\ r_{R_T} \end{bmatrix} \tag{3.19}$$

The scalar forms of this matrix equation in terms of Euler angles are:

$$\dot{\phi} = p + q \sin\phi \tan\theta + r \cos\phi \tan\theta \tag{3.20}$$

$$\dot{\theta} = q \cos\phi - r \sin\phi \tag{3.21}$$

$$\dot{\psi} = (q \sin\phi + r \cos\phi) \sec\theta \tag{3.22}$$

where note that both the orientation, (ψ, θ, ϕ), and the angular velocity, (p, q, r), of the receiver are relative to the tanker.

3.5 Rotational Dynamics Equations

The matrix form of the rotational dynamics of the receiver is also modeled as

$$\begin{aligned}\dot{\omega}_{B_R B_T} &= \underline{\underline{\mathbf{I}}}_{\mathbf{R}}^{-1} M_{B_R} + \underline{\underline{\mathbf{I}}}_{\mathbf{R}}^{-1}\mathbf{S}(\omega_{\mathbf{B_R B_T}} + \mathbf{R}_{\mathbf{B_R B_T}}\omega_{\mathbf{B_T}})\underline{\underline{\mathbf{I}}}_{\mathbf{R}}\left(\omega_{B_R B_T} + \mathbf{R}_{\mathbf{B_R B_T}}\omega_{B_T}\right) \\ &\quad -\mathbf{S}(\omega_{\mathbf{B_R B_T}})\mathbf{R}_{\mathbf{B_R B_T}}\omega_{B_T} - \mathbf{R}_{\mathbf{B_R B_T}}\dot{\omega}_{B_T} \qquad (3.23)\end{aligned}$$

where $\underline{\underline{\mathbf{I}}}_{\mathbf{R}}$ is the inertia matrix of the receiver aircraft, M_{B_R} is the moment of the external forces around the origin of the receiver body frame and expressed in the receiver body frame as

$$M_{B_R} = \begin{bmatrix} \mathcal{L} \\ \mathcal{M} \\ \mathcal{N} \end{bmatrix} \qquad (3.24)$$

The moment has two main components; due to aerodynamic forces and due to the thrust, thus

$$\mathcal{L} = \frac{1}{2}\rho V_R^2 \mathcal{S}_R b C_{\mathcal{L}} - \Delta_z T_y + \Delta_y T_z \qquad (3.25)$$

$$\mathcal{M} = \frac{1}{2}\rho V_R^2 \mathcal{S}_R c C_{\mathcal{M}} - \Delta_z T_x - \Delta_x T_z \qquad (3.26)$$

$$\mathcal{N} = \frac{1}{2}\rho V_R^2 \mathcal{S}_R b C_{\mathcal{N}} - \Delta_y T_x + \Delta_x T_y \qquad (3.27)$$

where b is the wingspan, c is the cord length of the receiver aircraft, and (Δ_x, Δ_y, Δ_z) are the moment arms of the thrust in the body frame of the receiver (see Fig. 3.1). The aerodynamic moment coefficients are

$$C_{\mathcal{L}} = C_{\mathcal{L}0} + C_{\mathcal{L}\delta_a}\delta_a + C_{\mathcal{L}\delta_r}\delta_r + C_{\mathcal{L}\beta}\beta + C_{\mathcal{L}p}\frac{b}{2V_R}p_{rel} + C_{\mathcal{L}r}\frac{b}{2V_R}r_{rel} \qquad (3.28)$$

$$C_{\mathcal{M}} = C_{\mathcal{M}0} + C_{\mathcal{L}\alpha}\alpha + C_{\mathcal{L}\delta_e}\delta_e + C_{\mathcal{M}q}\frac{c}{2V_R}q_{rel} \qquad (3.29)$$

$$C_{\mathcal{N}} = C_{\mathcal{N}0} + C_{\mathcal{N}\delta_a}\delta_a + C_{\mathcal{N}\delta_r}\delta_r + C_{\mathcal{N}\beta}\beta + C_{\mathcal{N}p}\frac{b}{2V_R}p_{rel} + C_{\mathcal{N}r}\frac{b}{2V_R}r_{rel} \qquad (3.30)$$

where (p_{rel},q_{rel},r_{rel}) are components of the angular velocity of the aircraft relative to the surrounding air. When the aircraft is in a vortex field as in the case of tanker's trailing

wake vortex field, these angular velocity components will be different from the angular velocity relative to the tanker.

The scalar forms of the rotational dynamics equation are given as:

$$
\begin{aligned}
\dot{p} \;=\; & \frac{(I_{zz}\mathcal{L} + I_{xz}\mathcal{N})}{(I_{xx}I_{zz} - I_{xz}^2)} \\
& + \frac{(I_{yy}I_{xx} - I_{zz}^2 - I_{xz}^2)}{(I_{xx}I_{zz} - I_{xz}^2)} \big[q + p_T \left(\cos\psi \sin\theta \sin\phi - \sin\psi \cos\phi\right) \\
& \qquad + q_T \left(\sin\psi \sin\theta \sin\phi + \cos\psi \cos\phi\right) + r_T \cos\theta \sin\phi \big] \\
& \qquad \big[r + p_T \left(\cos\psi \sin\theta \cos\phi + \sin\psi \sin\phi\right) \\
& \qquad + q_T \left(\sin\psi \sin\theta \cos\phi - \cos\psi \sin\phi\right) + r_T \cos\theta \cos\phi \big] \\
& + \frac{(I_{yy}I_{xz} - I_{xx}I_{xz} - I_{zz}I_{xz})}{(I_{xx}I_{zz} - I_{xz}^2)} \big[p + p_T \cos\psi \cos\theta + q_T \sin\psi \cos\theta - r_T \sin\theta \big] \\
& \qquad \big[-q + p_T \left(\sin\psi \cos\phi - \cos\psi \sin\theta \sin\phi\right) \\
& \qquad - q_T \left(\cos\psi \cos\phi - \sin\psi \sin\theta \sin\phi\right) - r_T \cos\theta \sin\phi \big] \\
& - r \big[p_T \left(\cos\psi \sin\theta \sin\phi - \sin\psi \cos\phi\right) + q_T \left(\sin\psi \sin\theta \sin\phi + \cos\psi \cos\phi\right) + r_T \cos\theta \sin\phi \big] \\
& + q \big[p_T \left(\cos\psi \sin\theta \cos\phi + \sin\psi \sin\phi\right) + q_T \left(\sin\psi \sin\theta \cos\phi - \cos\psi \sin\phi\right) \\
& \qquad + r_T \cos\theta \cos\phi \big] - \dot{p}_T \cos\psi \cos\theta - \dot{q}_T \sin\psi \cos\theta + \dot{r}_T \sin\theta
\end{aligned}
\tag{3.31}
$$

$$
\begin{aligned}
\dot{q} \;=\; & \frac{\mathcal{M}}{I_{yy}} - \frac{I_{xz}}{I_{yy}} \big[p + p_T \cos\psi \cos\theta + q_T \sin\psi \cos\theta - r_T \sin\theta \big]^2 \\
& + \frac{I_{xz}}{I_{yy}} \big[r + p_T \left(\cos\psi \sin\theta \cos\phi + \sin\psi \sin\phi\right) \\
& \qquad + q_T \left(\sin\psi \sin\theta \cos\phi - \cos\psi \sin\phi\right) + r_T \cos\theta \cos\phi \big]^2 \\
& + \frac{(I_{zz} - I_{xx})}{I_{yy}} \big[p + p_T \cos\psi \cos\theta + q_T \sin\psi \cos\theta - r_T \sin\theta \big] \\
& \big[r + p_T \left(\cos\psi \sin\theta \cos\phi + \sin\psi \sin\phi\right) + q_T \left(\sin\psi \sin\theta \cos\phi - \cos\psi \sin\phi\right) + r_T \cos\theta \cos\phi \big] \\
& + r \big[p_T \cos\psi \cos\theta + q_T \sin\psi \cos\theta - r_T \sin\theta \big] - \dot{q}_T \left(\sin\psi \sin\theta \sin\phi + \cos\psi \cos\phi\right) \\
& - p \big[p_T \left(\cos\psi \sin\theta \cos\phi + \sin\psi \sin\phi\right) + q_T \left(\sin\psi \sin\theta \cos\phi - \cos\psi \sin\phi\right) \\
& \qquad + r_T \cos\theta \cos\phi \big] + \dot{p}_T \left(\sin\psi \cos\phi - \cos\psi \sin\theta \sin\phi\right) - \dot{r}_T \cos\theta \sin\phi
\end{aligned}
\tag{3.32}
$$

$$
\begin{aligned}
\dot{r} \;=\; & \frac{(I_{xx}\mathcal{N} + I_{xz}\mathcal{L})}{(I_{xx}I_{zz} - I_{xz}^2)} \\
& + \frac{(I_{yy}I_{xz} - I_{xx}I_{xz} - I_{zz}I_{xz})}{(I_{xx}I_{zz} - I_{xz}^2)} \big[r + p_T \left(\cos\psi \sin\theta \cos\phi + \sin\psi \sin\phi\right) \\
& \qquad + q_T \left(\sin\psi \sin\theta \cos\phi - \cos\psi \sin\phi\right) + r_T \cos\theta \cos\phi \big] \\
& \big[q + p_T \left(\cos\psi \sin\theta \sin\phi - \sin\psi \cos\phi\right) + q_T \left(\sin\psi \sin\theta \sin\phi + \cos\psi \cos\phi\right) \\
& \quad + r_T \cos\theta \sin\phi \big] \\
& + \frac{(I_{xx}^2 - I_{xx}I_{yy} + I_{xz}^2)}{(I_{xx}I_{zz} - I_{xz}^2)} \big[p + p_T \cos\psi \cos\theta + q_T \sin\psi \cos\theta - r_T \sin\theta \big] \\
& \qquad \big[q + p_T \left(\cos\psi \sin\theta \sin\phi - \sin\psi \cos\phi\right) \\
& \qquad + q_T \left(\sin\psi \sin\theta \sin\phi + \cos\psi \sin\phi\right) + r_T \cos\theta \sin\phi \big] \\
& + p \big[p_T \left(\cos\psi \sin\theta \sin\phi - \sin\psi \cos\phi\right) \\
& \quad + q_T \left(\sin\psi \sin\theta \sin\phi + \cos\psi \cos\phi\right) + r_T \cos\theta \sin\phi \big] \\
& - q \big[p_T \cos\psi \cos\theta + q_T \sin\psi \cos\theta - r_T \sin\theta \big] - \dot{p}_T \left(\cos\psi \sin\theta \cos\phi + \sin\phi \sin\phi\right) \\
& - \dot{q}_T \left(\sin\psi \sin\theta \cos\phi - \cos\psi \sin\phi\right) - \dot{r}_T \cos\theta \cos\phi
\end{aligned}
\tag{3.33}
$$

where $I_{(\cdot)(\cdot)}$ is the moment or product of inertia of the receiver relative to the corresponding axis of the receiver body frame.

3.6 Engine Dynamics

As in the case of the tanker, the engine model of the receiver is also a first order transfer function with constant maximum thrust, obviously with different maximum thrust and different time constant.

3.7 Actuator Dynamics

For the present study, only the actuator saturation and rate limit effects are considered for the receiver. Other dynamics should be included in future work. The deflection

range attainable from the elevon is (-30 deg, 30 deg), from the pitch flap (-30 deg, 30 deg) and from the clamshells (-60 deg, 60 deg). All three control effectors have a rate limit of ±90 deg/sec. Likewise, the thrust vectoring has a limit of ± 30 deg in both directions and a rate limit of ±30 deg/sec.

3.8 Modeling the Vortex and Its Effect

It is to be noted that the wind effect terms constituting the elements W, $\dot{W}$ in the receiver's equations of motion presented earlier are considered to be based on the uniform wind distribution acting at the receiver's CM, expressed in its body frame. But, the vortex-induced wind field acting on the receiver aircraft is non-uniform in nature. Therefore, to be able to use the above aircraft equations of motion without doing any modifications, there is a need to approximate the non-uniform induced wind components and gradients by equivalent uniform wind and gradients. Once a fairly reasonable approximation can be achieved, the implementation of aerodynamic coupling between the tanker and the receiver becomes far more direct and computationally efficient than the conventional procedure which involves first the calculation of induced forces and moments from the wind distribution, and then inserting these forces and moments in the aircraft dynamics equations. The procedure for a simple and fairly accurate method of approximating the non-uniform vortex-induced wind field by its uniform equivalent is briefly explained in this section.

In our dynamic model for aerial refueling, the tanker is considered to produce two pairs of straight, semi-infinite trailing vortex filaments – one from the wings and one from the horizontal tail – that induce additional wind velocities on the body of the receiver aircraft (see Fig. 3.2). These vortex-induced wind velocities cause changes in the forces and moments experienced by the receiver. However, instead of attempting to directly estimate the induced forces and moments on the follower, the induced wind velocities

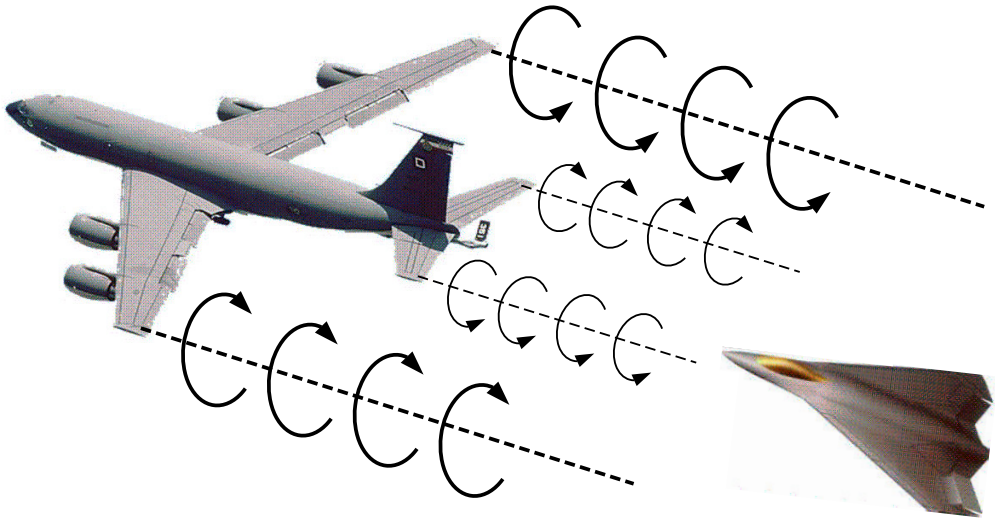

Figure 3.2. Trailing vortex from the wings and horizontal tail.

and wind gradients are computed. The induced wind velocities are written as a function of the relative separation as well as the relative orientation between the tanker and the receiver using a modified horseshoe vortex model based on the Helmholtz profile. Since the induced wind and wind gradients are non-uniform along the body dimensions of the receiver aircraft, an averaging technique is implemented to compute the effective wind and wind gradient as uniform approximations. The effective wind components and gradients are introduced into the nonlinear aircraft equations that include the components of wind and the temporal variation of wind in the body frame to determine the effect on the receiver's dynamics. The effect of vortex decay over time is also included in our model. Special care has been taken to accommodate different geometrical dimensions for the tanker and the receiver aircraft and also to include many useful geometrical parameters of the aircraft like the wing sweep angle, the dihedral angle and the relative distance between the center of mass of the aircraft and the aerodynamic center of the wing, in estimating the vortex-effect experienced during aerial refueling. Interested readers are

refered to Refs. [12, 13, 14, 10, 11, 15, 16, 17] for further details of the actual vortex model and the averaging technique used to estimate the vortex-effect on the receiver.

CHAPTER 4

CONTROL DESIGN

4.1 Control Design for Tanker

In an aerial refueling operation, the tanker aircraft flies in a pre-specified course while a receiver aircraft refuels and others fly in formation waiting for their turn for refueling. In general, the tanker aircraft flies at a constant altitude with a constant speed. The refueling flight course for the tanker aircraft is constituted by steady straight level flights and steady constant altitude turns such as in a "racetrack" maneuver.

4.1.1 Requirements

While a human pilot will fly the tanker aircraft in racetrack maneuvers for UAVs to refuel in real-life applications, in the computer simulation environment, a controller should be designed and implemented for the tanker aircraft to fly in any desired racetrack maneuver as at least a pilot would fly the aircraft. With the controller implemented in the simulation environment, the tanker aircraft should fly at any commanded altitude and with any commanded speed provided they are feasible for the tanker aircraft. Further, the tanker aircraft should be able to execute any steady turn as commanded. The steady turns, in this thesis, are specified by the yaw rate of the aircraft. The tanker aircraft should track commanded yaw rate changes with small transient and zero steady-state error. While starting and ending a turn, and during the turn, deviations in altitude and speed from their respective nominal values should be small and decay to zero at the steady-state. Overall, the closed-loop performance of the tanker aircraft, in the

simulation environment, should be similar to the flight of a piloted tanker aircraft in an actual racetrack maneuver.

4.1.2 Control Design Approach

To satisfy all the requirements, a combination of a multi-input-multi-output state-feedback LQR and integral control technique is employed in designing the altitude and speed hold, and yaw rate tracking controller. The control variables available for the tanker aircraft are the three conventional control surfaces and the throttle setting. The outputs to be controlled are the airspeed, altitude and yaw rate.

A gain scheduling scheme is implemented based on the commanded speed and yaw rate. The tanker's equations of motion which are given in the previous section are linearized at four different steady-state trimmed nominal conditions. Two of the nominal conditions correspond to tanker flying straight level at constant altitude with two different airspeeds and the other two correspond to tanker turning with a specifed turn rate at constant altitude with the same two airspeeds. These four nominal cases are summarized in Table 4.1.

Table 4.1. Nominal Conditions by Turn rate and Airspeed

Nominal Condition	Tanker Yaw Rate	Tanker Airspeed
1	$\dot{\psi}_{T,1}$	$V_{T,1}$
2	$\dot{\psi}_{T,1}$	$V_{T,2}$
3	$\dot{\psi}_{T,2}$	$V_{T,1}$
4	$\dot{\psi}_{T,2}$	$V_{T,2}$

Specification of the nominal conditions and the solution of the equations of motion for determining the nominal values of the tanker aircraft states and control variables at each nominal condition are presented in Appendix A. Note that the nominal conditions

are parameterized by the tanker yaw rate and speed. Thus, the nominal values of the states and the control variables are also functions of the two parameters. Once a set of nominal values for each of the four nominal conditions are determined, the equations of motion of the tanker are linearized at each nominal condition using the respective set of nominal values. In Appendix B, the linearization procedure for the tanker aircraft is summarized and the resultant matrices of the state-space representation are presented. Appendix E provides the nominal values of the states and control variables in each nominal conditions.

Followings are the four different sets of linearized equation of motion, in state-space form, for the tanker.

$$\Delta\underline{\dot{x}}_T = \mathbf{A}_{T,i}\ \Delta\underline{x}_T + \mathbf{B}_{T,i}\ \Delta\underline{u}_T \tag{4.1}$$

where $\mathbf{A}_{T,i} \in \Re^{9\times 9}$, $\mathbf{B}_{T,i} \in \Re^{9\times 4}$, $i \in \{1,2,3,4\}$, for the four nominal conditions described in Table 4.1, respectively. See Appendix B for the details of A_T and B_T and see Appendix G for the nominal values for A_T and B_T for the four nominal conditions. The state vector for the tanker aircraft is

$$\Delta\underline{x}_T = [\Delta V_T\ \ \Delta\beta_T\ \ \Delta\alpha_T\ \ \Delta p_T\ \ \Delta q_T\ \ \Delta r_T\ \ \Delta\theta_T\ \ \Delta\phi_T\ \ \Delta z_T\ \ ]^T \tag{4.2}$$

The control input vector is

$$\Delta\underline{u}_T = [\Delta\delta_{a_T}\ \ \Delta\delta_{e_T}\ \ \Delta\delta_{r_T}\ \ \Delta\xi_{t_T}\ \ ]^T \tag{4.3}$$

where $(\delta_{a_T}, \delta_{e_T}, \delta_{r_T})$ are the control surface deflections of the tanker and ξ_{t_T} is the throttle setting for the tanker. In all equations above, Δ indicates that the corresponding variable is the deviation from its nominal value. Since the requirements of the controller are to track commanded speed, altitude and yaw rate, the following output vector of the tanker aircraft is chosen

$$\underline{y}_T = \left[\Delta V_T\ \ \Delta z_T\ \ \Delta\dot{\psi}_T\right]^T \tag{4.4}$$

To ensure zero tracking error at steady state condition, the state space equations are augmented by three integrators for speed error, altitude error and yaw rate error:

$$\underline{\dot{e}}_T = \underline{y}_T - \underline{y}_{T,c} \tag{4.5}$$

where $\underline{y}_{T,c} = [\Delta V_{T,c}\ \Delta z_{T,c}\ \Delta\dot{\psi}_{T,c}]^T$ is the commanded output vector of the tanker. Thus, in scalar form

$$\begin{aligned} \dot{e}_{V_T} &= \Delta V_T - \Delta V_{T,c} \\ \dot{e}_{z_T} &= \Delta z_T - \Delta z_{T,c} \\ \dot{e}_{\dot{\psi}_T} &= \Delta\dot{\psi}_T - \Delta\dot{\psi}_{T,c} \end{aligned} \tag{4.6}$$

By including the augmentation states in the state–space equations, the augmented state equation becomes

$$\begin{bmatrix} \Delta\underline{\dot{x}}_T \\ \underline{\dot{e}}_T \end{bmatrix} = \begin{bmatrix} \mathbf{A}_{T,i} & \mathbf{0_{9\times 3}} \\ \mathbf{C_T} & \mathbf{0_{3\times 3}} \end{bmatrix} \begin{bmatrix} \Delta\underline{x}_T \\ \underline{e}_T \end{bmatrix} + \begin{bmatrix} \mathbf{B}_{T,i} \\ \mathbf{0_{3\times 4}} \end{bmatrix} \Delta\underline{u}_T - \begin{bmatrix} \mathbf{0_{9\times 3}} \\ \mathbf{I_{3\times 3}} \end{bmatrix} \underline{y}_{T,c} \tag{4.7}$$

Using LQR design technique, the state feedback gain matrix $[\mathbf{K_{T,x}}\mathbf{K_{T,e}}]$ is obtained to minimize the cost function:

$$J(\underline{u}_T) = \int_0^\infty \left\{ [\ \Delta\underline{x}_T^T \quad \underline{e}_T^T\ ]\mathbf{Q}_{T,i} \begin{bmatrix} \Delta\underline{x}_T \\ \underline{e}_T \end{bmatrix} + \Delta\underline{u}_T^T \mathbf{R}_{T,i}\, \Delta\underline{u} \right\} \mathrm{d}t \tag{4.8}$$

where $\mathbf{Q}_{T,i} \in \Re^{12\times 12}$ are symmetric positive semidefinite, $\mathbf{R}_{T,i} \in \Re^{4\times 4}$ are symmetric positive definite and $\mathbf{N}_{T,i} \in \Re^{12\times 4}$ are symmetric positive definite. Note that matrices $\mathbf{Q}_{T,i}$, $\mathbf{R}_{T,i}$ and $\mathbf{N}_{T,i}$ can be selected separately for each nominal condition. Thus, the state feedback control laws with the integral control are

$$\Delta\underline{u}_{T,i} = -\mathbf{K_{x_{T,i}}}\, \Delta\underline{x}_T - \mathbf{K_{e_{T,i}}}\, \underline{e}_T \tag{4.9}$$

where $i \in \{1, 2, 3, 4\}$, corresponding to the four nominal conditions. In the implementation of these controllers, a "scheduling" scheme should be employed, based on scheduling

parameters, $\dot{\psi}_T$ and V_T to determine effective values of the gains at a given flight condition. To formulate the overall non-linear controller based on the linear designs at the four nominal conditions, Lagrange interpolation scheme is utilized. Thus, the gain scheduling control law is

$$\Delta\underline{u} = \frac{\left(\dot{\psi}_{T,c} - \dot{\psi}_{T,2}\right)(V_{T,c} - V_{T,2})}{\left(\dot{\psi}_{T,1} - \dot{\psi}_{T,2}\right)(V_{T,1} - V_{T,2})}\,\underline{u}_1 + \frac{\left(\dot{\psi}_{T,c} - \dot{\psi}_{T,2}\right)(V_{T,c} - V_{T,1})}{\left(\dot{\psi}_{T,1} - \dot{\psi}_{T,2}\right)(V_{T,2} - V_{T,1})}\,\underline{u}_2$$
$$+\frac{\left(\dot{\psi}_{T,c} - \dot{\psi}_{T,1}\right)(V_{T,c} - V_{T,2})}{\left(\dot{\psi}_{T,2} - \dot{\psi}_{T,1}\right)(V_{T,1} - V_{T,2})}\,\underline{u}_3 + \frac{\left(\dot{\psi}_{T,c} - \dot{\psi}_{T,1}\right)(V_{T,c} - V_{T,1})}{\left(\dot{\psi}_{T,2} - \dot{\psi}_{T,1}\right)(V_{T,2} - V_{T,1})}\,\underline{u}_4 \tag{4.10}$$

Note that the control law assumes the availability of full state measurement or estimation for feedback. The control variables available for the tanker aircraft are the three conventional control surfaces and the throttle setting. The outputs to be controlled are the airspeed, altitude and yaw rate.

4.2 Control Design for Receiver

For successful aerial refueling operation, the receiver should approach the tanker, stay at the refueling contact position during the actual fuel transfer and fly away once the refueling is completed, all in a safe manner despite various sources of disturbance such as trailing wake vortex, fuel transfer and motion of the tanker. These three phases of aerial refueling can easily be addressed in a single framework by utilizing the equations of motion of the receiver, derived relative to the tanker. Since the motion of the receiver is defined in the tanker's body frame, the reference trajectory for the receiver can easily be defined relative to the tanker. Obviously, during the phase in which the receiver should stay at the refueling contact position (station-keeping phase), the reference trajectory for the receiver becomes a point in the body-frame of the tanker. Once a safe reference trajectory that consists of the approach from the observation position to the contact

position, the contact position and the fly-away are determined to ensure the overall safety of the receiver and the tanker, a trajectory-tracking controller is needed to make the receiver follow the reference trajectory in a safe and timely manner. Therefore, it is very important to have a controller that can fly the receiver close to the reference trajectories.

4.2.1 Requirements

The primary requirement of the control design is the tracking of the generated trajectories, with zero steady-state error in the x, y, z coordinates in the tanker's body frame, under the disturbance of trailing vortex, time variation of the inertia properties of the receiver and the possible steady maneuvers of the tanker's body frame. Meanwhile, the control inputs generated by the controller should not cause significant saturation on the magnitudes and rates of the actuators. Moreover, during the transient, overshoot or undershoot on trajectory response should be minimized to ensure the safety of the refueling. At the same time, the response of the closed loop system should be fast enough so that the approach and fly–away maneuvers are completed as planned and the high-wind regions of the trailing vortex field are exited in a timely fashion. Additionally, during the approach, fly–away and station-keeping maneuvers, the angle-of-attack and the airspeed should not be close to their corresponding stall values. In this regard, very big pitch angle should not be commanded. Finally, to ensure the safety of the aircraft, the bank angle should be small relative to its nominal value. As stated earlier, the controller should perform satisfactorily in all phases of the "racetrack" maneuver, i.e. while the tanker is in a straight wing–level flight, in a steady turn, in transition from straight flight to turn and in transition back to straight flight.

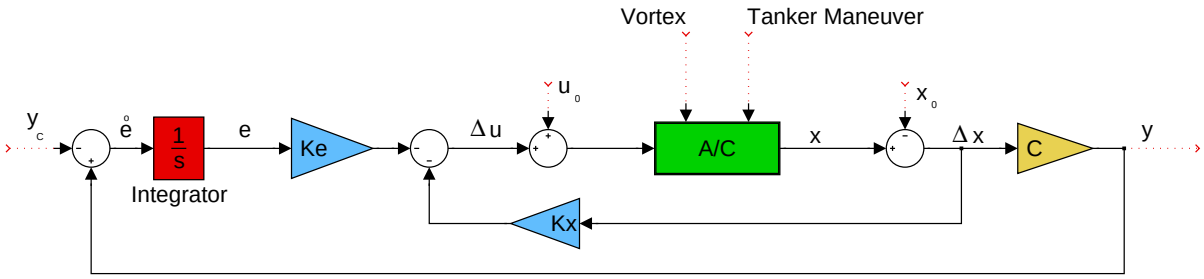

Figure 4.1. State feedback and integral control structure.

4.2.2 Control Design Approach

To satisfy all the requirements, similar to the tanker's case, a combination of a multi-input-multi-output state-feedback LQR and integral control technique is employed in designing the position tracking controller. Moreover, a gain scheduling scheme is implemented based on the speed and turn rate. The equations of motion given in Section 3 are linearized at four different steady-state trimmed nominal conditions. Two of the nominal conditions correspond to tanker flying straight level at constant altitude with two different airspeeds and the other two correspond to tanker turning with a specified turn rate at constant altitude with the same two airspeeds. These four nominal cases are described earlier in the tanker control design section.

To linearize the equations of motion of the receiver, the nominal values of its states should be determined at the four nominal conditions. However, first note that the translational and rotational dynamics equations of the receiver include Euler angles and angular velocity components of the tanker. Thus, the first step is to determine the nominal values of the tanker aircraft at the four nominal conditions. Recall that this task is carried out in Appendix A. Then, the nominal values of the receiver are determined at the four nominal conditions. Details of this procedure is given in Appendix

C. In Appendix D, the linearization procedure and the resultant state-space matrices are presented. This leads to four different sets of linearized equations of motion:

$$\Delta\underline{\dot{x}} = \mathbf{A}_i\ \Delta\underline{x} + \mathbf{B}_i\ \Delta\underline{u} + \mathbf{H}_i\ \Delta\underline{w} \tag{4.11}$$

where $\mathbf{A}_i \in \Re^{12\times12}$, $\mathbf{B}_i \in \Re^{12\times6}$, $\mathbf{H}_i \in \Re^{12\times6}$, $i \in \{1,2,3,4\}$, for the four nominal conditions described in Table 4.1, respectively. Appendix F provides the nominal values of the states and control variables in each nominal conditions. See Appendix H for the numerical values for A, B for four nominal conditions. The state vector is

$$\Delta\underline{x} = [\Delta V\ \ \Delta\beta\ \ \Delta\alpha\ \ \Delta p\ \ \Delta q\ \ \Delta r\ \ \Delta\psi\ \ \Delta\theta\ \ \Delta\phi\ \ \Delta x\ \ \Delta y\ \ \Delta z]^T \tag{4.12}$$

The control input vector is

$$\Delta\underline{u} = [\Delta\delta_a\ \ \Delta\delta_e\ \ \Delta\delta_r\ \ \Delta\xi\ \ \Delta\delta_y\ \ \Delta\delta_z]^T \tag{4.13}$$

The disturbance vector due to the motion of the tanker is

$$\Delta\underline{w} = [\Delta V_{xT}\ \ \Delta V_{yT}\ \ \Delta V_{zT}\ \ \Delta p_T\ \ \Delta q_T\ \ \Delta r_T\ \ \Delta\dot{p}_T\ \ \Delta\dot{q}_T\ \ \Delta\dot{r}_T\ \ \Delta\psi_T\ \ \Delta\theta_T\ \ \Delta\phi_T]^T \tag{4.14}$$

In all equations above, Δ indicates that the corresponding variable is the perturbation from its nominal value. Note that, since the nonlinear equations of motion are derived in terms of the states of the receiver relative to the tanker, in the linearized equations, the effect of the motion of the tanker on the relative motion is clearly identified by H_i matrices. However, H_i matrices are not utilized in the control design presented in this paper and this is left as a topic for future work.

Since the position tracking controller is to be designed for the receiver relative to the tanker, the outputs to be tracked are (Δx, Δy,Δz). Thus, output vector is chosen to be

$$\underline{y} = [\Delta x\ \ \Delta y\ \ \Delta z]^T \tag{4.15}$$

To ensure zero tracking error at steady state condition, the state space equations are augmented by three integrators, one for each position error:

$$\underline{\dot{e}} = \underline{y} - \underline{y_c} \tag{4.16}$$

where $\underline{y_c} = [\Delta x_c \ \Delta y_c \ \Delta z_c]^T$ is the commanded trajectory for the receiver in the body frame of the tanker for approaching the refueling contact position. Thus, in scalar form

$$\begin{aligned} \dot{e}_x &= \Delta x - \Delta x_c \\ \dot{e}_y &= \Delta y - \Delta y_c \\ \dot{e}_z &= \Delta z - \Delta z_c \end{aligned} \tag{4.17}$$

By including the augmentation states in the state–space equations, the augmented state equation becomes

$$\begin{bmatrix} \Delta\underline{\dot{x}} \\ \underline{\dot{e}} \end{bmatrix} = \begin{bmatrix} \mathbf{A}_i & \mathbf{0_{12\times 3}} \\ \mathbf{C} & \mathbf{0_{3\times 3}} \end{bmatrix} \begin{bmatrix} \Delta\underline{x} \\ \underline{e} \end{bmatrix} + \begin{bmatrix} \mathbf{B}_i \\ \mathbf{0_{3\times 6}} \end{bmatrix} \Delta\underline{u} + \begin{bmatrix} \mathbf{H}_i \\ \mathbf{0_{3\times 6}} \end{bmatrix} \Delta\underline{w} - \begin{bmatrix} \mathbf{0_{12\times 3}} \\ \mathbf{I_{3\times 3}} \end{bmatrix} \underline{y_c} \tag{4.18}$$

Using LQR design technique, the state feedback gain matrix $[\mathbf{K_x} \ \mathbf{K_e}]$ is obtained to minimize the cost function:

$$J(\underline{u}) = \int_0^\infty \left\{ [\ \Delta\underline{x}^T \quad \underline{e}^T\ ] \mathbf{Q}_i \begin{bmatrix} \Delta\underline{x} \\ \underline{e} \end{bmatrix} + \Delta\underline{u}^T \mathbf{R}_i \, \Delta\underline{u} \right\} \mathrm{d}t \tag{4.19}$$

where $\mathbf{Q}_i \in \Re^{15\times 15}$ are symmetric positive semidefinite and $\mathbf{R}_i \in \Re^{6\times 6}$ are symmetric positive definite. Note that matrices $\mathbf{Q}_i$ and $\mathbf{R}_i$ can be selected separately for each nominal condition. Thus, the state feedback control laws with the integral control are

$$\Delta\underline{u_i} = -\mathbf{K_{x_i}} \, \Delta\underline{x} - \mathbf{K_{e_i}} \, \underline{e} \tag{4.20}$$

where $i \in \{1, 2, 3, 4\}$, corresponding to the four nominal conditions. In the implementation of these controllers, a "scheduling" scheme should be employed, based on a specified

set of scheduling parameters, $\dot{\psi}_T$ and V_T to determine effective values of the gains at a given flight condition. To formulate the overall non-linear controller based on the linear designs at the four nominal conditions, Lagrange interpolation scheme is utilized. Thus, the gain scheduling control law is

$$\begin{aligned}\Delta\underline{u} = &\frac{\left(\dot{\psi}_{T,c} - \dot{\psi}_{T,2}\right)(V_{T,c} - V_{T,2})}{\left(\dot{\psi}_{T,1} - \dot{\psi}_{T,2}\right)(V_{T,1} - V_{T,2})}\,\underline{u}_1 + \frac{\left(\dot{\psi}_{T,c} - \dot{\psi}_{T,2}\right)(V_{T,c} - V_{T,1})}{\left(\dot{\psi}_{T,1} - \dot{\psi}_{T,2}\right)(V_{T,2} - V_{T,1})}\,\underline{u}_2 \\ &+\frac{\left(\dot{\psi}_{T,c} - \dot{\psi}_{T,1}\right)(V_{T,c} - V_{T,2})}{\left(\dot{\psi}_{T,2} - \dot{\psi}_{T,1}\right)(V_{T,1} - V_{T,2})}\,\underline{u}_3 + \frac{\left(\dot{\psi}_{T,c} - \dot{\psi}_{T,1}\right)(V_{T,c} - V_{T,1})}{\left(\dot{\psi}_{T,2} - \dot{\psi}_{T,1}\right)(V_{T,2} - V_{T,1})}\,\underline{u}_4 \end{aligned} \tag{4.21}$$

Note that the control law assumes the availability of full state measurement or estimation for feedback. As shown in Eq. (4.12), the states of the receiver consist of airspeed, side slip angle and angle-of-attack of the receiver as well as the angular velocity, orientation and position of the receiver relative to the tanker. Further, for the implementation of the gain scheduling scheme in Eq. (4.21), commanded speed and yaw rate of the tanker should be communicated to the receiver. While not used in this paper, if one wants to utilize the disturbance matrix in the control law, the disturbance states due to the motion of the tanker will need to be communicated to the receiver as well. As shown in Eq. (4.14), the disturbance vector consists of translational and angular velocity, angular acceleration and the orientation of the tanker relative to the inertial frame.

CHAPTER 5

SIMULATION RESULTS

5.1 Nomimal Conditions

The gain scheduling controller is designed based on four nominal conditions, which are: (1) $\dot{\psi}_T = 0$ and $V_T = 180\ m/s$, (2) $\dot{\psi}_T = 0$ and $V_T = 200\ m/s$, (3) $\dot{\psi}_T = 1.7\ deg/s$ and $V_T = 180\ m/s$, (4) $\dot{\psi}_T = 1.7\ deg/s$ and $V_T = 200\ m/s$. The linear LQR/Integral controllers are designed and implemented in such a way that various levels of control input allocations can be tested. The control variable allocation is achieved by varying the respective elements of the control weighting matrix $\mathbf{R}$ of the cost function in Eq. (4.19). Three different allocation cases simulated and compared are:

Case–1 : A combination of control effectors and thrust vectoring is used. $\mathbf{R}$ is chosen to be a diagonal matrix with the following elements

$$\mathbf{R}(i,i) = (10, 10, 100, 1000, 500, 100) \tag{5.1}$$

Case–2 : Only control effectors are used without any thrust vectoring. $\mathbf{R}$ is chosen to be a diagonal matrix with the following elements

$$\mathbf{R}(i,i) = (5, 1, 10, 700, 1000000, 1000000) \tag{5.2}$$

Case–3 : Pitch Flap and Clamshell are fixed at their nominal values. Elevon and thrust vectoring are the only control variables used. $\mathbf{R}$ is chosen to be a diagonal matrix with the following elements

$$\mathbf{R}(i,i) = (10, 10000000, 10000000, 1000, 50, 100) \tag{5.3}$$

In all the three cases, $\mathbf{Q}$ is chosen to be a diagonal matrix with the following elements

$$\mathbf{Q}(i,i) = 0.1 \times (1, 1, 1, 1, 1, 1, 1, 1, 100, 1, 0.1, 1, 1, 0.06, 1) \tag{5.4}$$

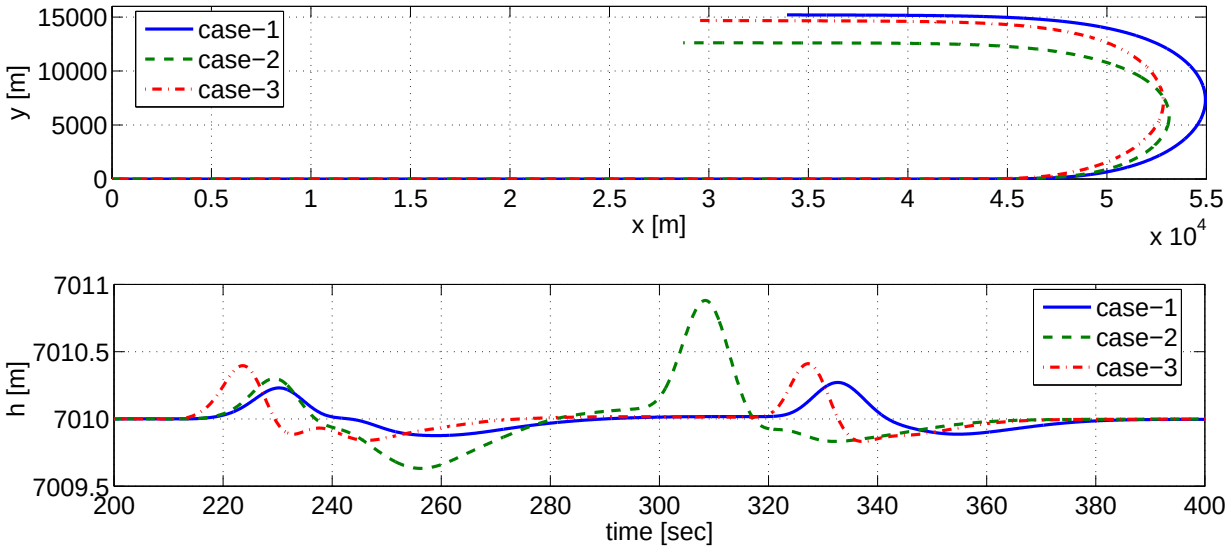

Figure 5.1. Target trajectories and altitude histories during turns with three different yaw rates.

5.2 Simulation Results

Since the performance of an aerial refueling operation depends on the motions of both the tanker and the receiver, the full 6-DOF nonlinear dynamics of both tanker and receiver are simulated in an integrated environment. The refueling is performed at the nominal altitude of 7010 *meters* while the tanker is flying at the speed of 200 m/sec. The simulation starts when the tanker is in a straight-level flight and stays in this condition until the receiver aircraft moves from the observation position to the refueling contact position. While the receiver is at this position, the tanker starts turning with a specified yaw rate until the yaw angle change is 180 *degrees* to complete the U-turn portion of the refueling maneuver. During this time, the receiver should be able to maintain the proximity of the refueling contact position without unacceptable deviation. Figure 5.1 shows three cases of tanker turn with different turning rates. In the rest of the paper,

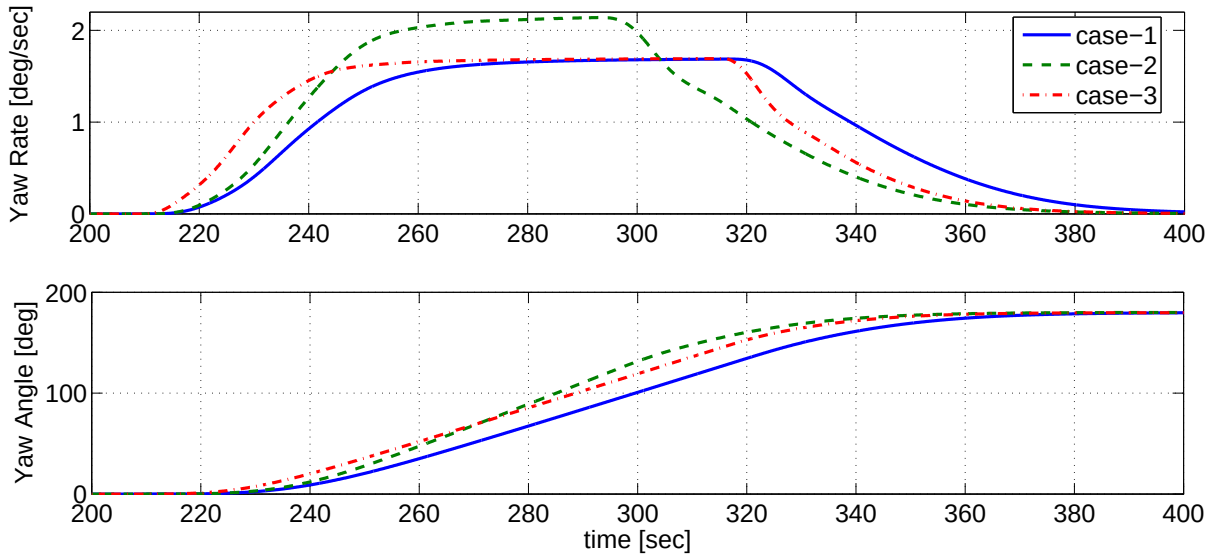

Figure 5.2. Time histories of yaw rate and yaw angle during three different turns.

these cases will be referred to as TANKER-CASE-1, TANKER-CASE-2 and TANKER-CASE-3. While the first plot of Figure 5.1 shows the xy-projections of the entire target trajectories, the second plot shows the altitude histories only during the turns. Note from the second plot of Figure 5.1 that tanker altitude slightly deviates from the nominal altitude during the turns. Even if the deviation is very small (less than 1 *meter*) for the tanker, as will be shown later, it might be very significant for the performance of the refueling. The three turns are generated with different turn rates as shown in Figure 5.2. The tanker model has its own gain scheduling controller to track commanded altitude, speed and yaw rate. The commanded yaw rate for TANKER-CASE-1 is generated from the 1.7 deg/sec step response of fourth order linear filter with time constants of 10, 10, 10 and 1 *seconds*. That for TANKER-CASE-2 is the 2.2 deg/sec step response of the same filter. TANKER-CASE-3 has the 1.7 deg/sec step response of a second order linear filter with two time constants of 10 *seconds*. Note that the yaw rates are scheduled so as for the yaw angle to end up to be 180 *degrees*. For the receiver's gain scheduling controller, the same step signals for the yaw rate, after passing through a first order filter with time

constant of 10 sec, are used for scheduling purposes in the interpolation scheme shown as $\dot{\psi}_{T,C}$ in Eq. (4.21).

Figure 5.3 shows the variation of airspeed, angle-of-attack and side-slip-angle of the tanker during the turns. This variations are important for the receiver aircraft because they affect the wind field in the wake of the tanker, particularly at the refueling position and, in turn, change the wind components and gradients that the receiver aircraft is exposed to.

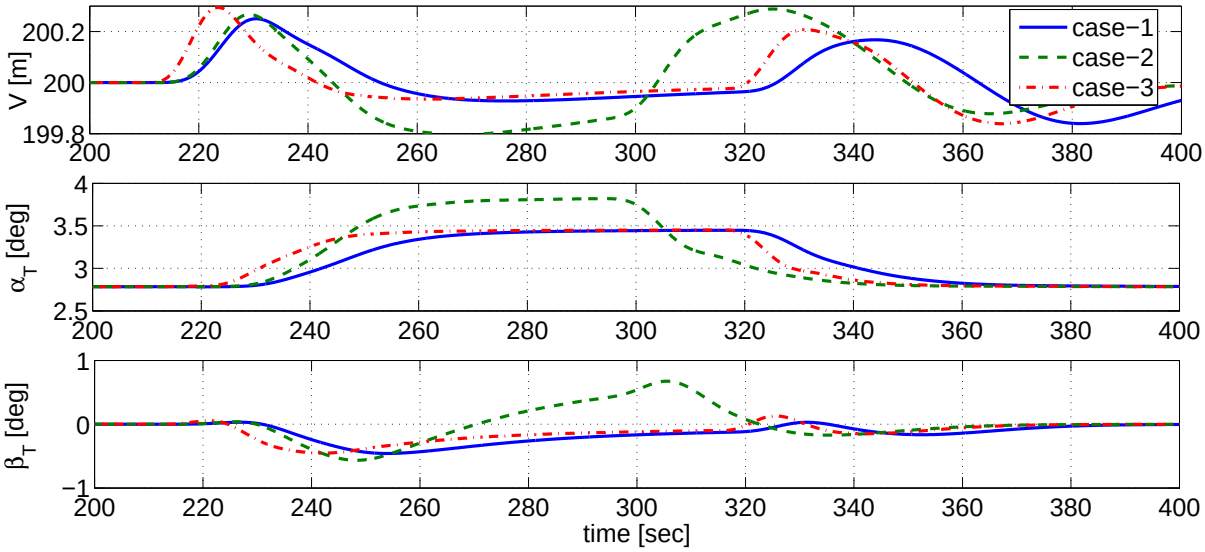

Figure 5.3. Airspeed, angle-of-attack and side-slip angle of tanker during the three turn cases.

Figure 5.4 shows the pitch and bank angles of the tanker. These variations are also important for the receiver aircraft because they directly change the relative orientation and thus cause the refueling position to move.

At the start of the simulation, the receiver aircraft is at the observation position, i.e., laterally offset from the tanker by 60.96 *meters*, longitudinally 15.24 *meters* behind the refueling contact position and vertically at the same level as the contact position.

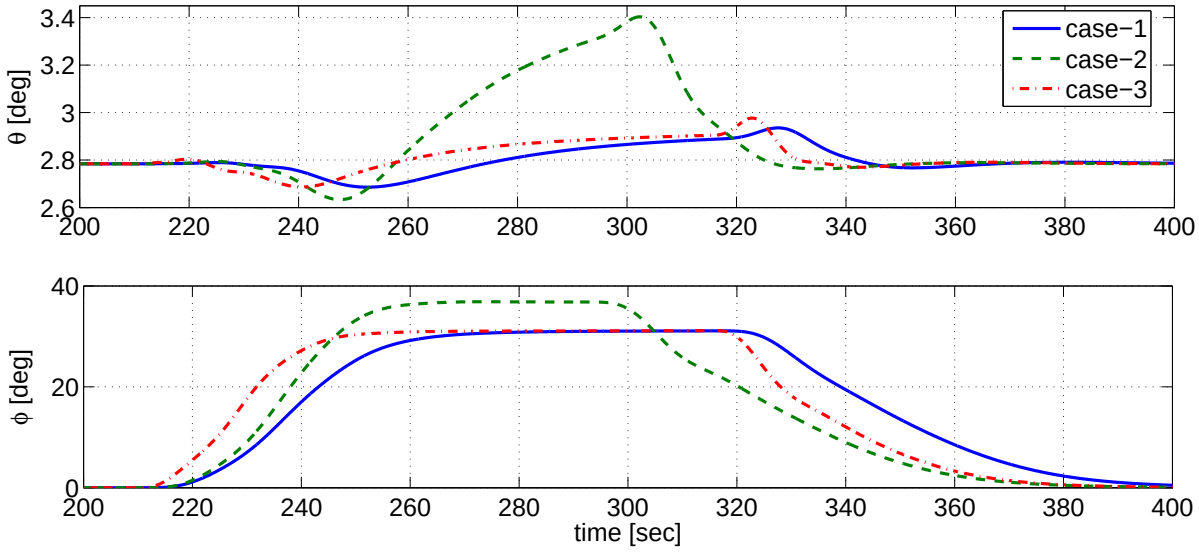

Figure 5.4. Pitch and bank angles of tanker during the turns.

The refueling contact position is 25.33 *meters* directly behind and 6.46 *meters* below the c.g. of the tanker without any lateral offset. In other words, the receiver is initially at (-40.56, 60.96, 6.46) in the body-frame of the tanker and should go to and stay at (-25.33, 0, 6.46) for refueling. The receiver should move from the initial position to the refueling contact position by first maneuvering laterally right behind the tanker and then moving forward to the contact position without any altitude change (see Figs 5.5 and 5.6).

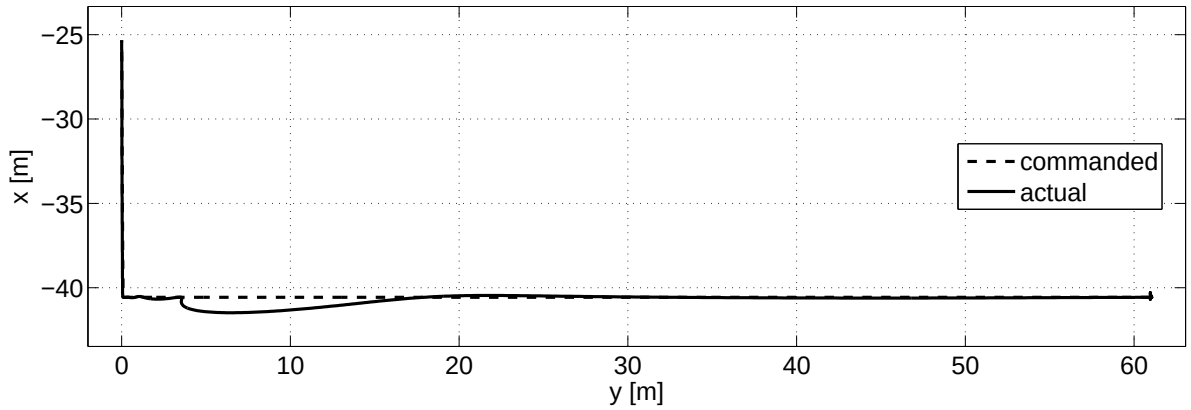

Figure 5.5. Trajectory of the aircraft relative to the tanker in xy-plane.

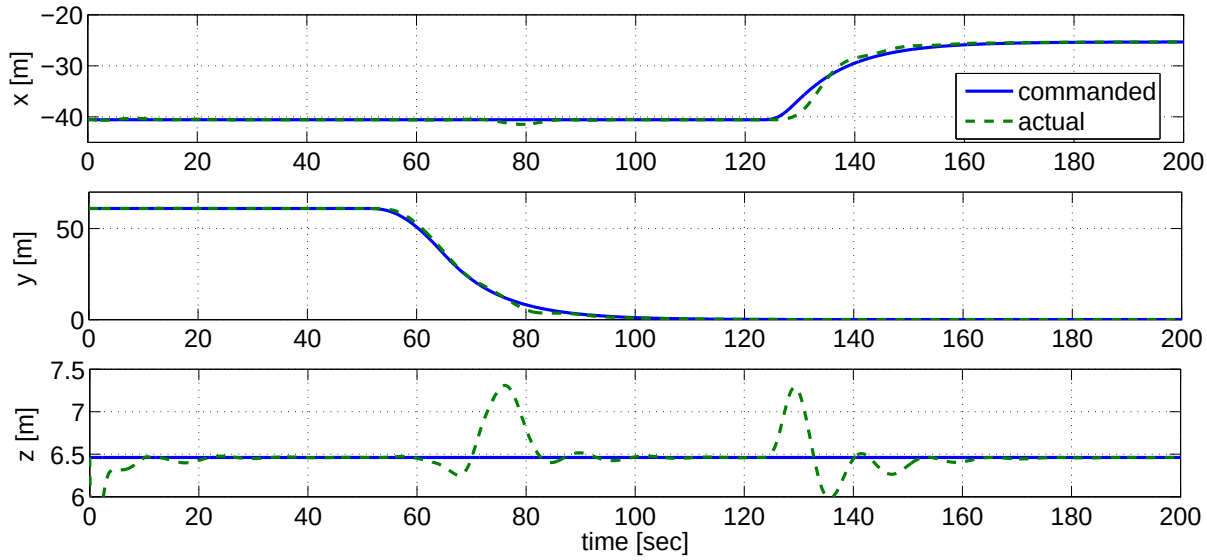

Figure 5.6. Commanded and actual x, y and z positions of the receiver during the approach maneuver.

Figure 5.5 shows the x- and y- components of both commanded and actual trajectory of the receiver in the body frame of the tanker in case-1. Fig 5.6 illustrates the x- , y- and z- components of the trajectory in time domain. As will be shown more clearly, when the simulation starts, the vortex induced wind is not on and at 10 *seconds*, the wind is turned on and gradually increased to the normal level. This is done to ensure the start of the simulation without any numerical problem and also to see the effect of the vortex in the initial flight configuration. As seen in Fig 5.6, the lateral maneuver is initiated at around 50 *seconds* and lasts about a minute until the receiver is directly behind the tanker at 110 *seconds*. Then at 125 *seconds*, the receiver starts moving forward towards and reaches the refueling contact position in about 50 *seconds*. The trajectories of the other two control allocation cases are not presented because they all are similar to each other. Both figures show that the commanded trajectories are closely tracked during the maneuver. Note that positive z-direction in down. Thus, the two spikes are in fact due

to slight altitude lost first when the lateral maneuver starts and second when the forward motion is initiated.

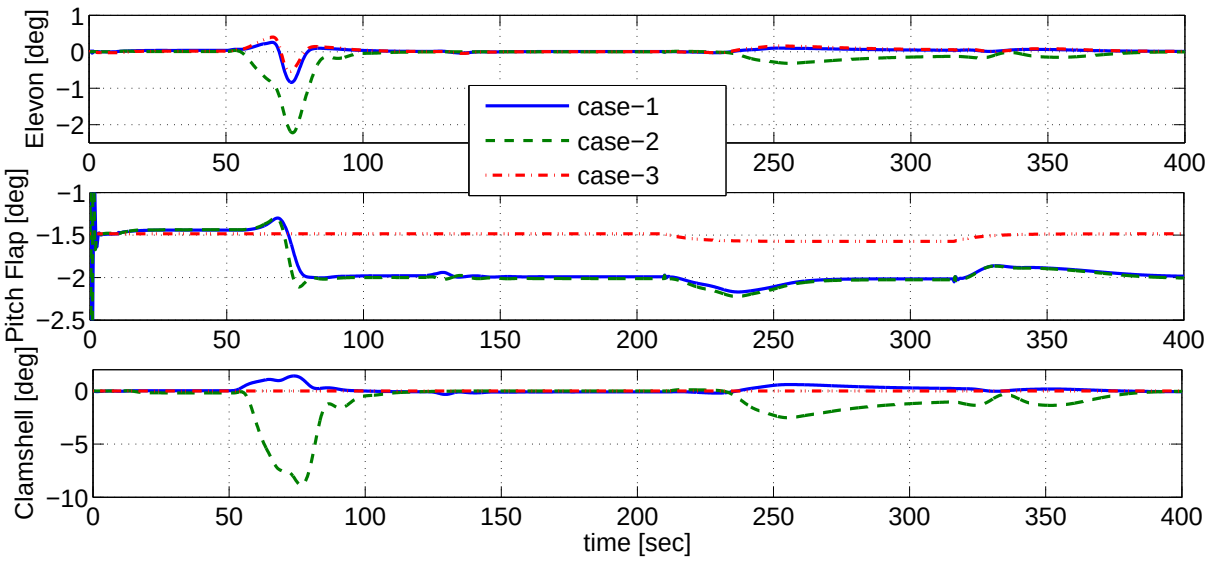

Figure 5.7. Deflection of the three control effectors in the three cases during the whole simulation.

Figure 5.7, 5.8 and 5.9 show the initial levels of the control variables, how they vary during the approach maneuver and when the tanker turns in all three control-allocation cases. These figures only shows TANKER-CASE-1 because the plots are similar in the other tanker-turn cases. Figure 5.7 illustrates the deflections of the three control effectors, elevon, pitch flap and clamshell. Note that the pitch flap and clamshell stay almost constant in case 3 because they are fixed at their nominal values. In all three cases, very small deflections and deflection rates (much smaller than their respective saturation levels) in all the three effectors are used to move the receiver to the refueling position and keep it there during the turns. Both elevon and clamshell, as expected, are mainly used during the lateral maneuver and stays almost constant during the forward motion in the approach maneuver. While the control effectors are used during the turn, their

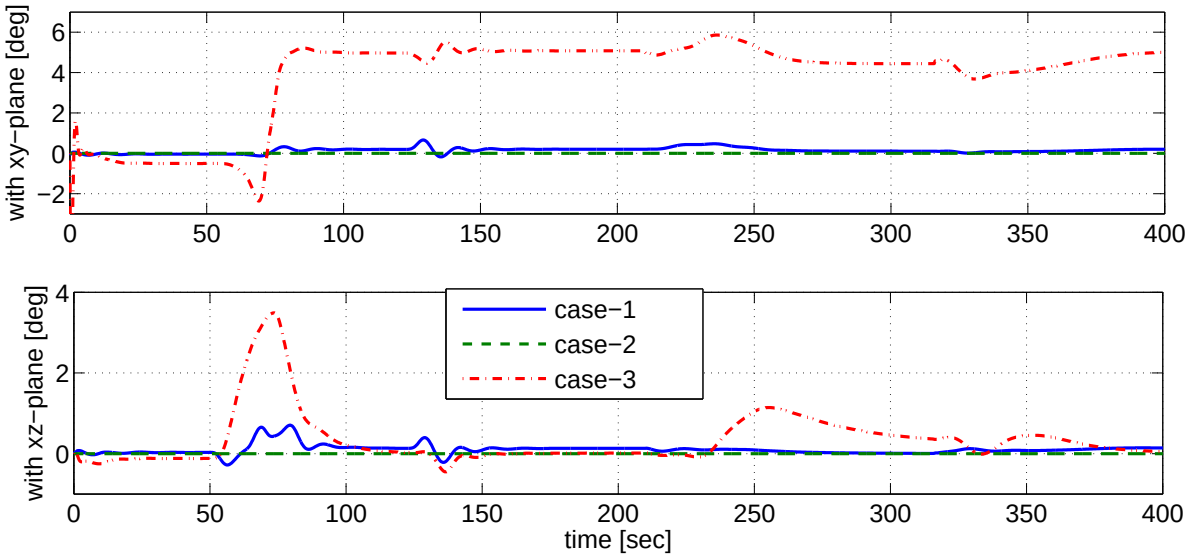

Figure 5.8. Thrust vectoring angle variation in the three cases during the whole simulation.

deflections are smaller compared to the deflections in the time of the approach maneuver. Note that elevon and clamshell deflect in the negative direction in case-2 when no thrust vectoring is used while elevon deflects positive in both cases-1 and -3 and clamshell deflects positive in case-1 during the turn. This implies the effect of thrust vectoring on the use of the control effectors. Figure 5.8 shows the rotation of the thrust vector in terms of its angles with the xy- and xz- planes of the body-frame of the receiver. Note that rotation of the thrust vector from xy-plane induces pitching moment while generating vertical force. Similarly, rotation of the thrust vector from xz-plane induces yawing moment while generating lateral force. Also note that both angles stay zero in case-2 since it represents no-thrust-vectoring configuration. As expected, the thrust vectoring is used the most in case-3 where the pitch flap and clamshell are fixed. The rotation of the thrust vector is small in case-1 because it is used in combination with the control surfaces.

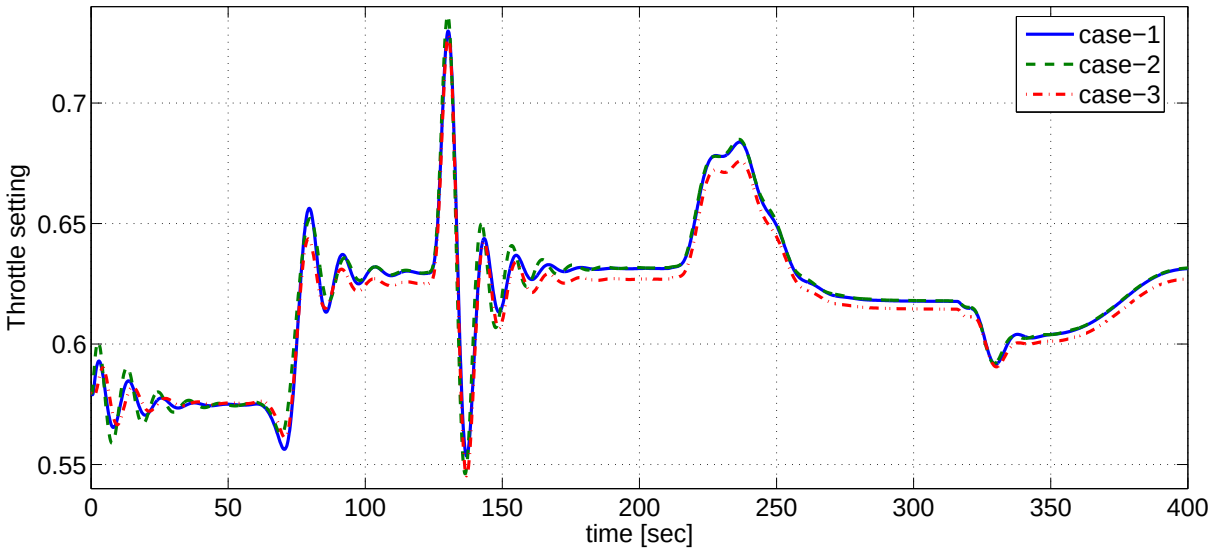

Figure 5.9. Variation in throttle level during the whole simulation in the three cases.

Figure 5.9 illustrates the level of throttle in the three cases. In all cases, the variation of throttle setting is very similar. Note the increase in the throttle setting (60 sec-100 sec) during the lateral maneuver to get right behind the tanker. This is because when the receiver aircraft is behind the tanker, it is subject to strong downwash, which results in higher required thrust. Note also that as the receiver approaches the refueling position, the level of throttle does not change significantly, except during the time of transient. This is due to the fact that the longitudinal variation of the vortex-induced wind is very small in this range. The slight difference in the level of throttle between the cases near 200 sec when the tanker is still in straight-level flight before it starts turning is due to the different thrust vectoring angles and different orientation of the aircraft at the refueling position. Variations of throttle setting in the three tanker-turn cases during the turn of the tanker (after 200 sec) are similar and the levels of throttle setting before the turn starts and after the turn ends are the same, as expected.

Figure 5.10 shows how the orientation of the receiver relative to the tanker changes during the approach maneuvers and the tanker turn in the three cases in terms of Euler

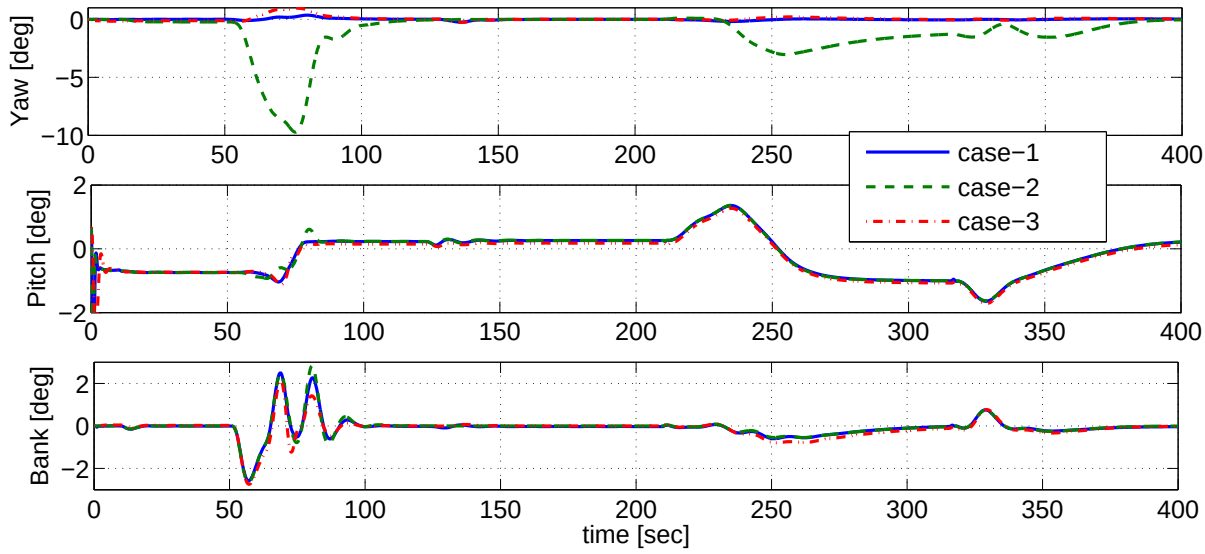

Figure 5.10. Orientation of the aircraft relative to the tanker in the three cases during the whole simulation.

angles. Note that both during the approach maneuver and tanker turn, all the angles are kept small, i.e. the orientation of the receiver is close to the orientation of the tanker. Comparison of yaw response in case-2 (no thrust vectoring) with the other two cases in which thrust vectoring is utilized indicates the positive effect of thrust vectoring in yaw motion during both lateral motion and tanker turn.

The vortex induced wind components and gradients are shown in Fig. 5.11 in control allocation case-1 and TANKER-CASE-1. In the other cases, the plots are similar. First note that at 10 *seconds*, the vortex is "turned on" and the aircraft is exposed to small upwash and sidewash and a slight "rolling" gradient. During the lateral maneuvers, as the receiver gets laterally closer to the tanker (starting at 50 sec), the magnitudes of both effective wind components and gradients increase. At about 70 *seconds* when the lateral distance to the tanker is about 60 percent of the tanker's wingspan, the highest upwash (negative W_z) is experienced. As the receiver gets closer to the tanker when the lateral distance to the tanker is about 45 percent of the tanker's wingspan, the receiver

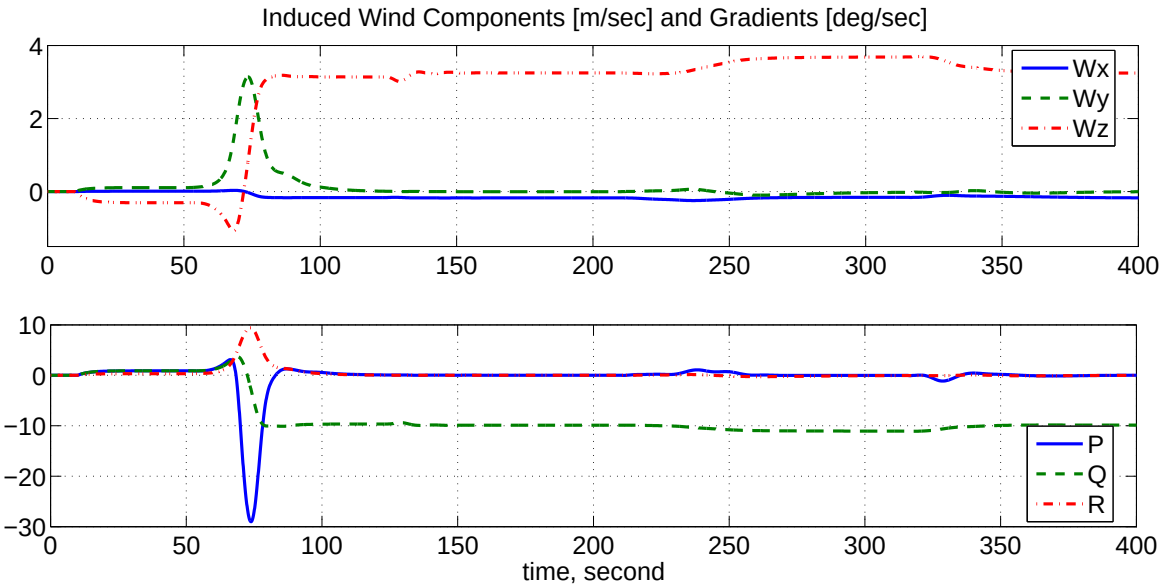

Figure 5.11. The wind components and gradients the receiver is exposed to in case-1 during the whole simulation.

experiences the greatest rolling vortex (P) and the upwash turns into downwash (positive W_z) while the sidewash (W_y) increases dramatically. This is manifested in the rolling oscillation as seen in Fig. 5.10 and altitude drop in Fig. 5.6. During this transition, a yawing vortex (R) gradient is experienced while a pitching vortex (Q) gradient develops. As the receiver gets even closer to a position right behind the tanker, the rolling vortex gradient and sidewash disappear and downwash increases to its highest level. When the receiver is right behind the tanker, two main vortex effects remain: strong downwash and pitching vortex. As stated earlier, when the receiver approaches the tanker from behind, the wind components and the gradients remain almost constant since wind variation is very small in this range of the longitudinal relative positions. Also note the small variation in the wind components and gradients during the tanker turn. This is partly because the receiver relative position and orientation experience small deviation and partly because the tanker's airspeed, angle-of-attack and sideslip angle changes while it turns. To quantify the effect of the trailing wake-vortex on the trajectory tracking

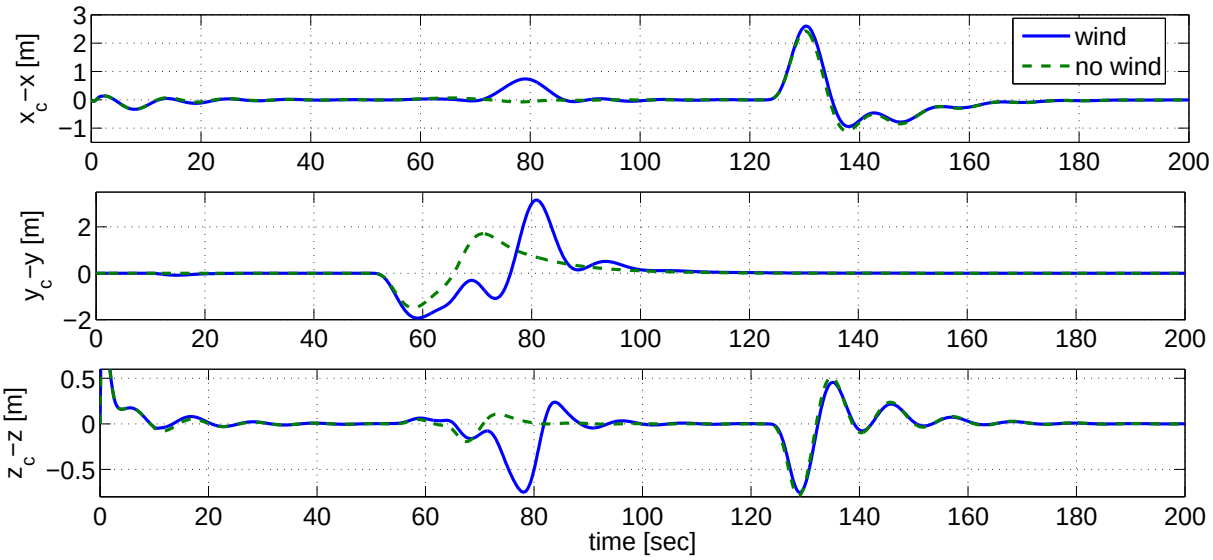

Figure 5.12. Comparision of the trajectory tracking errors in the presence and absence of the trailing wake-vortex.

performance, each control-allocation case is simulated with the vortex effect modeling turned off in addition to normal simulation in which the trailing wake-vortex is active as it should be. The simulations of all three control-allocation cases result in similar performance degradation due to the presence of the wake vortex. Thus, only case-2 (no thrust vectoring) is presented in Fig. 5.12, which shows the trajectory tracking error in three components with and without the wind effect. As seen in Fig. 5.12, the presence of the wake-vortex degrades the trailing performance during the time when the receiver moves laterally from the observation position to a point right behind the tanker. This result is consistent with the observation in Fig. 5.11, which shows, in summary, that the receiver experiences the highest variations in wind components and gradients during this time. During the time when the receiver moves forward to the contact position, the effect of the wake-vortex is minimal even if the aircraft is exposed to almost constant high level of downwash and pitching vortex.

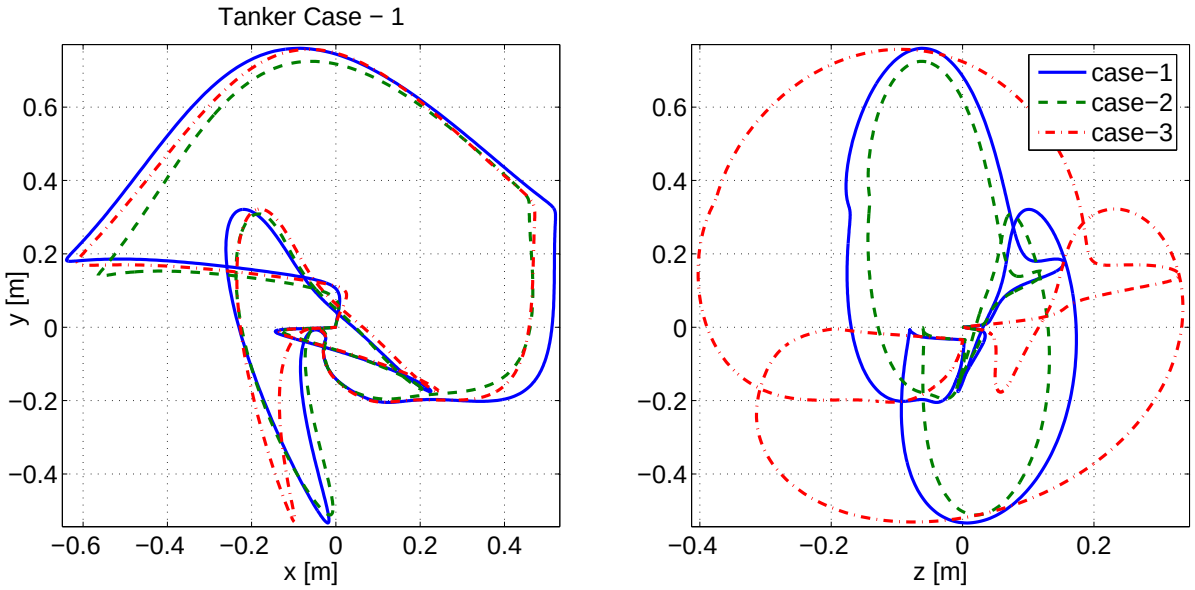

Figure 5.13. Deviation of the receiver position from the refueling position while the tanker turns in TANKER-CASE-1.

To be able to maintain the refueling contact while the target turns, the deviation from the refueling position should be minimal. At the same time, the relative orientation should stay small. To analyze the performance of the controllers in terms of these important requirements, phase portraits of position and orientation are presented as shown in Figs. 5.13 to 5.18. Note that the phase portraits are plotted based on the data only during the tanker turns (i.e. after 200 sec). Fig. 5.13 shows the position deviation from the refueling contact position while the tanker turns in TANKER-CASE-1. Note that y-deviation stays within 0.8 and -0.6 *meters* and x-deviation is between -0.6 and 0.5 *meters* in all three control allocation cases. Regarding z-deviation, case-3 is worse than the others. This is apparently due to the fact that the pitch flap is stuck and thrust vectoring is used instead to generate pitching moment. However, overall, all three cases result in small deviation in all three directions.

Figure 5.14 shows the phase portraits of Euler angles to illustrate the deviation of the receiver orientation from the tanker orientation. In all three cases, the receiver stays

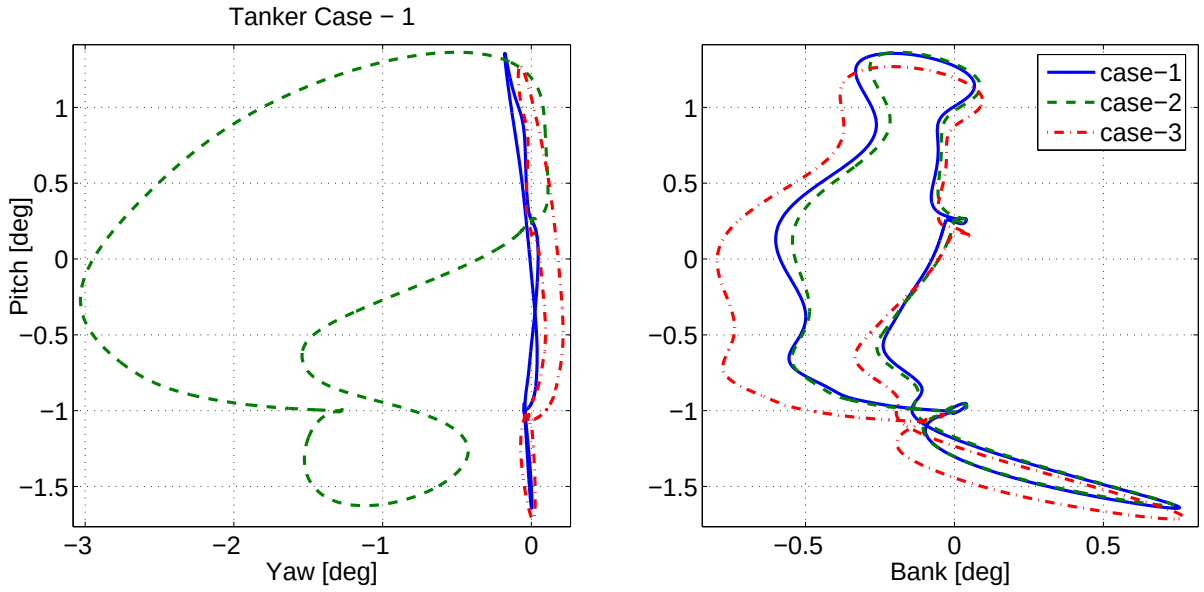

Figure 5.14. Deviation in relative orientation while the tanker turns in TANKER-CASE-1.

close to the tanker in terms of orientation. In the pitch angle, variation is about the same for all cases while cases-2 shows larger deviation in yaw and case-3 yields larger deviation in bank.

Figure 5.15 and 5.16 present the same information as Figs. 5.13 and 5.14 but in TANKER-CASE-2 where the tanker turns based on a larger yaw rate command. Fig. 5.15 shows similar trend as in the previous case in the sense that deviations in x and y are almost the same in all three cases while case-3 is worse in z-deviation. More importantly, amount of deviations in y- and z- directions are significantly increased while x-deviation is slightly changed. These results are as expected because, as shown in both nonlinear and linearized equations, the motion of the tanker acts as a source of disturbance and the magnitude of disturbance increases as the tanker maneuvers more sharply.

Deviation in orientation is also worsened, as compared to the previous tanker-turn case, as shown in Fig. 5.16, especially in bank angle. Figs. 5.17 and 5.18 show the same degradation in both position and orientation deviation in TANKER-CASE-3. Recall,

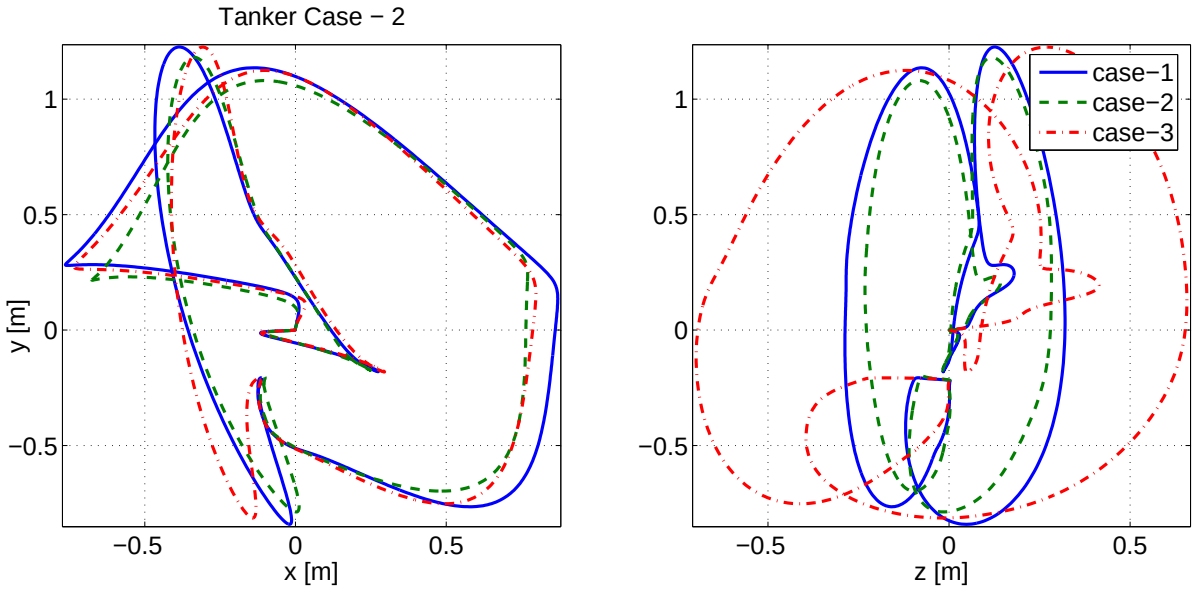

Figure 5.15. Deviation of the receiver position from the refueling position while the tanker turns in TANKER-CASE-2.

however, that while the commanded step change is still 1.7 deg/sec, the rate of change in yaw-rate is higher as a lower order filter is used.

Figures 5.19 to 5.24 are presented to show the comparison between the gain scheduling controller and the linear controller of the nominal condition 2 as summarized in Table 4.1. Further, these figures are used to show the effect of vortex in the performance of the controllers while the tanker turns. In all these figures, the tanker turns according to TANKER-CASE-2 as this is the worst case in terms of the receiver position and orientation deviation.

Figures 5.19 and 5.20 are for control allocation case-1, i.e. combination of thrust vectoring and control effectors are used. Figs. 5.21 and 5.22 are for control allocation case-2, i.e. no thrust vectoring is available. Figs. 5.23 and 5.24 are for control allocation case-3, namely pitch flap and clamshell are fixed. Note that case-1, case-2 and case-3, specified in the legends of each figure, imply (1) gain scheduling controller, (2) linear

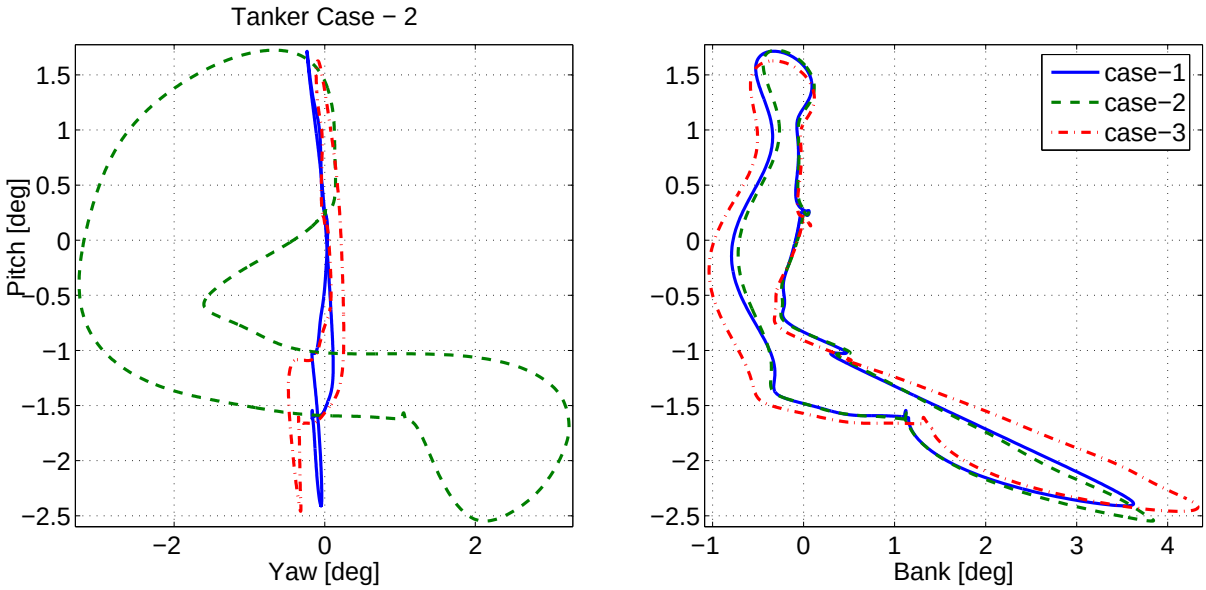

Figure 5.16. Deviation in relative orientation while the tanker turns in TANKER-CASE-2.

controller and (3) gain scheduling controller while the trailing wake vortex is "turned off".

The main observations commonly seen in these figures are as follows. The gain scheduling controller has small improvement over the linear controller. Particularly, in z-direction, the gain scheduling controller results in smaller deviations in all three control-allocation cases (Figs. 5.19, 5.21 and 5.23). Also, the yaw angle deviations in control-allocation cases 2 and 3 (Figs. 5.22 and 5.24) are smaller with gain scheduling. However, note that x-deviation in all three control-allocation cases (Figs. 5.19, 5.21 and 5.23) are larger with gain scheduling in the positive direction while little better in negative direction. In the y-deviation, there is no obvious benefit of gain scheduling. In terms of pitch and bank deviations (Figs. 5.20, 5.22 and 5.24), gain scheduling and linear controllers result in very similar performance.

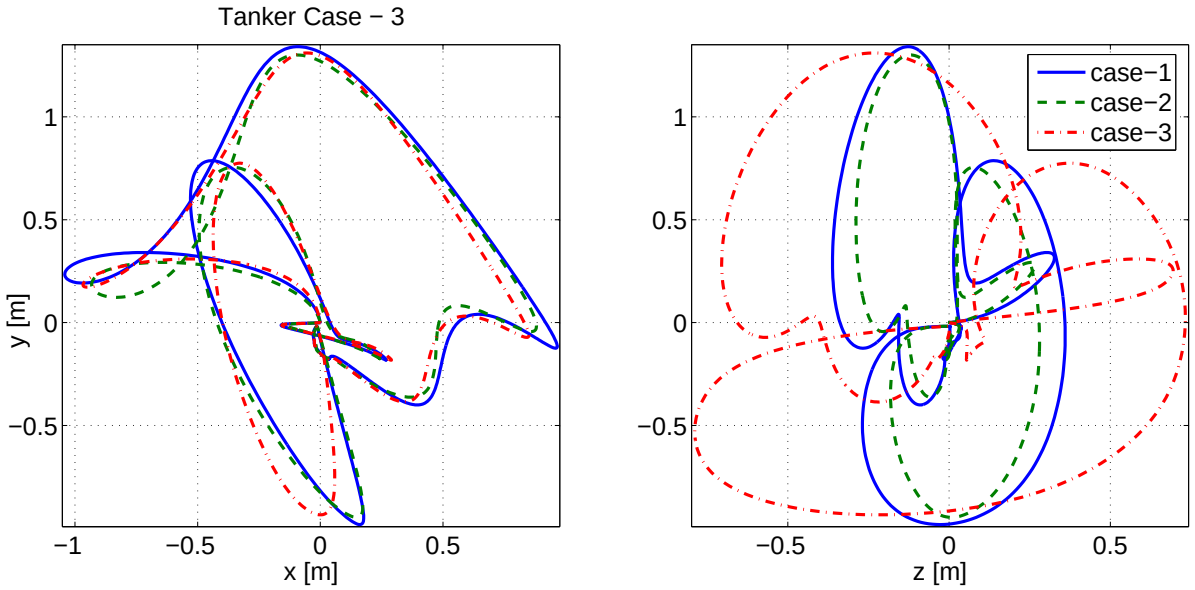

Figure 5.17. Deviation of the receiver position from the refueling position while the tanker turns in TANKER-CASE-3.

When case-1 and case-3 in all figures are compared, i.e., gain scheduling controller used with vortex and without vortex, degradation of performance due to the trailing wake vortex can be clearly seen. In all pitch angle and yaw angle graphs, and pitch angle and bank angle graphs, case 1 and case 3 has same pattern. However case 1 is shifted up compared with case 3 because the wind effect pushes the pitch angle up.

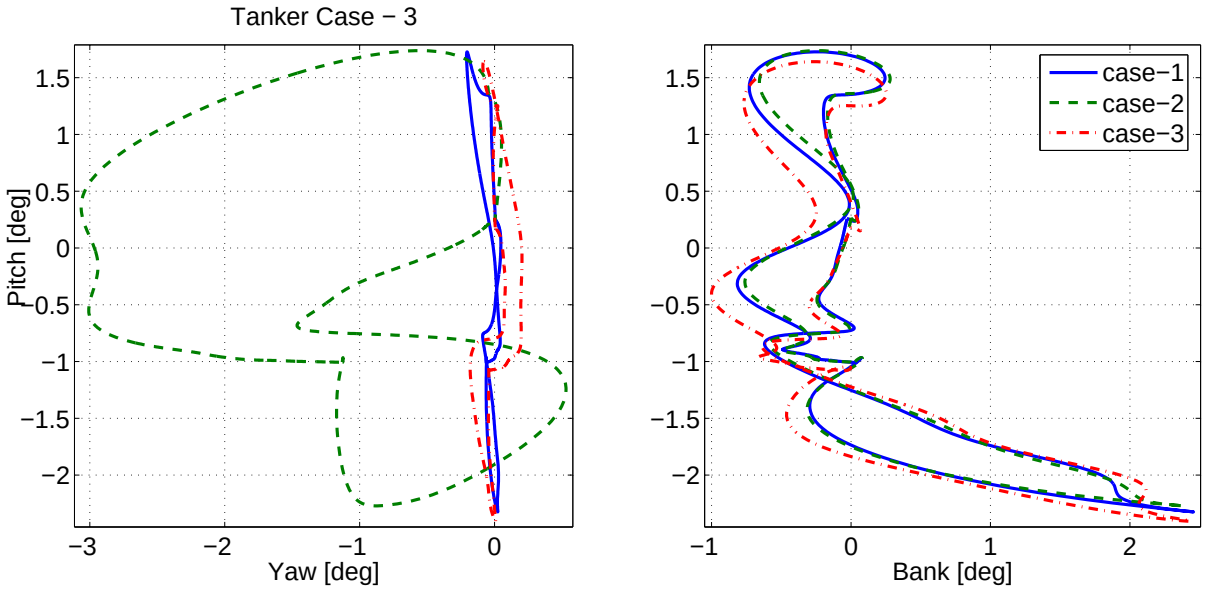

Figure 5.18. Deviation in relative orientation while tanker turns in TANKER-CASE-3.

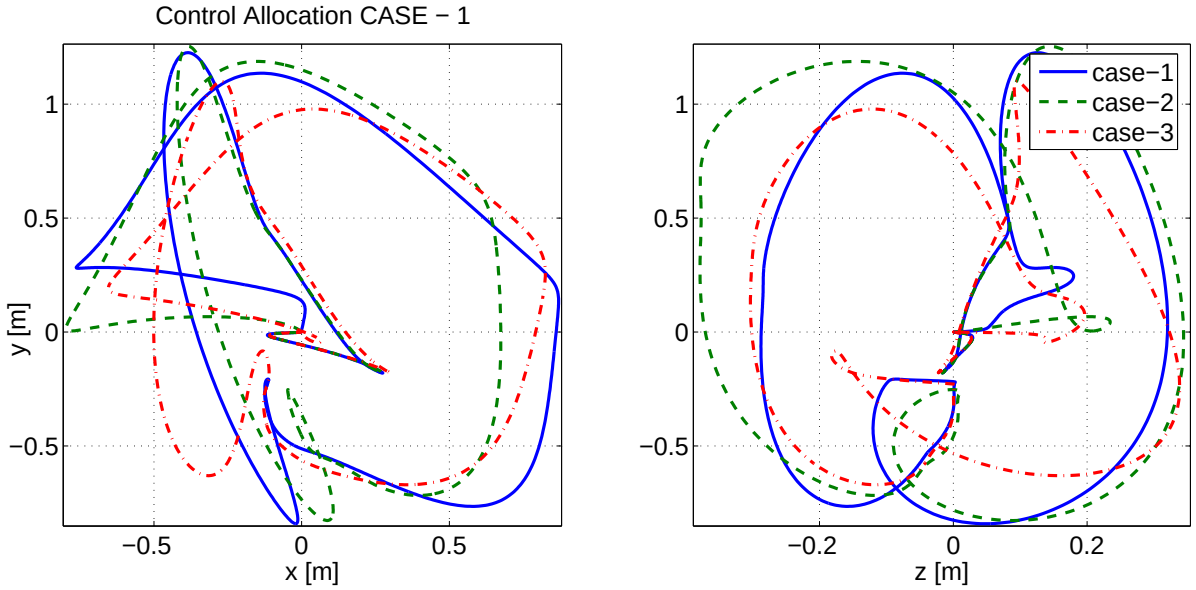

Figure 5.19. Deviation of the receiver position from the refueling position in TANKER-CASE-2.

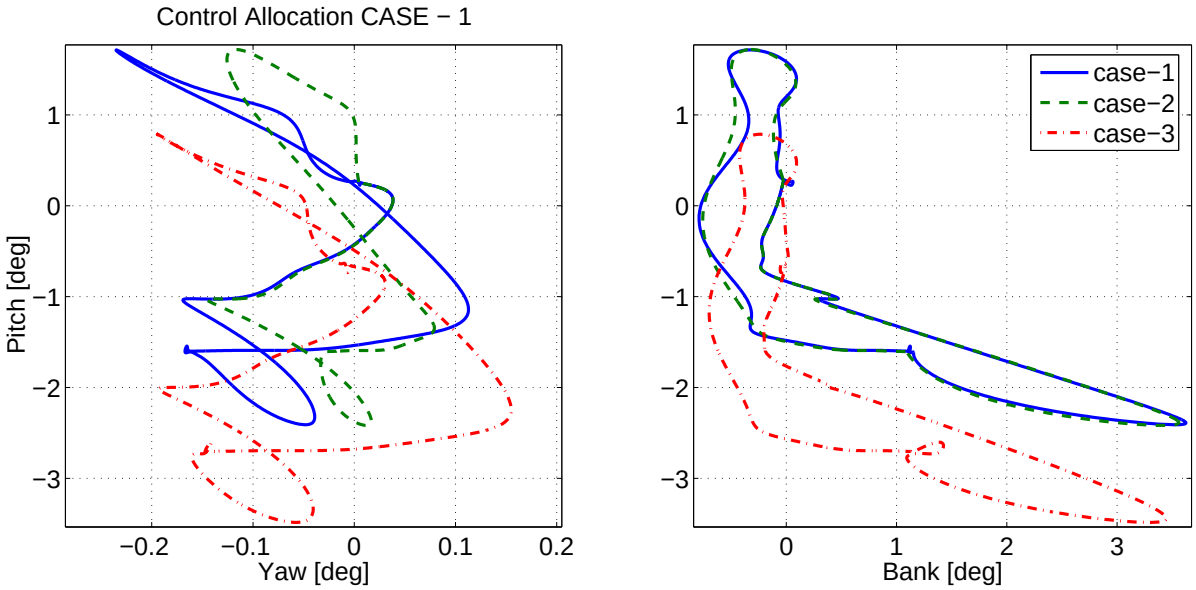

Figure 5.20. Deviation in relative orientation in TANKER-CASE-2.

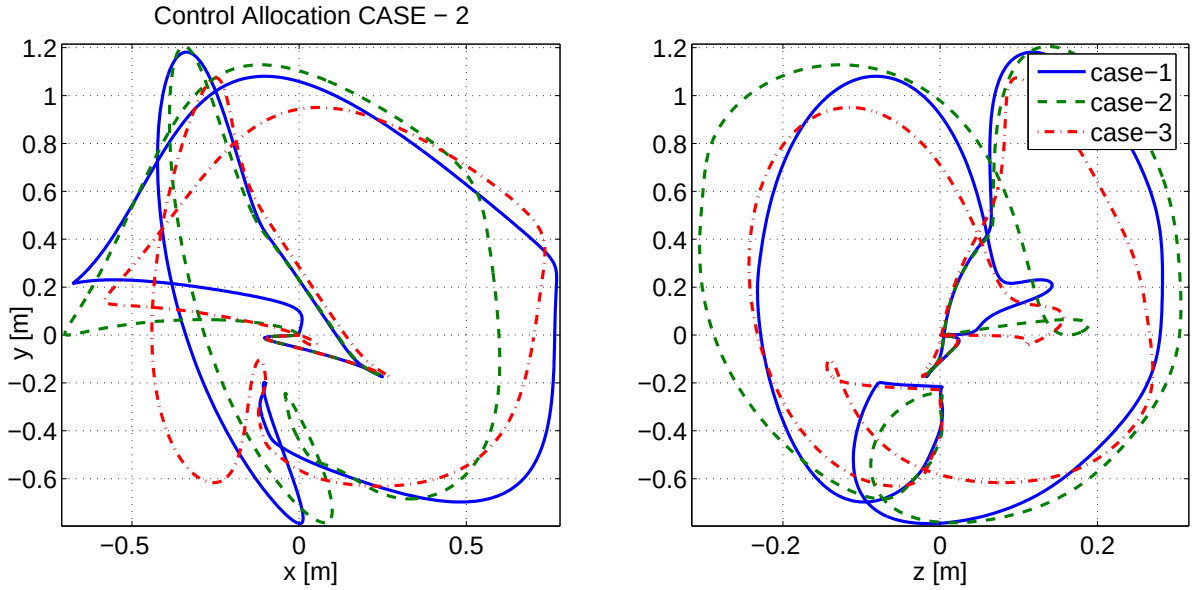

Figure 5.21. Deviation of the receiver position from the refueling position in TANKER-CASE-2.

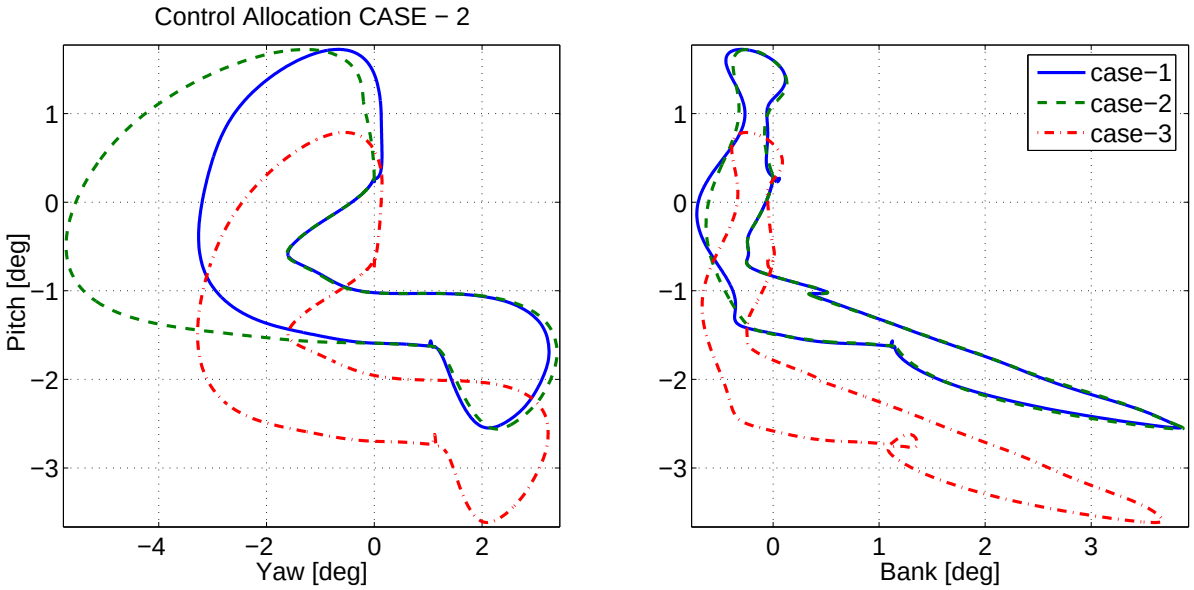

Figure 5.22. Deviation in relative orientation in TANKER-CASE-2.

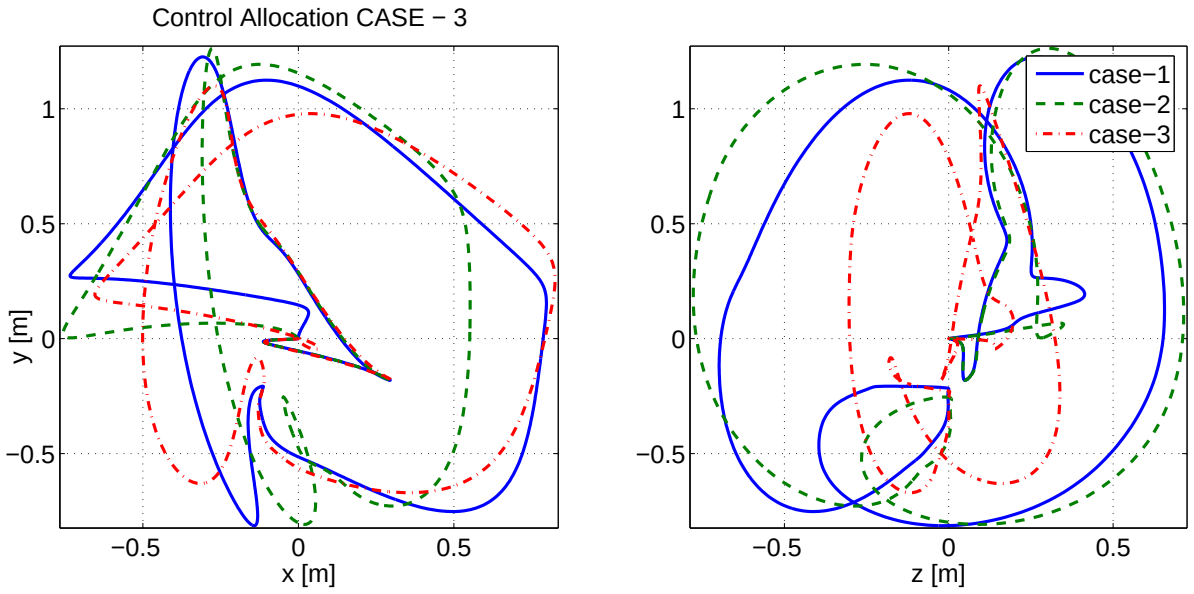

Figure 5.23. Deviation of the receiver position from the refueling position in TANKER-CASE-2.

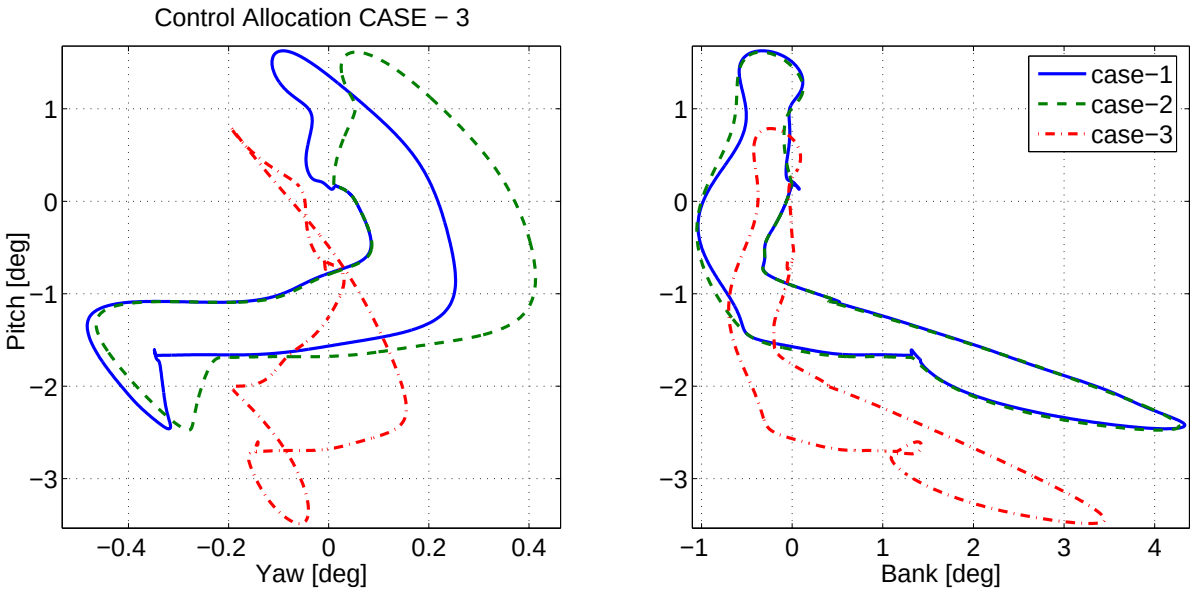

Figure 5.24. Deviation in relative orientation in TANKER-CASE-2.

CHAPTER 6

CONCLUSIONS AND RECOMMENDATION FOR FUTURE WORK

A trajectory tracking controller is designed to control the position and orientation of a receiver aircraft in a boom-receptacle aerial refueling operation. The controller can be used in all three phases of refueling operation by simply issuing an appropriate commanded trajectory: to move the receiver aircraft to the contact position; to keep it there during the fuel transfer; and then to move it away; while the tanker flies in a race-track maneuver. An LQR MIMO state-feedback and integral control method is employed to track the three components of the commanded position of the receiver relative to the tanker in the tanker's body frame. The gains of the controller are scheduled based on the turn rate and speed of the tanker. The tanker-receiver pair modeled and simulated are KC-135R and a tailless fighter aircraft with innovative control effectors (ICE) and thrust vectoring capability. Three versions of the controller are designed and simulated to investigate different control allocation schemes: (i) control effectors and thrust vectoring are simultaneously used, (ii) only control effectors are used and (iii) pitch flap and clamshell are stuck at their nominal values; elevon and thrust vectoring are used.

The performance of the controller is analyzed in an integrated simulation environment with 6-DOF nonlinear receiver and tanker dynamics including the aerodynamic coupling due to the tanker's trailing vortex. Since full 6-DOF nonlinear model of the tanker with its own controller is used in the simulation, the effect of the tanker maneuvers on the relative motion of the receiver is clearly shown. The maneuvering tanker influences the relative motion via two mechanisms: (i) As formulated in the nonlinear

and also the linearized equations, the tanker motion acts as a direct disturbance on the relative motion. For example, when tanker banks, the contact position laterally moves. (ii) The maneuvers of the tanker changes the trailing vortex field that the receiver aircraft is exposed to. For example, when the tanker turns, the velocity vector of the tanker rotates within its body frame, which, in turn, changes the induced wind at the contact position. This means that the receiver aircraft will be exposed to different induced wind when the tanker flies in straight-level than that when the tanker turns even if the receiver can maintain its relative position and orientation.

The equations of motion of the receiver derived previously and used in this study, formulate the motion of the receiver aircraft in terms of position and orientation states that are relative to the tanker aircraft. The linearization of these equations results in the clear manifestation of the tanker motion as disturbance on the relative motion. While not utilized in this paper, this formulation has the potential of improving the station-keeping performance during the tanker turns and will be the subject of future work.

The performance of the three control-allocation schemes are studied in three different race-track maneuvers of the tanker. These maneuvers differ in terms of the yaw rates of the tanker during the turns. In straight-level phase, all three maneuvers are effectively the same. While the tanker flies in straight-level, the controllers move the receiver aircraft from the observation position to the refueling contact position through a commanded trajectory. Simulation results show that all three control-allocation schemes can effectively follow the commanded trajectory without excessive control effort. Simulation results show that when thrust vectoring is not used, the control effector deflections are larger as one would expect. Similarly, when control effectors are stuck, the thrust vectoring is needed more to accomplish the same task. Simulation results also show that by adjusting the weighting matrices, the LQR method can easily provide an effective control allocation between the control effectors and thrust vectoring. When the receiver

moves behind the tanker through the commanded trajectory, the simulation can show how the induced wind components and the gradients vary depending on the position and orientation of the receiver relative to the tanker. Even if the controller are designed based on the linearized equations without the wind terms and thus do not have access to wind information, simulations have shown that all three control allocation can safely follow the commanded trajectory through the wind field.

In the simulations, the tanker starts the turn phase of the race-track maneuvers after the receiver moves to and stays at the contact position. The performances of the three control-allocation schemes in three cases of tanker turns are analyzed based on the phase-portraits of position deviations from the contact position and orientation deviations from the tanker orientation while the tanker starts and completes a full U-turn, and goes back to the straight-level flight. Phase-portrait plots demonstrate that the station-keeping performance while the tanker turns is affected by the rate of turn much more than by the control-allocation scheme used. The tanker turn is quantified by yaw rate of the tanker. The simulation results show that the station-keeping performance degrades more as the tanker-turn sharper. Particularly, variation in yaw-rate rather than the yaw-rate itself (i.e., how fast the tanker goes in and out of a turn) has more influence on the deterioration of the performance, i.e. more deviation in relative position and orientation. A comparative analysis is carried out to see whether the gain scheduling brings any benefit to the performance using the phase-portraits. Instead of scheduling the gains, the gains are kept at their values computed based on the linearized model around the straight-level flight. Comparison of the simulation results reveals that the improvement due to gain scheduling is small. Given the fact that commanded speed and yaw rate for the tanker should be transmitted to the receiver to implement the gain scheduling, linear controller might be considered more favorable. Finally, the effect of wake vortex is clearly shown by comparing simulation results with those generated by

turning off the wind. Both during the maneuver of the receiver to move to the contact position and during the tanker turn, the presence of induced wind and wind gradient increases the deviations of position from the commanded trajectory. As future work, the stochastic turbulence effect on the refueling performance will be studied.

APPENDIX A

NOMINAL CONDITION ANALYSIS FOR TANKER AIRCRAFT

Since the linearization is to be carried out for both steady straight-level flight and turn, the nominal condition analysis is carried out in such a way that both conditions are analyzed by the same formulation. The trimmed steady-state nominal condition is parameterized by V_{T0} and $\dot{\psi}_{T0}$. During the whole racetrack maneuver, the desired side slip angle is 0, and thus $\beta_{T0} = 0$. Airspeed and angle-of-attack are constants, i.e. $V_T = V_{T0}$ and $\alpha_T = \alpha_{T0}$. Further, since the altitude during the whole racetrack maneuver is desired to be constant, $\dot{z}_{T0} = 0$. Note also that for a given steady-state nominal flight condition, regardless whether it is a straight-level flight or turn, angular velocity components are also constants, i.e. $p_T = p_{T0}$, $q_T = q_{T0}$ and $r_T = r_{T0}$. Additionally, pitch and roll angles are constants, i.e. $\theta_T = \theta_{T0}$ and $\phi_T = \phi_{T0}$, and $\dot{\psi}_T = \dot{\psi}_{T0}$. Then the rotational kinematics equations at any nominal conditions yield

$$p_{T0} = -\sin\theta_{T0}\,\dot{\psi}_{T0} \tag{A.1}$$

$$q_{T0} = \sin\phi_{T0}\cos\theta_{T0}\,\dot{\psi}_{T0} \tag{A.2}$$

$$r_{T0} = \cos\phi_{T0}\cos\theta_{T0}\,\dot{\psi}_{T0} \tag{A.3}$$

Then, the translational dynamics equations in Eqs. (2.9) to (2.11) and the constitutive equations in Eqs. (2.12) to (2.19) at a steady-state trimmed flight condition yield.

$$\begin{aligned} 0 &= g\big(\cos\phi_{T0}\cos\theta_{T0}\sin\alpha_{T0} - \cos\alpha_{T0}\cos\theta_{T0}\big) + \frac{1}{m_T}\big[-\frac{1}{2}\rho V_{T0}^2 S_T(C_{D0} \\ &+C_{D\alpha}\alpha_{T0} + C_{D\alpha^2}\alpha_{T0}^2 + C_{D\delta_e}\delta_{e_{T0}}) + T_{T0}\cos(\alpha_{T0}+\delta_T)\big] \end{aligned} \tag{A.4}$$

$$\begin{aligned} 0 &= \cos\phi_{T0}\cos\theta_{T0}\sin\alpha_{T0}\dot{\psi}_{T0} + \sin\theta_{T0}\sin\alpha_{T0}\dot{\psi}_{T0} - \frac{g}{V_{T0}}\cos\theta_{T0}\sin\phi_{T0} \\ &+\frac{1}{2m_T}\rho V_{T0} S_T(C_{S0} + C_{S\delta_r}\delta_{r_{T0}} + C_{S\delta_a}\delta_{a_{T0}}) \end{aligned} \tag{A.5}$$

$$\begin{aligned} 0 &= \sin\phi_{T0}\cos\theta_{T0}\dot{\psi}_{T0} + \frac{g}{V_{T0}}(\cos\alpha_{T0}\cos\phi_{T0}\cos\theta_{T0} + \sin\alpha_{T0}\sin\theta_{T0}) \\ &-\frac{1}{2m_T}\rho V_{T0} S_T(C_{L0} + C_{L\alpha}\alpha_{T0} + C_{L\alpha^2}(\alpha_{T0} - \alpha_{ref}^2) \\ &+C_{Lq}\frac{c}{2V_{T0}}\sin\phi_{T0}\cos\theta_{T0}\dot{\phi}_{T0} + C_{L\delta_e}\delta_{e_{T0}}) - \frac{1}{m_T V_{T0}}T_{T0}\sin(\alpha_{T0}+\delta_T) \end{aligned} \tag{A.6}$$

The rotational dynamics equations in Eqs. (2.27) to (2.29) and the contitutive equations in Eqs. (2.30) to (2.35) yield

$$
\begin{aligned}
0 &= \frac{1}{I_{xx}I_{zz}-I_{xz}^2}\big[-I_{xz}(I_{xx}-I_{yy}+I_{zz})\sin\theta_{T0}\cos\theta_{T0}\sin\phi_{T0}\dot{\psi}_{T0}^2 \\
&+(I_{yy}I_{zz}-I_{zz}^2-I_{xz}^2)\sin\phi_{T0}\cos\phi_{T0}\cos\theta_{T0}^2\dot{\psi}_{T0}^2 \\
&+\frac{1}{2}\rho V_{T0}^2 S_T b_T I_{zz}(C_{\mathcal{L}_0}+C_{\mathcal{L}\delta_a}\delta_{a_{T0}}+C_{\mathcal{L}\delta_r}\delta_{r_{T0}}-C_{\mathcal{L}_p}\frac{b_T}{2V_{T0}}\sin\theta_{T0}\dot{\psi}_{T0} \\
&+C_{\mathcal{L}_r}\frac{b_T}{2V_{T0}}\cos\phi_{T0}\cos\theta_{T0}\dot{\psi}_{T0}) \\
&+\frac{1}{2}\rho V_{T0}^2 S_T b_T I_{xz}(C_{\mathcal{N}_0}+C_{\mathcal{N}\delta_a}\delta_{a_{T0}}+C_{\mathcal{N}\delta_r}\delta_{r_{T0}}-C_{\mathcal{N}_p}\frac{b_T}{2V_{T0}}\sin\theta_{T0}\dot{\psi}_{T0} \\
&+C_{\mathcal{N}_r}\frac{b_T}{2V_{T0}}\cos\phi_{T0}\cos\theta_{T0}\dot{\psi}_{T0})\big]
\end{aligned} \tag{A.7}
$$

$$
\begin{aligned}
0 &= \frac{1}{I_{yy}}\big[(I_{xx}-I_{zz})\sin\theta_{T0}\cos\theta_{T0}\cos\phi_{T0}\dot{\psi}_{T0}^2+I_{xz}\cos\theta_{T0}^2\dot{\psi}_{T0}^2(\cos\phi_{T0}^2-1) \\
&+\frac{1}{2}\rho V_{T0}^2 S_{T0}^2 c(C_{\mathcal{M}0}+C_{\mathcal{M}\alpha}\alpha_{T0}+C_{\mathcal{M}\delta_e}\delta_{e_{T0}}+C_{\mathcal{M}_q}\frac{c}{2V_{T0}}\sin\phi_{T0}\cos\theta_{T0}\dot{\psi}_{T0}) \\
&+\Delta_{z_T}T_{T0}\cos\delta_T+\Delta_{x_T}T_{T0}\sin\delta_T\big]
\end{aligned} \tag{A.8}
$$

$$
\begin{aligned}
0 &= \frac{1}{I_{xx}I_{zz}-I_{xz}^2}\big[-(I_{xx}^2-I_{xx}I_{yy}+I_{xz}^2)\sin\theta_{T0}\cos\theta_{T0}\sin\phi_{T0}\dot{\psi}_{T0}^2 \\
&+I_{xz}(-I_{xx}+I_{yy}-I_{zz})\sin\phi_{T0}\cos\phi_{T0}\cos\theta_{T0}^2\dot{\psi}_{T0}^2 \\
&+\frac{1}{2}\rho V_{T0}^2 S_T b_T I_{xz}(C_{\mathcal{L}_0}+C_{\mathcal{L}\delta_a}\delta_{a_{T0}}+C_{\mathcal{L}\delta_r}\delta_{r_{T0}}-C_{\mathcal{L}_p}\frac{b_T}{2V_{T0}}\sin\theta_{T0}\dot{\psi}_{T0} \\
&+C_{\mathcal{L}_r}\frac{b_T}{2V_{T0}}\cos\phi_{T0}\cos\theta_{T0}\dot{\psi}_{T0}) \\
&+\frac{1}{2}\rho V_{T0}^2 S_T b_T I_{xx}(C_{\mathcal{N}_0}+C_{\mathcal{N}\delta_a}\delta_{a_{T0}}+C_{\mathcal{N}\delta_r}\delta_{r_{T0}}-C_{\mathcal{N}_p}\frac{b_T}{2V_{T0}}\sin\theta_{T0}\dot{\psi}_{T0} \\
&+C_{\mathcal{N}_r}\frac{b_T}{2V_{T0}}\cos\phi_{T0}\cos\theta_{T0}\dot{\psi}_{T0})\big]
\end{aligned} \tag{A.9}
$$

Additionally, since altitude is constant, $\dot{z}_T$ equation in Eq. (2.4) at a steady-state trimmed flight condition yields

$$
0 = \sin\alpha_{T0}\cos\phi_{T0}\cos\theta_{T0}-\cos\alpha_{T0}\sin\theta_{T0} \tag{A.10}
$$

Note that in these seven algebraic equations, there are seven unknowns: α_{T0}, θ_{T0}, ϕ_{T0}, T_{T0}, $\delta_{a_{T0}}, \delta_{e_{T0}}, \delta_{r_{T0}}$. By solving these seven equations, the nominal values of the unknowns

are completed. Further, using Eqs. (A.1), (A.2), and (A.3), the nominal values of the angular velocity components, p_{T0}, q_{T0} and r_{T0}, are calculated.

Note that this nominal condition analysis is parameterized by $\dot{\psi}_{T0}$. That is, if a straight-level flight is to be analyzed, $\dot{\psi}_{T0}$ is set to 0. If a specific turn is to be analyzed, then $\dot{\psi}_{T0}$ is set to the desired turn rate.

APPENDIX B

TANKER'S MATRICES IN THE STATE-SPACE EQUATIONS

Linearization of the tanker's equations of motion is carried out by two steps. The equations of motion in Eqs. (2.9) to (2.11) (translational dynamics), (2.27) to (2.29) (rotational dynamics), Eqs. (2.22) and (2.23) ($\dot{\phi}_T$ and $\dot{\theta}_T$ equations in rotational kinematics) and Eq. (2.4) ($\dot{z}_T$ equation) can be written in compact form as

$$\underline{\dot{x}} = \underline{f}(\underline{x}, \underline{v}) \tag{B.1}$$

where

$$\begin{aligned} \underline{x} &= [V_T\ \beta_T\ \alpha_T\ p_T\ q_T\ r_T\ \theta_T\ \phi_T\ z_T]^T \\ \underline{v} &= [D_T\ S_T\ L_T\ \mathcal{L}_T\ \mathcal{M}_T\ \mathcal{N}_T\ T_T]^T \end{aligned}$$

Note that the constitutive equations in Eqs. (2.12) to (2.19), (2.30) to (2.35), and (2.36) can also be written in compact form as

$$\underline{v} = \underline{g}(\underline{x}, \underline{u}) \tag{B.2}$$

where $\underline{u} = [\delta_{a_T}\ \delta_{e_T}\ \delta_{r_T}\ \xi_T]^T$. Note that in this formulation the first order engine dynamics is not included.

Instead of carrying out the linearization after substituting $\underline{v}$ from (B.2) into (B.1), Eqs. (B.1) and (B.2) are linearized separately. This significantly simplifies the linearization procedure. Further, if the constitutive equations need to be modified for some reason, there would be no need to carry out the whole linearization; only new set of constitutive equations would need to be linearized. The linearization of Eqs. (B.1) and (B.2) yields respectively.

$$\Delta\underline{\dot{x}} = A\ \Delta\underline{x} + B\ \Delta\underline{v} \tag{B.3}$$

$$\Delta\underline{v} = E\ \Delta\underline{x} + F\ \Delta\underline{u} \tag{B.4}$$

substituting $\Delta\underline{v}$ into (B.3) results in the linearized equations of motion for the tanker

$$\Delta\underline{\dot{x}} = A_{T,i}\ \Delta\underline{x} + B_{T,i}\ \Delta\underline{u} \tag{B.5}$$

where index i denotes a specific nominal condition and

$$\begin{aligned} A_{T,i} &= A + BE \\ B_{T,i} &= BF \end{aligned}$$

Note that for nominal conditions specified in Table 4.1, Eq. (B.5) yields Eq. (4.1). In the remainder of this Appendix, matrices A, B, E, and F are presented in detail.

$$\begin{aligned}
A &= a(i,j), A \in \Re^{9\times 9}, i = \{1,...,9\}, j = \{1,...,9\} \\
a(1,1) &= 0 \\
a(1,2) &= g\cos\theta_{T0}\sin\phi_{T0} \\
a(1,3) &= g\cos\phi_{T0}\cos\theta_{T0}\cos\alpha_{T0} + g\sin\alpha_{T0}\sin\theta_{T0} - \tfrac{T_{T0}}{m_T}\sin(\alpha_{T0}+\delta_T) \\
a(1,4:6) &= 0 \\
a(1,7) &= -g\sin\alpha_{T0}\sin\theta_{T0}\cos\phi_{T0} - g\cos\alpha_{T0}\cos\theta_{T0} \\
a(1,8) &= -g\sin\alpha_{T0}\sin\phi_{T0}\cos\theta_{T0} \\
a(1,9) &= 0 \\
a(2,1) &= -\tfrac{g}{V_{T0}^2}\cos\theta_{T0}\sin\phi_{T0} + \tfrac{S_T}{m_T V_{T0}^2} \\
a(2,2) &= -\tfrac{g}{V_{T0}}\cos\phi_{T0}\cos\theta_{T0}\sin\alpha_{T0} + \tfrac{g}{V_{T0}}\sin\theta_{T0}\cos\alpha_{T0} - \tfrac{T_{T0}}{m_T V_{T0}}\cos(\alpha_{T0}+\delta_T) \\
a(2,3) &= r_{T0}\sin\alpha_{T0} + p_{T0}\cos\alpha_{T0} \\
a(2,4) &= \sin\alpha_{T0} \\
a(2,5) &= 0 \\
a(2,6) &= -\cos\alpha_{T0} \\
a(2,7) &= -\tfrac{g}{V_{T0}}\sin\theta_{T0}\sin\phi_{T0} \\
a(2,8) &= \tfrac{g}{V_{T0}}\cos\theta_{T0}\cos\phi_{T0} \\
a(2,9) &= 0 \\
a(3,1) &= q_{T0} \\
a(3,2) &= -p_{T0}\cos\alpha_{T0} - r_{T0}\sin\alpha_{T0}
\end{aligned}$$

$$
\begin{aligned}
a(3,3) &= -\tfrac{g}{V_{T0}}\sin\alpha_{T0}\cos\phi_{T0}\cos\theta_{T0} + \tfrac{g}{V_{T0}}\sin\theta_{T0}\cos\alpha_{T0} - \tfrac{T_{T0}}{m_T V_{T0}}\cos(\alpha_{T0}+\delta_T)\\
a(3,4) &= 0\\
a(3,5) &= 1\\
a(3,6) &= 0\\
a(3,7) &= -\tfrac{g}{V_{T0}}\cos\alpha_{T0}\cos\phi_{T0}\sin\theta_{T0} + \tfrac{g}{V_{T0}}\sin\alpha_{T0}\cos\theta_{T0}\\
a(3,8) &= -\tfrac{g}{V_{T0}}\cos\alpha_{T0}\sin\phi_{T0}\cos\theta_{T0}\\
a(3,9) &= 0\\
a(4,1:3) &= 0\\
a(4,4) &= (I_{xx}-I_{yy}+I_{zz})I_{xz}q_{T0}\tfrac{1}{I_{xx}I_{zz}-I_{xz}^2}\\
a(4,5) &= ((I_{xx}-I_{yy}+I_{zz})I_{xz}p_{T0} + (I_{yy}I_{zz}-I_{zz}^2-I_{xz}^2)r_{T0})\tfrac{1}{I_{xx}I_{zz}-I_{xz}^2}\\
a(4,6) &= (I_{yy}I_{zz}-I_{zz}^2-I_{xz}^2)q_{T0}\tfrac{1}{I_{xx}I_{zz}-I_{xz}^2}\\
a(4,7:9) &= 0\\
a(5,1:3) &= 0\\
a(5,4) &= \tfrac{(I_{zz}-I_{xx})r_{T0}-2I_{xz}p_{T0}}{I_{yy}}\\
a(5,5) &= 0\\
a(5,6) &= \tfrac{(I_{zz}-I_{xx})p_{T0}+2I_{xz}r_{T0}}{I_{yy}}\\
a(5,7:9) &= 0\\
a(6,1:3) &= 0\\
a(6,4) &= \tfrac{(I_{xx}^2-I_{xx}I_{yy}+I_{xz}^2)q_{T0}}{I_{xx}I_{zz}-I_{xz}^2}\\
a(6,5) &= \tfrac{(I_{xx}^2-I_{xx}I_{yy}+I_{xz}^2)p_{T0}+(I_{yy}-I_{xx}-I_{zz})I_{xz}r_{T0}}{I_{xx}I_{zz}-I_{xz}^2}\\
a(6,6) &= \tfrac{(I_{yy}-I_{xx}-I_{zz})I_{xz}q_{T0}}{I_{xx}I_{zz}-I_{xz}^2}\\
a(6,7:9) &= 0\\
a(7,1:4) &= 0\\
a(7,5) &= \cos\phi_{T0}\\
a(7,6) &= -\sin\phi_{T0}
\end{aligned}
$$

$$
\begin{aligned}
a(7,7) &= 0 \\
a(7,8) &= -q_{T0}\sin\phi_{T0} - r_{T0}\cos\phi_{T0} \\
a(7,9) &= 0 \\
a(8,1:3) &= 0 \\
a(8,4) &= 1 \\
a(8,5) &= \sin\phi_{T0}\tan\theta_{T0} \\
a(8,6) &= \cos\phi_{T0}\tan\theta_{T0} \\
a(8,7) &= q_{T0}\sin\phi_{T0}\sec\theta_{T0}^2 + r_{T0}\cos\phi_{T0}\sec\theta_{T0}^2 \\
a(8,8) &= q_{T0}\cos\phi_{T0}\tan\theta_{T0} - r_{T0}\sin\phi_{T0}\tan\theta_{T0} \\
a(8,9) &= 0 \\
a(9,1) &= -\cos\alpha_{T0}\sin\theta_{T0} + \sin\alpha_{T0}\cos\phi_{T0}\cos\theta_{T0} \\
a(9,2) &= V_{T0}\sin\phi_{T0}\cos\theta_{T0} \\
a(9,3) &= V_{T0}\sin\theta_{T0}\sin\alpha_{T0} + V_{T0}\cos\theta_{T0}\cos\phi_{T0}\cos\alpha_{T0} \\
a(9,4:6) &= 0 \\
a(9,7) &= -V_{T0}\cos\alpha_{T0}\cos\theta_{T0} - V_{T0}\sin\alpha_{T0}\cos\phi_{T0}\sin\theta_{T0} \\
a(9,8) &= -V_{T0}\cos\theta_{T0}\sin\alpha_{T0}\sin\phi_{T0} \\
a(9,9) &= 0
\end{aligned}
$$

$$
B = b(i,j), B \in \Re^{9\times 7}, i = \{1,...,9\}, j = \{1,...,7\}
$$

$$
\begin{aligned}
b(1,1) &= -\tfrac{1}{m_T} \\
b(1,2:6) &= 0 \\
b(1,7) &= \tfrac{\cos(\alpha_{T0}+\delta_T)}{m_T} \\
b(2,1) &= 0 \\
b(2,2) &= -\tfrac{1}{m_T V_{T0}} \\
b(2,3:7) &= 0
\end{aligned}
$$

$$
\begin{aligned}
b(3,1:2) &= 0 \\
b(3,3) &= -\frac{1}{m_T V_{T0}} \\
b(3,4:6) &= 0 \\
b(3,7) &= -\frac{\sin(\alpha_{T0}+\delta_T)}{m_T V_{T0}} \\
b(4,1:3) &= 0 \\
b(4,4) &= \frac{I_{zz}}{I_{xx}I_{zz}-I_{xz}^2} \\
b(4,5) &= 0 \\
b(4,6) &= \frac{I_{xz}}{I_{xx}I_{zz}-I_{xz}^2} \\
b(4,7) &= 0 \\
b(5,1:4) &= 0 \\
b(5,5) &= \frac{1}{I_{yy}} \\
b(5,6:7) &= 0 \\
b(6,1:3) &= 0 \\
b(6,4) &= \frac{I_{xz}}{I_{xx}I_{zz}-I_{xz}^2} \\
b(6,5) &= 0 \\
b(6,6) &= \frac{I_{xx}}{I_{xx}I_{zz}-I_{xz}^2} \\
b(6,7) &= 0 \\
b(7,1:7) &= 0 \\
b(8,1:7) &= 0 \\
b(9,1:7) &= 0
\end{aligned}
$$

$$
E = e(i,j), E \in \Re^{7\times 8}, i = \{1,...,7\}, j = \{1,...,8\}
$$

$$
\begin{aligned}
e(1,1) &= \rho V_{T0} S_T (C_{D0} + D_{D\alpha}\alpha_{T0} + C_{D\alpha^2}\alpha_{T0}^2 + C_{C\delta_e}\delta_{e_{T0}}) \\
e(1,2) &= 0 \\
e(1,3) &= \tfrac{1}{2}\rho V_{T0}^2 S_T (C_{D\alpha} + 2\alpha_{T0} C_{D\alpha^2})
\end{aligned}
$$

$$
\begin{aligned}
e(1,4:8) &= 0 \\
e(2,1) &= \rho V_{T0} S_T (C_{S0} + C_{S\delta_r}\delta_{r_{T0}} + C_{S\delta_a}\delta_{a_{T0}}) \\
e(2,2) &= \tfrac{1}{2}\rho V_{T0}^2 S_T C_{S\beta} \\
e(2,3:8) &= 0 \\
e(3,1) &= \rho V_{T0} S_T (C_{L0} + C_{L\alpha}\alpha_{T0} + C_{L\alpha^2}(\alpha_{T0} - \alpha_{ref})^2 + C_{L\delta_e}\delta_{e_{T0}} + C_{Lq}\tfrac{c}{4V_{T0}} q_{T0}) \\
e(3,2) &= 0 \\
e(3,3) &= \tfrac{1}{2}\rho V_{T0}^2 S_T (C_{L\alpha} + 2C_{L\alpha^2}(\alpha_{T0} - \alpha_{ref})) \\
e(3,4) &= 0 \\
e(3,5) &= \tfrac{c}{4}\rho V_{T0} S_T C_{Lq} \\
e(3,6:8) &= 0 \\
e(4,1) &= \rho V_{T0} S_T b_T (C_{\mathcal{L}0} + C_{\mathcal{L}\delta_a}\delta_{a_{T0}} + C_{\mathcal{L}\delta_r}\delta_{r_{T0}} + \tfrac{b}{8V_{T0}} C_{\mathcal{L}p} p_{T0} + \tfrac{b}{8V_{T0}} C_{\mathcal{L}r} r_{T0}) \\
e(4,2) &= \tfrac{1}{2}\rho V_{T0}^2 S_T b_T C_{\mathcal{L}\beta} \\
e(4,3) &= 0 \\
e(4,4) &= \tfrac{1}{4}\rho V_{T0} S_T b_T^2 C_{\mathcal{L}p} \\
e(4,5) &= 0 \\
e(4,6) &= \tfrac{1}{4}\rho V_{T0} S_T b_T^2 C_{\mathcal{L}r} \\
e(4,7:8) &= 0 \\
e(5,1) &= \rho V_{T0} S_T c_T (C_{\mathcal{M}0} + C_{\mathcal{M}\alpha}\alpha_{T0} + C_{\mathcal{M}\delta_e}\delta_{e_{T0}} + C_{\mathcal{M}q}\tfrac{c}{4V_{T0}} q_{T0}) \\
e(5,2) &= 0 \\
e(5,3) &= \tfrac{1}{2}\rho V_{T0}^2 S_T c_T C_{\mathcal{M}\alpha} \\
e(5,4) &= 0 \\
e(5,5) &= \tfrac{1}{4}\rho V_{T0} S_T c_T^2 C_{\mathcal{M}q} \\
e(5,6:8) &= 0 \\
e(6,1) &= \rho V_{T0} S_T b_T (C_{\mathcal{N}0} + C_{\mathcal{N}\delta_a}\delta_{a_{T0}} + C_{\mathcal{N}\delta_r}\delta_{r_{T0}} + \tfrac{b}{4V_{T0}} C_{\mathcal{N}p} p_{T0} + \tfrac{b}{4V_{T0}} C_{\mathcal{N}r} r_{T0}) \\
e(6,2) &= \tfrac{1}{2}\rho V_{T0}^2 S_T b_T C_{\mathcal{N}\beta}
\end{aligned}
$$

$$
\begin{aligned}
e(6,3) &= 0 \\
e(6,4) &= \tfrac{1}{4}\rho V_{T0} S_T b_T^2 C_{\mathcal{N}p} \\
e(6,5) &= 0 \\
e(6,6) &= \tfrac{1}{4}\rho V_{T0} S_T b_T^2 C_{\mathcal{N}r} \\
e(6,7:8) &= 0 \\
e(7,1:8) &= 0
\end{aligned}
$$

$$
F = f(i,j), F \in \Re^{7\times 4}, i = \{1,...,7\}, j = \{1,...,4\}
$$

$$
\begin{aligned}
f(1,1) &= 0 \\
f(1,2) &= \tfrac{1}{2}\rho V_{T0}^2 S_T C_{D\delta_e} \\
f(1,3:4) &= 0 \\
f(2,1) &= \tfrac{1}{2}\rho V_{T0}^2 S_T C_{S\delta_a} \\
f(2,2) &= 0 \\
f(2,3) &= \tfrac{1}{2}\rho V_{T0}^2 S_T C_{S\delta_r} \\
f(2,4) &= 0 \\
f(3,1) &= 0 \\
f(3,2) &= \tfrac{1}{2}\rho V_{T0}^2 S_T C_{L\delta_e} \\
f(3,3:4) &= 0 \\
f(4,1) &= \tfrac{1}{2}\rho V_{T0}^2 S_T b_T C_{\mathcal{L}\delta_a} \\
f(4,2) &= 0 \\
f(4,3) &= \tfrac{1}{2}\rho V_{T0} S_T b_T^2 C_{\mathcal{L}\delta_r} \\
f(4,4) &= 0 \\
f(5,1) &= 0 \\
f(5,2) &= \tfrac{1}{2}\rho V_{T0}^2 S_T c_T C_{\mathcal{M}\delta_e} \\
f(5,3) &= 0
\end{aligned}
$$

$$
\begin{aligned}
f(5,4) &= T_{max_T}(\Delta_{z_T 0}\cos\delta_{T0} + \Delta_{x_T 0}\sin\delta_{T0}) \\
f(6,1) &= \tfrac{1}{2}\rho V_{T0}^2 S_T b_T C_{\mathcal{N}\delta_a} \\
f(6,2) &= 0 \\
f(6,3) &= \tfrac{1}{2}\rho V_{T0}^2 S_T b_T C_{\mathcal{N}\delta_r} \\
f(6,4) &= 0 \\
f(7,1:3) &= 0 \\
f(7,4) &= T_{max_T}
\end{aligned}
$$

APPENDIX C

NOMINAL CONDITION ANALYSIS FOR RECEIVER AIRCRAFT

In aerial refueling operation, the receiver aircraft should maintain its position and orientation relative to the tanker aircraft. Thus, the nominal conditions for the receiver should be closely related to the nominal conditions of the tanker. Recall that the presence of the wake induced wind acting on the receiver is ignored during the linearization procedure. Further, note that the seven algebraic equations derived for the nominal condition analysis of the tanker, in Appendix A, are valid for any other aircraft. Since the objective is to maintain relative position and orientation, translational and angular velocity components of the receiver should be same as those of the tanker. Thus, for nominal condition analysis; $V_0 = V_{T0}, p_0 = p_{T0}, q_0 = q_{T0}$ and $r_0 = r_{T0}$. Further, yaw rates of the tanker and the receiver should be the same, i.e., $\dot{\psi}_0 = \dot{\psi}_{T0}$. Similar to tanker, side slip angle of the receiver at the nominal conditions is set to zero, i.e., $\beta_0 = 0$. Also, the receiver maintains its altitude, i.e., $\dot{z}_0 = 0$. At nominal conditions, the thrust vectoring angles are prefered to be zero, i.e. $\delta_{y0} = 0$ and $\delta_{z0} = 0$. Thus, the same set of algebraic equations, in Appendix A, is used for determining the nominal values of other states and control variables, using the receiver aircraft data. As in the case of the tanker analysis, the seven algebraic equations are solved for $\alpha_0, \theta_{0,I}, \phi_{0,I}, T_0, \delta_{a0}, \delta_{e0}, \delta_{r0}$. Note that $\theta_{0,I}$ and $\phi_{0,I}$ are the Euler angles of the receiver aircraft relative to the inertial frame since the equations used are based on the equations of motion relative to the inertial frame. Recall that in the equations of motion of the receiver aircraft, Euler angles are the parameterization of the receiver aircraft relative to the tanker. While all the other nominal values are directly applicable, the relative Euler angles need to be computed. Note that

$$\mathbf{R_{B_R I}} = \mathbf{R_{B_R B_T} R_{B_T I}} \tag{C.1}$$

where $\mathbf{R_{B_R I}}$ is the rotation matrix from the inertial frame to the receiver's body frame, $\mathbf{R_{B_R B_T}}$ is the rotation matrix from the tanker's body frame to the receiver's body frame,

and $\mathbf{R_{B_TI}}$ is the rotation matrix from the inertial frame to the tanker's body frame. Eq. (C.1) can be written in terms of 3-2-1 Euler angles,

$$R(\psi_I, \theta_I, \phi_I) = R(\psi, \theta, \phi)R(\psi_T, \theta_T, \phi_T) \tag{C.2}$$

where $(\psi_I, \theta_I, \phi_I)$ are the Euler angles of the receiver relative to the inertial frame, (ψ, θ, ϕ) are the Euler angles of the receiver relative to the tanker's body frame and $(\psi_T, \theta_T, \phi_T)$ are the Euler angles of the tanker relative to the inertial frame. At the nominal conditions, set the relative yaw angle to zero, i.e. $\psi_0 = 0$. Note that this is justified by the fact that both receiver and the tanker turn at the same yaw rate at the nominal conditions. Rewriting Eq. (C.2) at the nominal conditions yield

$$R(\psi_{0,I}(t), \theta_{0,I}, \phi_{0,I}) = R(0, \theta_0, \phi_0)R(\psi_{T0}(t), \theta_{T0}, \phi_{T0}) \tag{C.3}$$

where there are only two unknowns, θ_0 and ϕ_0. To solve for these two unknowns, the 1^{st} raw and 3^{rd} column entries of the left and right sides yield the first equation

$$-\sin\theta_{0,I} = -\cos\theta_0 \sin\theta_{T0} - \sin\theta_0 \cos\phi_{T0} \cos\theta_{T0} \tag{C.4}$$

The 2^{nd} raw and 3^{rd} column entries of the left and right sides gives the second equation

$$\begin{aligned} \sin\phi_{0,I} \cos\theta_{0,I} = & -\sin\phi_0 \sin\theta_0 \sin\theta_{T0} + \cos\phi_0 \sin\phi_{T0} \cos\theta_{T0} \\ & + \sin\phi_0 \cos\theta_0 \cos\phi_{T0} \cos\theta_{T0} \end{aligned} \tag{C.5}$$

These two equations are solved for the unknowns θ_0 and ϕ_0.

APPENDIX D

RECEIVER'S MATRICES IN THE STATE-SPACE EQUATIONS

Linearization of the receiver equations of motion is also carried out by two steps as was done for the tanker. Equations of motion in Eqs. (3.15) to (3.17) (translational dynamics), (3.31) to (3.33) (rotational dynamics), (3.20) to (3.22) (rotational kinematics) and (3.2) (3.4) (translational kinematics) are written in compact form as

$$\underline{\dot{x}} = \underline{f}(\underline{x}, \underline{v}, \underline{w}) \tag{D.1}$$

where

$$\begin{aligned} \underline{x} &= [V\ \beta\ \alpha\ p\ q\ r\ \psi\ \theta\ \phi\ x\ y\ z]^T \\ \underline{v} &= [D\ S\ L\ \mathcal{L}\ \mathcal{M}\ \mathcal{N}\ T_x\ T_y\ T_z]^T \\ \underline{w} &= [V_{xT}\ V_{yT}\ V_{zT}\ \psi_T\ \theta_T\ \phi_T\ p_T\ q_T\ r_T\ \dot{p}_T\ \dot{q}_T\ \dot{r}_T]^T \end{aligned}$$

The constitutive equations in Eqs. (3.9) to (3.14), (3.25) to (3.30), (3.8) to (3.9) and the thrust as the product of maximum thrust available and throttle setting (ξ) can also be written in compact form as

$$\underline{v} = \underline{g}(\underline{x}, \underline{u}, \underline{w}) \tag{D.2}$$

where

$$\underline{u} = [\delta_a\ \delta_e\ \delta_r\ \xi\ \delta_y\ \delta_z]^T$$

The linearization of Eqs. (D.1) and (D.2) yields respectively

$$\Delta\underline{\dot{x}} = A\,\underline{x} + B\,\underline{v} + H\,\underline{w} \tag{D.3}$$

$$\underline{v} = E\,\underline{x} + F\,\underline{u} + G\,\underline{w} \tag{D.4}$$

Substituting Δv into Eqs. (D.3) results in the linearized equations of motion for the receiver

$$\Delta\underline{\dot{x}} = A_i\,\Delta\underline{x} + B_i\,\underline{u} + H_i\,\underline{w} \tag{D.5}$$

where index i denotes a specific nominal condition, and

$$\begin{aligned} A_i &= A + BE \\ B_i &= BF \\ H_i &= BG + H \end{aligned}$$

Note that for nominal conditions specified in Table 4.1, Eq. (D.5) yields Eq. (4.11). In the remainder of this Appendix, matrices A, B, H, E, F and G are presented in detail.

$$\begin{aligned}
A &= a(i,j), A \in \Re^{12\times 12}, i = \{1,...,12\}, j = \{1,...,12\} \\
a(1,1) &= 0 \\
a(1,2) &= g\sin\phi_{T0}\cos\theta_{T0} + \tfrac{T_{y0}}{m_R} \\
a(1,3) &= g\sin\theta_{T0}\sin\alpha_0 + g\cos\phi_{T0}\cos\theta_{T0}\cos\alpha_0 - \tfrac{(T_{x0}\sin\alpha_0 + T_{z0}\cos\alpha_0)}{m_R} \\
a(1,4:6) &= 0 \\
a(1,7) &= g\sin\phi_{T0}\cos\alpha_0\cos\theta_{T0} \\
a(1,8) &= -g(\cos\phi_{T0}\cos\theta_{T0}\cos\alpha_0 + \sin\theta_{T0}\sin\alpha_0) \\
a(1,9) &= -g\sin\phi_{T0}\cos\theta_{T0}\sin\alpha_0 \\
a(1,10:12) &= 0 \\
a(2,1) &= -\tfrac{r_{T0}}{V_0}\cos\alpha_0 + \tfrac{p_{T0}}{V_0}\sin\alpha_0 \\
a(2,2) &= \tfrac{g}{V_0}(\sin\theta_{T0}\cos\alpha_0 - \cos\phi_{T0}\cos\theta_{T0}\sin\alpha_0) \\
&\quad -\tfrac{1}{m_R V_0}(T_{x0}\cos\alpha_0 + T_{z0}\sin\alpha_0) \\
a(2,3) &= r_{T0}\sin\alpha_0 + P_{T0}\cos\alpha_0 \\
a(2,4) &= \sin\alpha_0 \\
a(2,5) &= 0 \\
a(2,6) &= -\cos\alpha_0 \\
a(2,7) &= q_{T0}\sin\alpha_0 + \tfrac{g}{V_0}\sin\theta_{T0} \\
a(2,8) &= -p_{T0}\cos\alpha_0 - r_{T0}\sin\alpha_0
\end{aligned}$$

$$
\begin{aligned}
a(2,9) &= \tfrac{g}{V_0}\cos\phi_{T0}\cos\theta_{T0} + q_{T0}\cos\alpha_0 \\
a(2,10:12) &= 0 \\
a(3,1) &= \tfrac{q_{T0}}{V_0} \\
a(3,2) &= -r_{T0}\sin\alpha_0 - p_{T0}\cos\alpha_0 \\
a(3,3) &= \tfrac{g}{V_0}(\sin\theta_{T0}\cos\alpha_0 - \cos\phi_{T0}\cos\theta_{T0}\sin\alpha_0) \\
&\quad -\tfrac{1}{m_R V_0}(T_{x0}\cos\alpha_0 + T_{z0}\sin\alpha_0) \\
a(3,4) &= 0 \\
a(3,5) &= 1 \\
a(3,6) &= 0 \\
a(3,7) &= -p_{T0} - \tfrac{g}{V_0}\sin\phi_{T0}\cos\theta_{T0}\sin\alpha_0 \\
a(3,8) &= \tfrac{g}{V_0}(\cos\phi_{T0}\cos\theta_{T0}\sin\alpha_0 - \sin\theta_{T0}\cos\alpha_0) \\
a(3,9) &= r_{T0} - \tfrac{g}{V_0}\sin\phi_{T0}\cos\theta_{T0}\cos\alpha_0 \\
a(3,10:12) &= 0 \\
a(4,1:3) &= 0 \\
a(4,4) &= \tfrac{(I_{xx}-I_{yy}+I_{zz})I_{xz}q_{T0}}{I_{xx}I_{zz}-I_{xz}^2} \\
a(4,5) &= \tfrac{I_{zz}I_{yy}-I_{zz}^2-I_{xz}^2}{I_{xx}I_{zz}-I_{xz}^2}r_{T0} + \tfrac{I_{xx}-I_{yy}+I_{zz}}{I_{xx}I_{zz}-I_{xz}^2}I_{xz}p_{T0} + r_{T0} \\
a(4,6) &= \tfrac{I_{yy}I_{zz}-I_{zz}^2-I_{xz}^2}{I_{xx}I_{zz}-I_{xz}^2}q_{T0} - q_{T0} \\
a(4,7) &= \tfrac{I_{yy}I_{zz}-I_{zz}^2-I_{xz}^2}{I_{xx}I_{zz}-I_{xz}^2}(-p_{T0}r_{T0}) + \tfrac{I_{yy}-I_{xx}-I_{zz}}{I_{xx}I_{zz}-I_{xz}^2}I_{xz}(p_{T0}^2 - q_{T0}^2) \\
a(4,8) &= \tfrac{I_{yy}I_{zz}-I_{zz}^2-I_{xz}^2}{I_{xx}I_{zz}-I_{xz}^2}p_{T0}q_{T0} + \tfrac{I_{yy}-I_{xx}-I_{zz}}{I_{xx}I_{zz}-I_{xz}^2}I_{xz}q_{T0}r_{T0} \\
a(4,9) &= \tfrac{I_{yy}I_{zz}-I_{zz}^2-I_{xz}^2}{I_{xx}I_{zz}-I_{xz}^2}(-q_{T0}^2 + r_{T0}^2) + \tfrac{I_{xx}-I_{yy}+I_{zz}}{I_{xx}I_{zz}-I_{xz}^2}I_{xz}p_{T0}r_{T0} \\
a(4,10:12) &= 0 \\
a(5,1:3) &= 0 \\
a(5,4) &= -2\tfrac{I_{xz}}{I_{yy}}p_{T0} + \tfrac{I_{zz}-I_{xx}}{I_{yy}}r_{T0} - r_{T0} \\
a(5,5) &= 0 \\
a(5,6) &= 2\tfrac{I_{xz}}{I_{yy}}r_{T0} + \tfrac{I_{zz}-I_{xx}}{I_{yy}}p_{T0} + p_{T0}
\end{aligned}
$$

$$
\begin{aligned}
a(5,7) &= -2\tfrac{I_{xz}}{I_{yy}} p_{T0} q_{T0} + \tfrac{I_{zz}-I_{xx}}{I_{yy}} r_{T0} q_{T0} \\
a(5,8) &= 4\tfrac{I_{xz}}{I_{yy}} r_{T0} p_{T0} + \tfrac{I_{zz}-I_{xx}}{I_{yy}} (-r_{T0}^2 + p_{T0}^2) \\
a(5,9) &= 2\tfrac{I_{xz}}{I_{yy}} r_{T0} q_{T0} - \tfrac{I_{zz}-I_{xx}}{I_{yy}} p_{T0} q_{T0} \\
a(5,10:12) &= 0 \\
a(6,1:3) &= 0 \\
a(6,4) &= \tfrac{I_{xx}^2 - I_{xx} I_{yy} + I_{xz}^2}{I_{xx} I_{zz} - I_{xz}^2} q_{T0} + q_{T0} \\
a(6,5) &= \tfrac{I_{yy}-I_{xx}-I_{zz}}{I_{xx} I_{zz} - I_{xz}^2} I_{xz} r_{T0} + \tfrac{I_{xx}^2 - I_{xx} I_{yy} + I_{xz}^2}{I_{xx} I_{zz} - I_{xz}^2} p_{T0} - p_{T0} \\
a(6,6) &= \tfrac{I_{yy}-I_{xx}-I_{zz}}{I_{xx} I_{zz} - I_{xz}^2} I_{xz} q_{T0} \\
a(6,7) &= \tfrac{I_{xx}-I_{yy}+I_{zz}}{I_{xx} I_{zz} - I_{xz}^2} I_{xz} p_{T0} r_{T0} + \tfrac{I_{xx}^2 - I_{xx} I_{yy} + I_{xz}^2}{I_{xx} I_{zz} - I_{xz}^2} (q_{T0}^2 - p_{T0}^2) \\
a(6,8) &= \tfrac{I_{yy}-I_{xx}-I_{zz}}{I_{xx} I_{zz} - I_{xz}^2} I_{xz} p_{T0} q_{T0} + \tfrac{I_{xx}^2 - I_{xx} I_{yy} + I_{xz}^2}{I_{xx} I_{zz} - I_{xz}^2} (-q_{T0} r_{T0}) \\
a(6,9) &= \tfrac{I_{yy}-I_{xx}-I_{zz}}{I_{xx} I_{zz} - I_{xz}^2} I_{xz} (-q_{T0}^2 + r_{T0}^2) + \tfrac{I_{xx}^2 - I_{xx} I_{yy} + I_{xz}^2}{I_{xx} I_{zz} - I_{xz}^2} p_{T0} r_{T0} \\
a(6,10:12) &= 0 \\
a(7,1:5) &= 0 \\
a(7,6) &= 1 \\
a(7,7:12) &= 0 \\
a(8,1:4) &= 0 \\
a(8,5) &= 1 \\
a(8,6:12) &= 0 \\
a(9,1:3) &= 0 \\
a(9,4) &= 1 \\
a(9,5:12) &= 0 \\
a(10,1) &= \cos\alpha_0 \\
a(10,2) &= 0 \\
a(10,3) &= -V_0 \sin\alpha_0 \\
a(10,4:7) &= 0
\end{aligned}
$$

$$
\begin{aligned}
a(10,8) &= V_0 \sin\alpha_0 \\
a(10,9:10) &= 0 \\
a(10,11) &= r_{T0} \\
a(10,12) &= -q_{T0} \\
a(11,1) &= 0 \\
a(11,2) &= V_0 \\
a(11,3:6) &= 0 \\
a(11,7) &= V_0 \cos\alpha_0 \\
a(11,8) &= 0 \\
a(11,9) &= -V_0 \sin\alpha_0 \\
a(11,10) &= -r_{T0} \\
a(11,11) &= 0 \\
a(11,12) &= p_{T0} \\
a(12,1) &= \sin\alpha_0 \\
a(12,2) &= 0 \\
a(12,3) &= V_0 \cos\alpha_0 \\
a(12,4:7) &= 0 \\
a(12,8) &= -V_0 \cos\alpha_0 \\
a(12,9) &= 0 \\
a(12,10) &= q_{T0} \\
a(12,11) &= -p_{T0} \\
a(12,12) &= 0
\end{aligned}
$$

$$
B = b(i,j), B \in \Re^{12\times 9}, i = \{1,...,12\}, j = \{1,...,9\}
$$

$$
b(1,1) = -\frac{1}{m_R}
$$

$$
\begin{aligned}
b(1,2:6) &= 0 \\
b(1,7) &= \tfrac{1}{m_R}\cos\alpha_0 \\
b(1,8) &= 0 \\
b(1,9) &= \tfrac{1}{m_R}\sin\alpha_0 \\
b(2,1) &= 0 \\
b(2,2) &= -\tfrac{1}{m_R V_0} \\
b(2,3:7) &= 0 \\
b(2,8) &= \tfrac{1}{m_R V_0} \\
b(2,9) &= 0 \\
b(3,1:2) &= 0 \\
b(3,3) &= -\tfrac{1}{m_R V_0} \\
b(3,4:6) &= 0 \\
b(3,7) &= -\tfrac{1}{m_R V_0}\sin\alpha_0 \\
b(3,8) &= 0 \\
b(3,9) &= \tfrac{1}{m_R V_0}\cos\alpha_0 \\
b(4,1:3) &= 0 \\
b(4,4) &= \tfrac{I_{zz}}{I_{xx}I_{zz}-I_{xz}^2} \\
b(4,5) &= 0 \\
b(4,6) &= \tfrac{I_{xz}}{I_{xx}I_{zz}-I_{xz}^2} \\
b(4,7:9) &= 0 \\
b(5,1:4) &= 0 \\
b(5,5) &= \tfrac{1}{I_{yy}} \\
b(5,6:9) &= 0 \\
b(6,1:3) &= 0 \\
b(6,4) &= \tfrac{I_{xz}}{I_{xx}I_{zz}-I_{xz}^2}
\end{aligned}
$$

$$
\begin{aligned}
b(6,5) &= 0 \\
b(6,6) &= \tfrac{I_{xx}}{I_{xx}I_{zz}-I_{xz}^2} \\
b(6,7:9) &= 0 \\
b(7,1:9) &= 0 \\
b(8,1:9) &= 0 \\
b(9,1:9) &= 0 \\
b(10,1:9) &= 0 \\
b(11,1:9) &= 0 \\
b(12,1:9) &= 0
\end{aligned}
$$

$$
H = h(i,j), H \in \Re^{12\times 12}, i = \{1,...,12\}, j = \{1,...,12\}
$$

$$
\begin{aligned}
h(1,10) &= 0 \\
h(1,11) &= -g(\cos\theta_{T0}\cos\alpha_0 + \cos\phi_{T0}\sin\theta_{T0}\sin\alpha_0) \\
h(1,12) &= -g(\sin\phi_{T0}\cos\theta_{T0}\sin\alpha_0) \\
h(2,1:3) &= 0 \\
h(2,4) &= \sin\alpha_0 \\
h(2,5) &= 0 \\
h(2,6) &= -\cos\alpha_0 \\
h(2,7:10) &= 0 \\
h(2,11) &= -\tfrac{g}{V_0}\sin\phi_{T0}\sin\theta_{T0} \\
h(2,12) &= \tfrac{g}{V_0}\cos\theta_{T0}\cos\phi_{T0} \\
h(3,1:4) &= 0 \\
h(3,5) &= 1 \\
h(3,6:10) &= 0 \\
h(3,11) &= \tfrac{g}{V_0}(\sin\alpha_0\cos\theta_{T0} - \cos\alpha_0\cos\phi_{T0}\sin\theta_{T0})
\end{aligned}
$$

$$
\begin{aligned}
h(3,12) &= -\tfrac{g}{V_0}\cos\alpha_0\cos\theta_{T0}\sin\phi_{T0} \\
h(4,1:3) &= 0 \\
h(4,4) &= \tfrac{I_{xx}-I_{yy}+I_{zz}}{I_{xx}I_{zz}-I_{xz}^2}I_{xz}q_{T0} \\
h(4,5) &= \tfrac{I_{yy}I_{zz}-I_{zz}^2-I_{xz}^2}{I_{xx}I_{zz}-I_{xz}^2}r_{T0} + \tfrac{I_{xx}-I_{yy}+I_{zz}}{I_{xx}I_{zz}-I_{xz}^2}I_{xz}p_{T0} \\
h(4,6) &= \tfrac{I_{yy}I_{zz}-I_{zz}^2-I_{xz}^2}{I_{xx}I_{zz}-I_{xz}^2}q_{T0} \\
h(4,7) &= \text{-1} \\
h(4,8:12) &= 0 \\
h(5,1:3) &= 0 \\
h(5,4) &= -2\tfrac{I_{xz}}{I_{yy}}p_{T0} + \tfrac{I_{zz}-I_{xx}}{I_{yy}}r_{T0} \\
h(5,5) &= 0 \\
h(5,6) &= 2\tfrac{I_{xz}}{I_{yy}}r_{T0} + \tfrac{I_{zz}-I_{xx}}{I_{yy}}p_{T0} \\
h(5,7) &= 0 \\
h(5,8) &= \text{-1} \\
h(5,9:12) &= 0 \\
h(6,1:3) &= 0 \\
h(6,4) &= \tfrac{I_{xx}^2-I_{xx}I_{yy}+I_{xz}^2}{I_{xx}I_{zz}-I_{xz}^2}q_{T0} \\
h(6,5) &= \tfrac{I_{yy}-I_{xx}-I_{zz}}{I_{xx}I_{zz}-I_{xz}^2}I_{xz}r_{T0} + \tfrac{I_{xx}^2-I_{xx}I_{yy}+I_{xz}^2}{I_{xx}I_{zz}-I_{xz}^2}p_{T0} \\
h(6,6) &= \tfrac{I_{yy}-I_{xx}-I_{zz}}{I_{xx}I_{zz}-I_{xz}^2}I_{xz}q_{T0} \\
h(6,7:8) &= 0 \\
h(6,9) &= \text{-1} \\
h(6,10:12) &= 0 \\
h(7,1:12) &= 0 \\
h(8,1:12) &= 0 \\
h(9,1:12) &= 0 \\
h(10,1) &= -\cos\theta_{T0}\cos\psi_{T0}
\end{aligned}
$$

$$
\begin{aligned}
h(10,2) &= -\cos\theta_{T0}\sin\psi_{T0} \\
h(10,3) &= \sin\theta_{T0} \\
h(10,4) &= 0 \\
h(10,5) &= -z_0 \\
h(10,6) &= y_0 \\
h(10,7:9) &= 0 \\
h(10,10) &= V_{xT0}\cos\theta_{T0}\sin\psi_{T0} - V_{yT0}\cos\theta_{T0}\cos\psi_{T0} \\
h(10,11) &= V_{xT0}\cos\psi_{T0}\sin\theta_{T0} - V_{yT0}\sin\theta_{T0}\sin\psi_{T0} + V_{zT0}\cos\theta_{T0} \\
h(10,12) &= 0 \\
h(11,1) &= \cos\phi_{T0}\sin\psi_{T0} - \sin\phi_{T0}\sin\theta_{T0}\cos\psi_{T0} \\
h(11,2) &= -\cos\phi_{T0}\cos\psi_{T0} - \sin\phi_{T0}\sin\theta_{T0}\sin\psi_{T0} \\
h(11,3) &= -\sin\phi_{T0}\cos\theta_{T0} \\
h(11,4) &= z_0 \\
h(11,5) &= 0 \\
h(11,6) &= -x_0 \\
h(11,7:9) &= 0 \\
h(11,10) &= V_{xT0}\cos\phi_{T0}\cos\psi_{T0} + V_{xT0}\sin\phi_{T0}\sin\theta_{T0}\sin\psi_{T0} \\
&\quad + V_{yT0}\cos\phi_{T0}\sin\psi_{T0} - V_{yT0}\sin\phi_{T0}\sin\theta_{T0}\cos\psi_{T0} \\
h(11,11) &= -V_{xT0}\cos\psi_{T0}\sin\phi_{T0}\cos\theta_{T0} - V_{yT0}\sin\psi_{T0}\sin\phi_{T0}\cos\theta_{T0} \\
&\quad + V_{zT0}\sin\phi_{T0}\sin\theta_{T0} \\
h(11,12) &= -V_{xT0}\sin\phi_{T0}\sin\psi_{T0} - V_{xT0}\cos\psi_{T0}\sin\theta_{T0}\cos\phi_{T0} \\
&\quad + V_{yT0}\cos\psi_{T0}\sin\phi_{T0} - V_{yT0}\sin\psi_{T0}\sin\theta_{T0}\cos\phi_{T0} \\
&\quad - V_{zT0}\cos\theta_{T0}\cos\phi_{T0} \\
h(12,1) &= -\sin\phi_{T0}\sin\psi_{T0} - \cos\psi_{T0}\cos\phi_{T0}\sin\theta_{T0} \\
h(12,2) &= \sin\phi_{T0}\cos\psi_{T0} - \cos\phi_{T0}\sin\theta_{T0}\sin\psi_{T0}
\end{aligned}
$$

$$
\begin{aligned}
h(12,3) &= -\cos\phi_{T0}\cos\theta_{T0} \\
h(12,4) &= -y_0 \\
h(12,5) &= x_0 \\
h(12,6:9) &= 0 \\
h(12,10) &= -V_{xT0}\sin\phi_{T0}\cos\psi_{T0} + V_{xT0}\sin\psi_{T0}\cos\phi_{T0}\sin\theta_{T0} \\
&\quad -V_{yT0}\sin\phi_{T0}\sin\psi_{T0} - V_{yT0}\cos\psi_{T0}\cos\phi_{T0}\sin\theta_{T0} \\
h(12,11) &= -V_{xT0}\cos\psi_{T0}\cos\phi_{T0}\cos\theta_{T0} - V_{yT0}\sin\psi_{T0}\cos\phi_{T0}\cos\theta_{T0} \\
&\quad +V_{zT0}\cos\phi_{T0}\sin\theta_{T0} \\
h(12,12) &= -V_{xT0}\sin\psi_{T0}\cos\phi_{T0} + V_{xT0}\cos\psi_{T0}\sin\theta_{T0}\sin\phi_{T0} \\
&\quad +V_{yT0}\cos\psi_{T0}\cos\phi_{T0} + V_{yT0}\sin\psi_{T0}\sin\theta_{T0}\sin\phi_{T0} \\
&\quad +V_{zT0}\cos\theta_{T0}\sin\phi_{T0}
\end{aligned}
$$

$$
E = e(i,j), E \in \Re^{9\times 12}, i = \{1,...,9\}, j = \{1,...,12\}
$$

$$
\begin{aligned}
e(1,1) &= \rho V_0 S(C_{D0} + C_{D\alpha}\alpha_0 + C_{D\alpha^2}\alpha_0^2 + C_{D\delta_e}\delta_{e0}) \\
e(1,2) &= 0 \\
e(1,3) &= \tfrac{1}{2}\rho V_0^2 S(C_{D\alpha} + 2\alpha_0 C_{D\alpha^2}) \\
e(1,4:12) &= 0 \\
e(2,1) &= \rho V_0 S(C_{S0} + C_{S\delta_r}\delta_{r0} + C_{S\delta_a}\delta_{a0}) \\
e(2,2) &= \tfrac{1}{2}\rho V_0^2 S C_{S\beta} \\
e(2,3:12) &= 0 \\
e(3,1) &= \tfrac{4m_R\rho V_0 S}{4m_R+\rho S C_{L\dot\alpha} c}(C_{L0} + C_{L\alpha}\alpha_0 + C_{L\alpha^2}(\alpha_0\alpha_{ref})^2 + C_{L\delta_e}\delta_{e0} + \tfrac{C_{L\dot\alpha} c q_{T0}}{4V_0}) \\
e(3,2) &= -\tfrac{m_R\rho V_0 S C_{L\dot\alpha} c}{4m_R+\rho S C_{L\dot\alpha} c}(r_{T0}\sin\alpha_0 + p_{T0}\cos\alpha_0) \\
e(3,3) &= \tfrac{m_R\rho V_0 S}{4m_R+\rho S C_{L\dot\alpha} c}[2V_0 C_{L\alpha} + 4V_0 C_{L\alpha^2}(\alpha_0 - \alpha_{ref}) \\
&\quad +\tfrac{gcC_{L\dot\alpha}}{V_0}(\sin\theta_{T0}\cos\alpha_0 - \cos\phi_{T0}\cos\theta_{T0}\sin\alpha_0) \\
&\quad -\tfrac{C_{L\dot\alpha} c}{m_R V_0}(T_{x0}\cos\alpha_0 + T_{z0}\sin\alpha_0)]
\end{aligned}
$$

$$
\begin{aligned}
e(3,4) &= 0 \\
e(3,5) &= \tfrac{m_R\rho V_0 Sc}{4m_R+\rho SC_{L\dot{\alpha}}c}(C_{Lq}+C_{L\dot{\alpha}}) \\
e(3,6) &= 0 \\
e(3,7) &= -\tfrac{m_R\rho V_0 SC_{L\dot{\alpha}}c}{4m_R+\rho SC_{L\dot{\alpha}}c}\ (p_{T0}+\tfrac{g}{V_0}\sin\phi_{T0}\cos\theta_{T0}\sin\alpha_0) \\
e(3,8) &= \tfrac{m_R\rho V_0 SC_{L\dot{\alpha}}c}{4m_R+\rho SC_{L\dot{\alpha}}c}\ (g\cos\phi_{T0}\cos\theta_{T0}\sin\alpha_0 - g\sin\theta_{T0}\cos\alpha_0) \\
e(3,9) &= \tfrac{m_R\rho V_0 SC_{L\dot{\alpha}}c}{4m_R+\rho SC_{L\dot{\alpha}}c}\ (r_{T0}-\tfrac{g}{V_0}\sin\phi_{T0}\cos\theta_{T0}\cos\alpha_0) \\
e(3,10:12) &= 0 \\
e(4,1) &= \rho V_0 Sb(C_{\mathcal{L}0}+C_{\mathcal{L}\delta_a}\delta_{a0}+C_{\mathcal{L}\delta_r}\delta_{r0}) \\
e(4,2) &= \tfrac{1}{2}\rho V_0^2 SbC_{\mathcal{L}\beta} \\
e(4,3) &= 0 \\
e(4,4) &= \tfrac{1}{4}\rho V_0 Sb^2 C_{\mathcal{L}p} \\
e(4,5) &= 0 \\
e(4,6) &= \tfrac{1}{4}\rho V_0 Sb^2 C_{\mathcal{L}r} \\
e(4,7:12) &= 0 \\
e(5,1) &= \rho V_0 Sc(C_{\mathcal{M}0}+C_{\mathcal{M}\alpha}\alpha_0+C_{\mathcal{M}\delta_e}\delta_{e0}+\tfrac{c}{4V_0}C_{\mathcal{M}\dot{\alpha}}q_{T0}) \\
&\quad -\tfrac{\rho^2 V_0 S^2 c^2 C_{\mathcal{M}\dot{\alpha}}}{4m_R+\rho SC_{L\dot{\alpha}}c}\ (C_{L0}+C_{L\alpha}\alpha_0+C_{L\alpha^2}(\alpha_0-\alpha_{ref})^2+C_{L\delta_e}\delta_{e0}+\tfrac{C_{L\dot{\alpha}}cq_{T0}}{4V_0}) \\
e(5,2) &= -\tfrac{1}{4}\rho V_0 SC^2 C_{\mathcal{M}\dot{\alpha}}(r_{T0}\sin\alpha_0+p_{T0}\cos\alpha_0) \\
&\quad +\tfrac{\rho^2 V_0 S^2 c^3 C_{\mathcal{M}\dot{\alpha}}C_{L\dot{\alpha}}}{4(4m_R+\rho SC_{L\dot{\alpha}}c)}\ (r_{T0}\sin\alpha_0+p_{T0}\cos\alpha_0) \\
e(5,3) &= \tfrac{1}{2}\rho V_0^2 ScC_{\mathcal{M}\alpha}+\tfrac{1}{4}\rho Sc^2 C_{\mathcal{M}\dot{\alpha}}\ [g\sin\theta_{T0}\cos\alpha_0 - g\cos\phi_{T0}\cos\theta_{T0}\sin\alpha_0 \\
&\quad -\tfrac{1}{m_R}(T_{x0}\cos\alpha_0+T_{z0}\sin\alpha_0)] \\
&\quad -\tfrac{\rho^2 S^2 V_0 c^2 C_{\mathcal{M}\dot{\alpha}}}{4(4m_R+\rho SC_{L\dot{\alpha}}c)}\ [2V_0 C_{L\alpha}+4V_0 C_{L\alpha^2}(\alpha_0-\alpha_{ref}) \\
&\quad +\tfrac{gC_{L\dot{\alpha}}c}{V_0}(\sin\theta_{T0}\cos\alpha_0-\cos\phi_{T0}\cos\theta_{T0}\sin\alpha_0) \\
&\quad -\tfrac{C_{L\dot{\alpha}}c}{m_R V_0}(T_{x0}\cos\alpha_0+T_{z0}\sin\alpha_0)] \\
e(5,4) &= 0 \\
e(5,5) &= \tfrac{1}{4}\rho V_0 Sc^2(C_{\mathcal{M}q}+C_{\mathcal{M}\dot{\alpha}})\ -\tfrac{\rho^2 V_0 S^2 c^3 C_{\mathcal{M}\dot{\alpha}}}{4(4m_R+\rho SC_{L\dot{\alpha}}c)}(C_{Lq}+C_{L\dot{\alpha}})
\end{aligned}
$$

$$
\begin{aligned}
e(5,6) &= 0 \\
e(5,7) &= \tfrac{1}{4}\rho V_0 S c C_{\mathcal{M}\dot{\alpha}} \left(\tfrac{\rho S c^2 C_{L\dot{\alpha}}}{4m_R+\rho S C_{L\dot{\alpha}} c} - 1\right) \left(p_{T0} + \tfrac{g}{V_0}\sin\phi_{T0}\cos\theta_{T0}\sin\alpha_0\right) \\
e(5,8) &= \tfrac{1}{4}\rho S c^2 C_{\mathcal{M}\dot{\alpha}} g \left(1 - \tfrac{m_R \rho S c C_{L\dot{\alpha}}}{4m_R+\rho S C_{L\dot{\alpha}} c}\right)\left(\cos\phi_{T0}\cos\theta_{T0}\sin\alpha_0 - \sin\theta_{T0}\cos\alpha_0\right) \\
e(5,9) &= \tfrac{1}{4}\rho V_0 S c^2 C_{\mathcal{M}\dot{\alpha}} \left(1 - \tfrac{\rho S c C_{L\dot{\alpha}}}{4m_R+\rho S C_{L\dot{\alpha}} c}\right) \left(r_{T0} - \tfrac{g}{V_0}\sin\phi_{T0}\cos\theta_{T0}\cos\alpha_0\right) \\
e(5,10:12) &= 0 \\
e(6,1) &= \rho V_0 S b (C_{\mathcal{N}0} + C_{\mathcal{N}\delta_a}\delta_{a0} + C_{\mathcal{N}\delta_r}\delta_{r0}) \\
e(6,2) &= \tfrac{1}{2}\rho V_0^2 S b C_{\mathcal{N}\beta} \\
e(6,3) &= 0 \\
e(6,4) &= \tfrac{1}{4}\rho V_0 S b^2 C_{\mathcal{N}p} \\
e(6,5) &= 0 \\
e(6,6) &= \tfrac{1}{4}\rho V_0 S b^2 C_{\mathcal{N}r} \\
e(6,7:12) &= 0 \\
e(7,1:12) &= 0 \\
e(8,1:12) &= 0 \\
e(9,1:12) &= 0
\end{aligned}
$$

$$
F = f(i,j), F \in \Re^{9\times 6}, i = \{1,...,9\}, j = \{1,...,6\}
$$

$$
\begin{aligned}
f(1,1) &= 0 \\
f(1,2) &= \tfrac{1}{2}\rho V_0^2 S C_{D\delta_e} \\
f(1,3:6) &= 0 \\
f(2,1) &= \tfrac{1}{2}\rho V_0^2 S C_{S\delta_a} \\
f(2,2) &= 0 \\
f(2,3) &= \tfrac{1}{2}\rho V_0^2 S C_{S\delta_r} \\
f(2,4:6) &= 0 \\
f(3,1) &= 0
\end{aligned}
$$

$$
\begin{aligned}
f(3,2) &= \tfrac{2m_R\rho V_0^2 SC_{L\delta_e}}{4m_R+\rho SC_{L\dot{\alpha}}c} \\
f(3,3) &= 0 \\
f(3,4) &= \tfrac{\rho SC_{L\dot{\alpha}}c}{4m_R+\rho SC_{L\dot{\alpha}}c}\ \cos\delta_{z0}T_{max}(\cos\alpha_0\sin\delta_{y0}-\sin\alpha_0\cos\delta_{y0}) \\
f(3,5) &= \tfrac{\rho SC_{L\dot{\alpha}}c}{4m_R+\rho SC_{L\dot{\alpha}}c}\ T_0\cos\delta_{z0}(\sin\alpha_0\sin\delta_{y0}+\cos\alpha_0\cos\delta_{y0}) \\
f(3,6) &= \tfrac{\rho SC_{L\dot{\alpha}}c}{4m_R+\rho SC_{L\dot{\alpha}}c}\ \sin\delta_{z0}(T_0\sin\alpha_0\cos\delta_{y0}-\cos\alpha_0\sin\delta_{y0}) \\
f(4,1) &= \tfrac{1}{2}\rho V_0^2 SbC_{\mathcal{L}\delta_a} \\
f(4,2) &= 0 \\
f(4,3) &= \tfrac{1}{2}\rho V_0^2 SbC_{\mathcal{L}\delta_r} \\
f(4,4) &= T_{max}(\triangle_{y0}\cos\delta_{z0}\cos\delta_{y0}-\triangle_{z0}\sin\delta_{z0}) \\
f(4,5) &= -\triangle_{y0}T_0\cos\delta_{z0}\sin\delta_{y0} \\
f(4,6) &= -T_0(\triangle_{y0}\sin\delta_{z0}\cos\delta_{y0}+\cos\delta_{z0}) \\
f(5,1) &= 0 \\
f(5,2) &= \tfrac{1}{2}\rho V_0^2 ScC_{\mathcal{M}\delta_e}\ -\tfrac{\rho^2V_0^2S^2c^2C_{\mathcal{M}\dot{\alpha}}C_{L\delta_e}}{2(4m_R+\rho SC_{L\dot{\alpha}}c)} \\
f(5,3) &= 0 \\
f(5,4) &= \cos\delta_{z0}T_{max}(\triangle_{z0}\cos\delta_{y0}-\triangle_{x0}\sin\delta_{y0}) \\
&\quad +\tfrac{1}{4m_R}\rho Sc^2C_{\mathcal{M}\dot{\alpha}}\cos\delta_{z0}T_{max}(\cos\alpha_0\sin\delta_{y0}-\sin\alpha_0\cos\delta_{y0}) \\
&\quad +\tfrac{\rho^2S^2c^3C_{\mathcal{M}\dot{\alpha}}C_{L\dot{\alpha}}}{4m_R(4m_R+\rho ScC_{L\dot{\alpha}})}\ \cos\delta_{z0}T_{max}(\sin\alpha_0\cos\delta_{y0}-\cos\alpha_0\sin\delta_{y0}) \\
f(5,5) &= -T_0\cos\delta_{z0}(\triangle_{z0}\sin\delta_{y0}+\triangle_{x0}\cos\delta_{y0}) \\
&\quad +\tfrac{1}{4m_R}\rho Sc^2C_{\mathcal{M}\dot{\alpha}}T_0\cos\delta_{z0}\ (\sin\alpha_0\sin\delta_{y0}+\cos\alpha_0\cos\delta_{y0}) \\
&\quad -\tfrac{\rho^2S^2c^3C_{\mathcal{M}\dot{\alpha}}C_{L\dot{\alpha}}}{4m_R(4m_R+\rho ScC_{L\dot{\alpha}})}\ (\sin\alpha_0\sin\delta_{y0}+\cos\alpha_0\cos\delta_{y0})T_0\cos\delta_{z0} \\
f(5,6) &= T_0\sin\delta_{z0}(\triangle_{x0}\sin\delta_{y0}-\triangle_{z0}\cos\delta_{y0}) \\
&\quad +\tfrac{1}{4m_R}\rho Sc^2C_{\mathcal{M}\dot{\alpha}}T_0\sin\delta_{z0}\ (\sin\alpha_0\cos\delta_{y0}-\cos\alpha_0\sin\delta_{y0}) \\
&\quad +\tfrac{\rho^2S^2c^3C_{\mathcal{M}\dot{\alpha}}C_{L\dot{\alpha}}}{4m_R(4m_R+\rho ScC_{L\dot{\alpha}})}\ T_0\sin\delta_{z0}(\cos\alpha_0\sin\delta_{y0}-\sin\alpha_0\cos\delta_{y0}) \\
f(6,1) &= \tfrac{1}{2}\rho V_0^2 SbC_{\mathcal{N}\delta_a} \\
f(6,2) &= 0
\end{aligned}
$$

$$
\begin{aligned}
f(6,3) &= \tfrac{1}{2}\rho V_0^2 SbC_{\mathcal{N}\delta_r} \\
f(6,4) &= T_{max}(\triangle_{x0}\sin\delta_{z0} - \triangle_{y0}\cos\delta_{z0}\cos\delta_{y0}) \\
f(6,5) &= \triangle_{y0} T_0 \cos\delta_{z0}\sin\delta_{y0} \\
f(6,6) &= T_0(\triangle_{x0}\cos\delta_{z0} + \triangle_{y0}\sin\delta_{z0}\cos\delta_{y0}) \\
f(7,1:3) &= 0 \\
f(7,4) &= \cos\delta_{z0}\cos\delta_{y0} T_{max} \\
f(7,5) &= -T_0\cos\delta_{z0}\sin\delta_{y0} \\
f(7,6) &= -T_0\sin\delta_{z0}\cos\delta_{y0} \\
f(8,1:3) &= 0 \\
f(8,4) &= \sin\delta_{z0} T_{max} \\
f(8,5) &= 0 \\
f(8,6) &= T_0\cos\delta_{z0} \\
f(9,1:3) &= 0 \\
f(9,4) &= \cos\delta_{z0}\sin\delta_{y0} T_{max} \\
f(9,5) &= -T_0\sin\delta_{y0}\sin\delta_{z0} \\
f(9,6) &= T_0\cos\delta_{z0}\cos\delta_{y0}
\end{aligned}
$$

$$
G = g(i,j), G \in \Re^{9\times 12}, i = \{1,...,9\}, j = \{1,...,12\}
$$

$$
\begin{aligned}
g(1,1:12) &= 0 \\
g(2,1:12) &= 0 \\
g(3,1:4) &= 0 \\
g(3,5) &= \tfrac{m_R\rho V_0 ScC_{L\dot{\alpha}}}{4m_R+\rho ScC_{L\dot{\alpha}}} \\
g(3,6:10) &= 0 \\
g(3,11) &= \tfrac{m_R\rho ScC_{L\dot{\alpha}}}{4m_R+\rho ScC_{L\dot{\alpha}}}\ (g\sin\alpha_0\cos\theta_{T0} - g\cos\alpha_0\cos\phi_{T0}\sin\theta_{T0}) \\
g(3,12) &= -\tfrac{m_R\rho ScgC_{L\dot{\alpha}}}{4m_R+\rho ScC_{L\dot{\alpha}}}\cos\alpha_0\cos\theta_{T0}\sin\phi_{T0}
\end{aligned}
$$

$$
\begin{aligned}
g(4,1:12) &= 0 \\
g(5,1:4) &= 0 \\
g(5,5) &= \tfrac{1}{4}\rho V_0 S c^2 C_{\mathcal{M}\dot{\alpha}} - \tfrac{\rho^2 V_0 S^2 c^3 C_{L\dot{\alpha}} C_{\mathcal{M}\dot{\alpha}}}{4(4m_R+\rho S c C_{L\dot{\alpha}})} \\
g(5,6:10) &= 0 \\
g(5,11) &= \tfrac{1}{4}\rho S c^2 g C_{\mathcal{M}\dot{\alpha}} \left(1 - \tfrac{\rho S c^2 C_{L\dot{\alpha}}}{4m_R+\rho S c C_{L\dot{\alpha}}}\right) \left(\sin\alpha_0 \cos\theta_{T0} - \cos\alpha_0 \cos\phi_{T0} \sin\theta_{T0}\right) \\
g(5,12) &= \tfrac{1}{4}\rho S c^2 g C_{\mathcal{M}\dot{\alpha}} \cos\alpha_0 \cos\theta_{T0} \sin\phi_{T0} \left(\tfrac{\rho S c C_{L\dot{\alpha}}}{4m_R+\rho S c C_{L\dot{\alpha}}} - 1\right) \\
g(6,1:12) &= 0 \\
g(7,1:12) &= 0 \\
g(8,1:12) &= 0 \\
g(9,1:12) &= 0
\end{aligned}
$$

APPENDIX E

NOMINAL VALUES OF TANKER STATES AND CONTROL VARIABLES

Nominal values of tanker states

$$\underline{x}_T = [V_T \ \beta_T \ \alpha_T \ p_T \ q_T \ r_T \ \theta_T \ \phi_T \ z_T]^T$$

The units of the states are respectively;

$$[m/s \ rad \ rad \ rad/s \ rad/s \ rad/s \ rad \ rad \ m]^T$$

Nominal values of tanker control inputs are

$$\underline{u}_T = [\delta_{a_T} \ \delta_{e_T} \ \delta_{r_T} \ \xi_{t_T}]^T$$

The units of the states are respectively;

$$[rad \ rad \ rad \ unitless]^T$$

$$\underline{x}_{T01} = [\ 180 \ \ 0 \ \ 0.0651 \ \ 0 \ \ 0 \ \ 0 \ \ 0.0651 \ \ 0 \ \ -7010\ ]^T$$

$$\underline{x}_{T02} = [\ 200 \ \ 0 \ \ 0.0485 \ \ 0 \ \ 0 \ \ 0 \ \ 0.0485 \ \ 0 \ \ -7010\ ]^T$$

$$\underline{x}_{T03} = [\ 180 \ \ 0 \ \ 0.0769 \ \ -0.0020 \ \ 0.0137 \ \ 0.0262 \ \ 0.0682 \ \ 0.4827 \ \ -7010\ ]^T$$

$$\underline{x}_{T04} = [\ 200 \ \ 0 \ \ 0.0602 \ \ -0.0015 \ \ 0.0149 \ \ 0.0256 \ \ 0.0521 \ \ 0.5273 \ \ -7010\ ]^T$$

$$\underline{u}_{T01} = [\ 0 \ \ -0.0662 \ \ 0 \ \ 0.0922\ ]^T$$

$$\underline{u}_{T02} = [\ 0 \ \ -0.0474 \ \ 0 \ \ 0.1117\ ]^T$$

$$\underline{u}_{T03} = [\ 0.0093 \ \ -0.0814 \ \ -0.0019 \ \ 0.0936\ ]^T$$

$$\underline{u}_{T04} = [\ 0.0079 \ \ -0.0625 \ \ -0.0017 \ \ 0.1131\ ]^T$$

APPENDIX F

NOMINAL VALUES OF RECEIVER STATES AND CONTROL VARIABLES

Nominal values of receiver states

$$\underline{x} \;=\; [V \;\; \beta \;\; \alpha \;\; p \;\; q \;\; r \;\; \psi \;\; \theta \;\; \phi \;\; x \;\; y \;\; z]^T$$

The units of the state are respectively;

$$[m/s \;\; rad \;\; rad \;\; rad/s \;\; rad/s \;\; rad/s \;\; rad \;\; rad \;\; rad \;\; m \;\; m \;\; m]^T$$

Nominal values of receiver control inputs are

$$\underline{u} \;=\; [\delta_a \;\; \delta_e \;\; \delta_r \;\; \xi \;\; \delta_y \;\; \delta_z]^T$$

The units of the states are respectively;

$$[rad \;\; rad \;\; rad \;\; unitless \;\; rad \;\; rad]^T$$

$$\underline{x}_{01} = [\; 180 \;\; 0 \;\; 0.0516 \;\; 0 \;\; 0 \;\; 0 \;\; 0 \;\; 0.0135 \;\; 0 \;\; -25.33 \;\; 0 \;\; 6.46 \;]^T$$

$$\underline{x}_{02} = [\; 200 \;\; 0 \;\; 0.0371 \;\; 0 \;\; 0 \;\; 0 \;\; 0 \;\; 0.0115 \;\; 0 \;\; -25.33 \;\; 0 \;\; 6.46 \;]^T$$

$$\underline{x}_{03} = [\; 180 \;\; 0 \;\; 0.0662 \;\; 0 \;\; 0 \;\; 0 \;\; 0 \;\; 0.0154 \;\; 0.0173 \;\; -25.33 \;\; 0 \;\; 6.46 \;]^T$$

$$\underline{x}_{04} = [\; 200 \;\; 0 \;\; 0.0475 \;\; 0 \;\; 0 \;\; 0 \;\; 0 \;\; 0.0132 \;\; 0.0176 \;\; -25.33 \;\; 0 \;\; 6.46 \;]^T$$

$$\underline{u}_{01} = [\; 0 \;\; -0.0281 \;\; 0 \;\; 0.4878 \;\; 0 \;\; 0 \;]^T$$

$$\underline{u}_{02} = [\; 0 \;\; -0.0259 \;\; 0 \;\; 0.5795 \;\; 0 \;\; 0 \;]^T$$

$$\underline{u}_{03} = [\; -0.1272 \times 10^{-4} \;\; -0.0297 \;\; 0.2207 \times 10^{-4} \;\; 0.5049 \;\; 0 \;\; 0 \;]^T$$

$$\underline{u}_{04} = [\; -0.1082 \times 10^{-4} \;\; -0.0275 \;\; 0.1707 \times 10^{-4} \;\; 0.5951 \;\; 0 \;\; 0 \;]^T$$

APPENDIX G

STATE AND CONTROL MATRICES FOR TANKER

$$A_{T,1} = \begin{bmatrix} -0.0079 & 0 & 8.9178 & 0 & 0 & 0 & -9.8066 & 0 & 0 \\ 0 & 0.1061 & 0 & 0.0651 & 0 & -0.9979 & 0 & 0.0544 & 0 \\ -0.0006 & 0 & -0.6542 & 0 & 0.9869 & 0 & 0 & 0 & 0 \\ 0 & -4.2119 & 0 & -0.8270 & 0 & 0.4023 & 0 & 0 & 0 \\ -0.0002 & 0 & -2.5095 & 0 & -0.2965 & 0 & 0 & 0 & 0 \\ 0 & 1.5329 & 0 & -0.0208 & 0 & -0.2186 & 0 & 0 & 0 \\ 0 & 0 & 0 & 0 & 1.0000 & 0 & 0 & 0 & 0 \\ 0 & 0 & 0 & 1.0000 & 0 & 0.0652 & 0 & 0 & 0 \\ 0 & 0 & 180 & 0 & 0 & 0 & -180 & 0 & 0 \end{bmatrix}$$

$$B_{T,1} = \begin{bmatrix} 0 & 0 & 0 & 7.7056 \\ 0 & 0 & -0.0249 & 0 \\ 0 & -0.0257 & 0 & -0.0030 \\ -1.1947 & 0 & 0.4413 & 0 \\ 0 & -2.2006 & 0 & 0.1941 \\ 0.0883 & 0 & -0.9179 & 0 \\ 0 & 0 & 0 & 0 \\ 0 & 0 & 0 & 0 \\ 0 & 0 & 0 & 0 \end{bmatrix}$$

$$A_{T,2} = \begin{bmatrix} -0.0086 & 0 & 8.9880 & 0 & 0 & 0 & -9.8067 & 0 & 0 \\ 0 & 0.1179 & 0 & 0.0486 & 0 & -0.9988 & 0 & 0.0490 & 0 \\ -0.0005 & 0 & -0.7268 & 0 & 0.9869 & 0 & 0 & 0 & 0 \\ 0 & -5.1998 & 0 & -0.9189 & 0 & 0.4470 & 0 & 0 & 0 \\ -0.0002 & 0 & -3.0981 & 0 & -0.3295 & 0 & 0 & 0 & 0 \\ 0 & 1.8925 & 0 & -0.0231 & 0 & -0.2429 & 0 & 0 & 0 \\ 0 & 0 & 0 & 0 & 1.0000 & 0 & 0 & 0 & 0 \\ 0 & 0 & 0 & 1.0000 & 0 & 0.0486 & 0 & 0 & 0 \\ 0 & 0 & 200 & 0 & 0 & 0 & -200 & 0 & 0 \end{bmatrix}$$

$$B_{T,2} = \begin{bmatrix} 0 & 0 & 0 & 7.7135 \\ 0 & 0 & -0.0277 & 0 \\ 0 & -0.0286 & 0 & -0.0020 \\ -1.4750 & 0 & 0.5448 & 0 \\ 0 & -2.7168 & 0 & 0.1941 \\ 0.1090 & 0 & -1.1332 & 0 \\ 0 & 0 & 0 & 0 \\ 0 & 0 & 0 & 0 \\ 0 & 0 & 0 & 0 \end{bmatrix}$$

$$A_{T,3} = \begin{bmatrix} -0.0080 & 4.5416 & 7.6407 & 0 & 0 & 0 & -9.8004 & -0.3494 & 0 \\ -0.0001 & 0.1060 & 0 & 0.0769 & 0 & -0.9970 & -0.0017 & 0.0481 & 0 \\ -0.0131 & 0 & -0.6543 & 0 & 0.9869 & 0 & 0.0009 & -0.0252 & 0 \\ 0.9566 & -4.2119 & 0 & -0.8268 & -0.0267 & 0.3883 & 0 & 0 & 0 \\ -0.0002 & 0 & -2.5095 & 0.0268 & -0.2965 & -0.0013 & 0 & 0 & 0 \\ 0.0069 & 1.5329 & 0 & -0.0205 & -0.0004 & -0.2188 & 0 & 0 & 0 \\ 0 & 0 & 0 & 0 & 0.8857 & -0.4642 & 0 & -0.0296 & 0 \\ 0 & 0 & 0 & 1.0000 & 0.0317 & 0.0605 & 0.0297 & 0 & 0 \\ 0 & 83.3615 & 159.5333 & 0 & 0 & 0 & -179.8852 & -6.4123 & 0 \end{bmatrix}$$

$$B_{T,3} = \begin{bmatrix} 0 & 0 & 0 & 7.6987 \\ 0 & 0 & -0.0249 & 0 \\ 0 & -0.0257 & 0 & -0.0035 \\ -1.1947 & 0 & 0.4413 & 0 \\ 0 & -2.2006 & 0 & 0.1941 \\ 0.0883 & 0 & -0.9179 & 0 \\ 0 & 0 & 0 & 0 \\ 0 & 0 & 0 & 0 \\ 0 & 0 & 0 & 0 \end{bmatrix}$$

$$A_{T,4} = \begin{bmatrix} -0.0087 & 4.9286 & 7.4627 & 0 & 0 & 0 & -9.8021 & -0.2970 & 0 \\ 0.0001 & 0.1179 & 0 & 0.0603 & 0 & -0.9982 & -0.0013 & 0.0423 & 0 \\ -0.0143 & 0 & -0.7269 & 0 & 0.9869 & 0 & 0.0007 & -0.0246 & 0 \\ 1.1533 & -5.1998 & 0 & -0.9186 & -0.0261 & 0.4318 & 0 & 0 & 0 \\ -0.0002 & 0 & -3.0981 & 0.0262 & -0.3295 & -0.0008 & 0 & 0 & 0 \\ 0.0084 & 1.8925 & 0 & -0.0227 & 0.0004 & -0.2431 & 0 & 0 & 0 \\ 0 & 0 & 0 & 0 & 0.8641 & -0.5033 & 0 & -0.0296 & 0 \\ 0 & 0 & 0 & 1.0000 & 0.0263 & 0.0451 & 0.0297 & 0 & 0 \\ 0 & 100.516 & 172.9061 & 0 & 0 & 0 & -199.9080 & -6.0563 & 0 \end{bmatrix}$$

$$B_{T,4} = \begin{bmatrix} 0 & 0 & 0 & 7.7081 \\ 0 & 0 & -0.0277 & 0 \\ 0 & -0.0286 & 0 & -0.0025 \\ -1.4750 & 0 & 0.5448 & 0 \\ 0 & -2.7168 & 0 & 0.1941 \\ 0.1090 & 0 & -1.1332 & 0 \\ 0 & 0 & 0 & 0 \\ 0 & 0 & 0 & 0 \\ 0 & 0 & 0 & 0 \end{bmatrix}$$

APPENDIX H

STATE, CONTROL AND DISTURBANCE MATRICES FOR RECEIVER

$$A_{01} = \begin{bmatrix} -0.0175 & 0 & 5.1342 & 0 & 0 & 0 & 0 & -9.8031 & 0 & 0 & 0 & 0 \\ 0 & 0.0092 & 0 & 0.0516 & 0 & -0.9987 & 0.0035 & 0 & 0.0543 & 0 & 0 & 0 \\ -0.0006 & 0 & -0.7446 & 0 & 0.9869 & 0 & 0 & -0.0015 & 0 & 0 & 0 & 0 \\ 0 & -5.6296 & 0 & -1.3291 & 0 & 0.0982 & 0 & 0 & 0 & 0 & 0 & 0 \\ 0.0004 & 0 & -1.7202 & 0 & -0.6979 & 0 & 0 & 0 & 0 & 0 & 0 & 0 \\ 0 & -1.3800 & 0 & -0.0429 & 0 & -0.0196 & 0 & 0 & 0 & 0 & 0 & 0 \\ 0 & 0 & 0 & 0 & 0 & 1.0001 & 0 & 0 & 0 & 0 & 0 & 0 \\ 0 & 0 & 0 & 0 & 1.0000 & 0 & 0 & 0 & 0 & 0 & 0 & 0 \\ 0 & 0 & 0 & 1.0000 & 0 & 0.0135 & 0 & 0 & 0 & 0 & 0 & 0 \\ 0.9993 & 0 & -6.8481 & 0 & 0 & 0 & 0 & 6.8481 & 0 & 0 & 0 & 0 \\ 0 & 180.0000 & 0 & 0 & 0 & 0 & 179.8697 & 0 & -9.2838 & 0 & 0 & 0 \\ 0.0380 & 0 & 179.8697 & 0 & 0 & 0 & 0 & -179.8697 & 0 & 0 & 0 & 0 \end{bmatrix}$$

$$A_{02} = \begin{bmatrix} -0.0188 & 0 & 5.6588 & 0 & 0 & 0 & 0 & -9.8041 & 0 & 0 & 0 & 0 \\ 0 & 0.0075 & 0 & 0.0371 & 0 & -0.9993 & 0.0024 & 0 & 0.0489 & 0 & 0 & 0 \\ -0.0005 & 0 & -0.8275 & 0 & 0.9869 & 0 & 0 & -0.0011 & 0 & 0 & 0 & 0 \\ 0 & -6.9501 & 0 & 0 & 0 & 0.1092 & 0 & 0 & 0 & 0 & 0 & 0 \\ 0.0004 & 0 & -2.1237 & -0.0477 & -0.7754 & 0 & 0 & 0 & 0 & 0 & 0 & 0 \\ 0 & -1.7038 & 0 & 0 & 0 & -0.0217 & 0 & 0 & 0 & 0 & 0 & 0 \\ 0 & 0 & 0 & 0 & 0 & 1.0001 & 0 & 0 & 0 & 0 & 0 & 0 \\ 0 & 0 & 0 & 0 & 1.0000 & 0 & 0 & 0 & 0 & 0 & 0 & 0 \\ 0 & 0 & 0 & 1.0000 & 0 & 0.0115 & 0 & 0 & 0 & 0 & 0 & 0 \\ 0.9997 & 0 & -5.1343 & 0 & 0 & 0 & 0 & 5.1343 & 0 & 0 & 0 & 0 \\ 0 & 200.0000 & 0 & 0 & 0 & 0 & 199.9341 & 0 & -7.4149 & 0 & 0 & 0 \\ 0.0257 & 0 & 199.9341 & 0 & 0 & 0 & 0 & -199.9341 & 0 & 0 & 0 & 0 \end{bmatrix}$$

$$A_{03} \;=\; \left[\; A1_{03} \;\mid\; A2_{03} \;\right]$$

where $A_{03} \in \Re^{12\times 12}$, $A1_{03} \in \Re^{12\times 6}$ and $A2_{03} \in \Re^{12\times 6}$.

$$A1_{03} = \begin{bmatrix} -0.0181 & 4.6903 & 2.9809 & 0 & 0 & 0 \\ 0 & 0.0093 & -0.0008 & 0.0621 & 0 & -0.9981 \\ -0.0006 & 0.0008 & -0.7449 & 0 & 0.9869 & 0 \\ 0 & -5.6296 & 0 & -1.3291 & -0.0024 & 0.0686 \\ 0.0004 & 0 & -1.7202 & -0.0008 & -0.6979 & -0.0053 \\ 0 & -1.3800 & 0 & -0.0352 & 0.0038 & -0.0194 \\ 0 & 0 & 0 & 0 & 0.0173 & 1.0000 \\ 0 & 0 & 0 & 0 & 0.9999 & -0.0173 \\ 0 & 0 & 0 & 1.0000 & 0.0003 & 0.0154 \\ 0.9989 & 0.0479 & -8.4105 & 0 & 0 & 0 \\ -0.0011 & 179.9732 & -3.0991 & 0 & 0 & 0 \\ 0.0467 & 3.1047 & 179.7769 & 0 & 0 & 0 \end{bmatrix}$$

$$A2_{03} = \begin{bmatrix} 4.5360 & -8.6876 & -0.2913 & 0 & 0 & 0 \\ 0.0044 & 0.0007 & 0.0618 & 0 & 0 & 0 \\ 0.0008 & -0.0015 & -0.0001 & 0 & 0 & 0 \\ -0.0001 & 0 & -0.0005 & 0 & 0 & 0 \\ 0.0004 & 0.0007 & 0 & 0 & 0 & 0 \\ -0.0001 & 0.0002 & 0 & 0 & 0 & 0 \\ 0 & 0 & 0 & 0 & 0 & 0 \\ 0 & 0 & 0 & 0 & 0 & 0 \\ 0 & 0 & 0 & 0 & 0 & 0 \\ 0.1929 & 8.4084 & -0.0003 & 0 & 0.0262 & -0.0137 \\ 179.8034 & 0 & -11.1786 & -0.0262 & 0 & -0.0020 \\ 0 & -179.8034 & -0.1928 & 0.0137 & 0.0020 & 0 \end{bmatrix}$$

$$A_{04} \;=\; \left[\; A1_{04} \;\mid\; A2_{04} \;\right]$$

where $A_{04} \in \Re^{12\times 12}$, $A1_{04} \in \Re^{12\times 6}$ and $A2_{04} \in \Re^{12\times 6}$.

$$A1_{04} = \begin{bmatrix} -0.0193 & 5.0770 & 3.0769 & 0 & 0 & 0 \\ -0.0001 & 0.0076 & -0.0007 & 0.0475 & 0 & -0.9987 \\ -0.0005 & 0.0007 & -0.8277 & 0 & 0.9869 & 0 \\ 0 & -6.9501 & 0 & -1.4769 & -0.0023 & 0.0770 \\ 0.0004 & 0 & -2.1237 & 0.0008 & -0.7754 & -0.0041 \\ 0 & -1.7038 & 0 & -0.0393 & 0.0003 & -0.0216 \\ 0 & 0 & 0 & 0 & 0.0176 & 0.9999 \\ 0 & 0 & 0 & 0 & 0.9998 & -0.0176 \\ 0 & 0 & 0 & 1.0000 & 0.0002 & 0.0132 \\ 0.9994 & 0.0467 & -6.8614 & 0 & 0 & 0 \\ -0.0008 & 199.9689 & -3.5233 & 0 & 0 & 0 \\ 0.0343 & 3.5270 & 199.8512 & 0 & 0 & 0 \end{bmatrix}$$

$$A2_{04} = \begin{bmatrix} 4.9253 & -8.4753 & -0.2413 & 0 & 0 & 0 \\ 0.0031 & 0.0006 & 0.0572 & 0 & 0 & 0 \\ 0.0007 & -0.0011 & 0 & 0 & 0 & 0 \\ 0 & 0 & -0.0004 & 0 & 0 & 0 \\ 0.0004 & -0.0007 & 0 & 0 & 0 & 0 \\ 0 & 0.0002 & 0 & 0 & 0 & 0 \\ 0 & 0 & 0 & 0 & 0 & 0 \\ 0 & 0 & 0 & 0 & 0 & 0 \\ 0 & 0 & 0 & 0 & 0 & 0 \\ 0.1676 & 6.8595 & -0.0022 & 0 & 0.0256 & -0.0149 \\ 199.8823 & 0 & -9.5043 & -0.0256 & 0 & -0.0015 \\ 0 & -199.8823 & -0.1676 & 0.0149 & 0.0015 & 0 \end{bmatrix}$$

$$B_{01} = \begin{bmatrix} 0 & 0 & 0 & 3.2621 & 0 & 0.0822 \\ 0 & 0 & 0 & 0 & 0 & 0.0089 \\ 0 & -0.2095 & 0 & -0.0009 & 0 & 0.0088 \\ -33.3885 & 0 & -1.0073 & 0 & 0 & -0.5498 \\ 0 & -12.1132 & 0 & -0.0748 & 1.1730 & 0 \\ -0.9884 & 0 & -1.1999 & 0 & 0 & -0.8371 \\ 0 & 0 & 0 & 0 & 0 & 0 \\ 0 & 0 & 0 & 0 & 0 & 0 \\ 0 & 0 & 0 & 0 & 0 & 0 \\ 0 & 0 & 0 & 0 & 0 & 0 \\ 0 & 0 & 0 & 0 & 0 & 0 \\ 0 & 0 & 0 & 0 & 0 & 0 \end{bmatrix}$$

$$B_{02} = \begin{bmatrix} 0 & 0 & 0 & 3.2642 & 0 & 0.0703 \\ 0 & 0 & 0 & 0 & 0 & 0.0095 \\ 0 & -0.2328 & 0 & -0.0006 & 0 & 0.0095 \\ -41.2203 & 0 & -1.2436 & 0 & 0 & -0.6532 \\ 0 & -14.9545 & 0 & -0.0748 & 1.3937 & 0 \\ -1.2203 & 0 & -1.4814 & 0 & 0 & -0.9946 \\ 0 & 0 & 0 & 0 & 0 & 0 \\ 0 & 0 & 0 & 0 & 0 & 0 \\ 0 & 0 & 0 & 0 & 0 & 0 \\ 0 & 0 & 0 & 0 & 0 & 0 \\ 0 & 0 & 0 & 0 & 0 & 0 \\ 0 & 0 & 0 & 0 & 0 & 0 \end{bmatrix}$$

$$B_{03} = \begin{bmatrix} 0 & 0 & 0 & 3.2601 & 0 & 0.1024 \\ 0 & 0 & 0 & 0 & 0 & 0.0092 \\ 0 & -0.2095 & 0 & -0.0011 & 0 & 0.0091 \\ -33.3885 & 0 & -1.0073 & 0 & 0 & -0.5691 \\ 0 & -12.1132 & 0 & -0.0748 & 1.2142 & 0 \\ -0.9884 & 0 & -1.1999 & 0 & 0 & -0.8665 \\ 0 & 0 & 0 & 0 & 0 & 0 \\ 0 & 0 & 0 & 0 & 0 & 0 \\ 0 & 0 & 0 & 0 & 0 & 0 \\ 0 & 0 & 0 & 0 & 0 & 0 \\ 0 & 0 & 0 & 0 & 0 & 0 \\ 0 & 0 & 0 & 0 & 0 & 0 \end{bmatrix}$$

$$B_{04} = \begin{bmatrix} 0 & 0 & 0 & 3.2628 & 0 & 0.0924 \\ 0 & 0 & 0 & 0 & 0 & 0.0097 \\ 0 & -0.2328 & 0 & -0.0008 & 0 & 0.0097 \\ -41.2203 & 0 & -1.2436 & 0 & 0 & -0.6708 \\ 0 & -14.9545 & 0 & -0.0748 & 1.4312 & 0 \\ -1.2203 & 0 & -1.4814 & 0 & 0 & -0.0213 \\ 0 & 0 & 0 & 0 & 0 & 0 \\ 0 & 0 & 0 & 0 & 0 & 0 \\ 0 & 0 & 0 & 0 & 0 & 0 \\ 0 & 0 & 0 & 0 & 0 & 0 \\ 0 & 0 & 0 & 0 & 0 & 0 \\ 0 & 0 & 0 & 0 & 0 & 0 \end{bmatrix}$$

Note ψ_{T0} in nominal condition 1 and ψ_{T0} in nominal condition 2 are different constants.

$$H_{01,02} = \left[\begin{array}{c} H1 \\ \hline H2 \mid H3 \end{array}\right]$$

where $H_{01,02} \in \Re^{12\times12}$, $H1 \in \Re^{9\times12}$, $H2 \in \Re^{3\times9}$ and $H3 \in \Re^{3\times3}$.

$$H1_{01} = \left[\begin{array}{cccccccccccc}
0 & 0 & 0 & 0 & 0 & 0 & 0 & 0 & 0 & 0 & -9.8058 & 0 \\
0 & 0 & 0 & 0.0516 & 0 & -0.9987 & 0 & 0 & 0 & 0 & 0.0000 & 0.0544 \\
0 & 0 & 0 & 0 & 1.0000 & 0 & 0 & 0 & 0 & 0 & -0.0007 & 0 \\
0 & 0 & 0 & 0 & 0 & 0 & -1.0000 & 0 & 0 & 0 & 0 & 0 \\
0 & 0 & 0 & 0 & 0 & 0 & 0 & -1.0000 & 0 & 0 & 0 & 0 \\
0 & 0 & 0 & 0 & 0 & 0 & 0 & 0 & -1.0000 & 0 & 0 & 0 \\
0 & 0 & 0 & 0 & 0 & 0 & 0 & 0 & 0 & 0 & 0 & 0 \\
0 & 0 & 0 & 0 & 0 & 0 & 0 & 0 & 0 & 0 & 0 & 0 \\
0 & 0 & 0 & 0 & 0 & 0 & 0 & 0 & 0 & 0 & 0 & 0
\end{array}\right]$$

$$H2_{01} = \left[\begin{array}{ccccccccc}
-0.5403\cos\psi_{T0} & -0.5403\sin\psi_{T0} & 0.8415 & 0 & -6.46 & 0 & 0 & 0 & 0 \\
\sin\psi_{T0} & -\cos\psi_{T0} & 0 & 6.46 & 0 & 25.33 & 0 & 0 & 0 \\
-0.0998\cos\psi_{T0} & -0.0998\sin\psi_{T0} & -0.9950 & 0 & -25.33 & 0 & 0 & 0 & 0
\end{array}\right]$$

$$H3_{01} = \left[\begin{array}{ccc}
-97.254\sin\psi_{T0} & 151.29\cos\psi_{T0} & 0 \\
180\cos\psi_{T0} & 0 & -17.964\cos\psi_{T0} \\
17.964\sin\psi_{T0} & -179.1\cos\psi_{T0} & -180\sin\psi_{T0}
\end{array}\right]$$

$$H1_{02} = \left[\begin{array}{cccccccccccc}
0 & 0 & 0 & 0 & 0 & 0 & 0 & 0 & 0 & 0 & -9.8060 & 0 \\
0 & 0 & 0 & 0.0371 & 0 & -0.9993 & 0 & 0 & 0 & 0 & 0 & 0.0490 \\
0 & 0 & 0 & 0 & 1.0000 & 0 & 0 & 0 & 0 & 0 & -0.0006 & 0 \\
0 & 0 & 0 & 0 & 0 & 0 & -1.0000 & 0 & 0 & 0 & 0 & 0 \\
0 & 0 & 0 & 0 & 0 & 0 & 0 & -1.0000 & 0 & 0 & 0 & 0 \\
0 & 0 & 0 & 0 & 0 & 0 & 0 & 0 & -1.0000 & 0 & 0 & 0 \\
0 & 0 & 0 & 0 & 0 & 0 & 0 & 0 & 0 & 0 & 0 & 0 \\
0 & 0 & 0 & 0 & 0 & 0 & 0 & 0 & 0 & 0 & 0 & 0 \\
0 & 0 & 0 & 0 & 0 & 0 & 0 & 0 & 0 & 0 & 0 & 0
\end{array}\right]$$

$$H2_{02} = \begin{bmatrix} -\cos\psi_{T0} & -\sin\psi_{T0} & 0 & 0 & -6.46 & 0 & 0 & 0 & 0 \\ \sin\psi_{T0} & -\cos\psi_{T0} & 0 & 6.46 & 0 & 25.33 & 0 & 0 & 0 \\ 0 & 0 & -1 & 0 & -25.33 & 0 & 0 & 0 & 0 \end{bmatrix}$$

$$H3_{02} = \begin{bmatrix} 200\sin\psi_{T0} & 0 & 0 \\ 200\cos\psi_{T0} & 0 & 0 \\ 0 & -200\cos\psi_{T0} & -200\sin\psi_{T0} \end{bmatrix}$$

Note in nominal conditions 3 and 4, $\psi_{T0}, V_{xT0}, V_{yT0}$ and V_{zT0} are time-varying as these conditions represent tanker turn.

$$H_{03,04} = \begin{bmatrix} H1 \\ H2 \mid H3 \mid H4 \mid H5 \mid H6 \end{bmatrix}$$

where $H_{03,04} \in \Re^{12\times12}$, $H1 \in \Re^{9\times12}$, $H2 \in \Re^{3\times2}$, $H3 \in \Re^{3\times7}$, $H4 \in \Re^{3\times1}$, $H5 \in \Re^{3\times1}$ and $H6 \in \Re^{3\times1}$.

$$H1_{03} = \begin{bmatrix} 0 & 0 & 0 & 0 & 0 & 0 & 0 & 0 & 0 & 0 & -9.8017 & -0.2821 \\ 0 & 0 & 0 & 0.0621 & 0 & -0.9981 & 0 & 0 & 0 & 0 & -0.0017 & 0.0481 \\ 0 & 0 & 0 & 0 & 1.0000 & 0 & 0 & 0 & 0 & 0 & 0.0001 & -0.0252 \\ 0 & 0 & 0 & -0.0001 & -0.0286 & -0.0150 & -1.0000 & 0 & 0 & 0 & 0 & 0 \\ 0 & 0 & 0 & 0.0271 & 0 & -0.0024 & 0 & -1.0000 & 0 & 0 & 0 & 0 \\ 0 & 0 & 0 & -0.0063 & 0.0012 & 0.0001 & 0 & 0 & -1.0000 & 0 & 0 & 0 \\ 0 & 0 & 0 & 0 & 0 & 0 & 0 & 0 & 0 & 0 & 0 & 0 \\ 0 & 0 & 0 & 0 & 0 & 0 & 0 & 0 & 0 & 0 & 0 & 0 \\ 0 & 0 & 0 & 0 & 0 & 0 & 0 & 0 & 0 & 0 & 0 & 0 \end{bmatrix}$$

$$H2_{03} = \begin{bmatrix} -0.5403\cos\psi_{T0} & -0.5403\sin\psi_{T0} \\ 0.8776\sin\psi_{T0} - 0.0479\cos\psi_{T0} & -0.8776\cos\psi_{T0} - 0.0479\sin\psi_{T0} \\ -0.4794\sin\psi_{T0} - 0.0876\cos\psi_{T0} & 0.4794\cos\psi_{T0} - 0.0876\sin\psi_{T0} \end{bmatrix}$$

$$H3_{03} = \begin{bmatrix} 0.8415 & 0 & -6.46 & 0 & 0 & 0 & 0 \\ -0.4770 & 6.46 & 0 & 25.33 & 0 & 0 & 0 \\ -0.8732 & 0 & -25.33 & 0 & 0 & 0 & 0 \end{bmatrix}$$

$$H4_{03} = \begin{bmatrix} -0.5403(V_{xT0}\sin\psi_{T0} - V_{yT0}\cos\psi_{T0}) \\ 0.8776(V_{xT0}\cos\psi_{T0} + V_{yT0}\sin\psi_{T0}) + 0.0478(V_{xT0}\sin\psi_{T0} - V_{yT0}\cos\psi_{T0}) \\ -0.4794(V_{xT0}\cos\psi_{T0} + V_{yT0}\sin\psi_{T0}) + 0.0876(V_{xT0}\sin\psi_{T0} - V_{yT0}\cos\psi_{T0}) \end{bmatrix}$$

$$H5_{03} = \begin{bmatrix} 0.8405(V_{xT0}\cos\psi_{T0} - V_{yT0}\sin\psi_{T0}) + 0.5403V_{zT0} \\ 0.4770(-V_{xT0}\cos\psi_{T0} - V_{yT0}\sin\psi_{T0} + V_{zT0}) \\ -0.8732(V_{xT0}\cos\psi_{T0} + V_{yT0}\sin\psi_{T0}) + 0.0876V_{zT0} \end{bmatrix}$$

$$H6_{03} = \begin{bmatrix} 0 \\ 0.4794(-V_{xT0}\sin\psi_{T0} + V_{yT0}\cos\psi_{T0}) - 0.0876(V_{xT0}\cos\psi_{T0} + V_{yT0}\sin\psi_{T0}) - 0.8732V_{zT0} \\ 0.8776(-V_{xT0}\sin\psi_{T0} + V_{yT0}\cos\psi_{T0}) + 0.0478(V_{xT0}\cos\psi_{T0} + V_{yT0}\sin\psi_{T0}) - 0.4770V_{zT0} \end{bmatrix}$$

$$H1_{04} = \begin{bmatrix} 0 & 0 & 0 & 0 & 0 & 0 & 0 & 0 & 0 & 0 & -9.8032 & -0.2343 \\ 0 & 0 & 0 & 0.0475 & 0 & -0.9989 & 0 & 0 & 0 & 0 & -0.0013 & 0.0423 \\ 0 & 0 & 0 & 0 & 1.0000 & 0 & 0 & 0 & 0 & 0 & 0.0001 & -0.0246 \\ 0 & 0 & 0 & -0.0001 & -0.0279 & -0.0163 & -1.0000 & 0 & 0 & 0 & 0 & 0 \\ 0 & 0 & 0 & 0.0264 & 0 & -0.0019 & 0 & -1.0000 & 0 & 0 & 0 & 0 \\ 0 & 0 & 0 & -0.0068 & 0.0009 & 0.0001 & 0 & 0 & -1.0000 & 0 & 0 & 0 \\ 0 & 0 & 0 & 0 & 0 & 0 & 0 & 0 & 0 & 0 & 0 & 0 \\ 0 & 0 & 0 & 0 & 0 & 0 & 0 & 0 & 0 & 0 & 0 & 0 \\ 0 & 0 & 0 & 0 & 0 & 0 & 0 & 0 & 0 & 0 & 0 & 0 \end{bmatrix}$$

$$H2_{04} = \begin{bmatrix} -0.5403\cos\psi_{T0} & -0.5403\sin\psi_{T0} \\ 0.8776\sin\psi_{T0} - 0.0479\cos\psi_{T0} & -0.8776\cos\psi_{T0} - 0.0479\sin\psi_{T0} \\ -0.4794\sin\psi_{T0} - 0.0876\cos\psi_{T0} & 0.4794\cos\psi_{T0} - 0.0876\sin\psi_{T0} \end{bmatrix}$$

$$H3_{04} = \begin{bmatrix} 0.8415 & 0 & -6.46 & 0 & 0 & 0 & 0 \\ -0.4770 & 6.46 & 0 & 25.33 & 0 & 0 & 0 \\ -0.8732 & 0 & -25.33 & 0 & 0 & 0 & 0 \end{bmatrix}$$

$$H4_{04} = \begin{bmatrix} -0.5403(V_{xT0}\sin\psi_{T0} - V_{yT0}\cos\psi_{T0}) \\ 0.8776(V_{xT0}\cos\psi_{T0} + V_{yT0}\sin\psi_{T0}) + 0.0478(V_{xT0}\sin\psi_{T0} - V_{yT0}\cos\psi_{T0}) \\ -0.4794(V_{xT0}\cos\psi_{T0} + V_{yT0}\sin\psi_{T0}) + 0.0876(V_{xT0}\sin\psi_{T0} - V_{yT0}\cos\psi_{T0}) \end{bmatrix}$$

$$H5_{04} = \begin{bmatrix} 0.8405(V_{xT0}\cos\psi_{T0} - V_{yT0}\sin\psi_{T0}) + 0.5403V_{zT0} \\ 0.4770(-V_{xT0}\cos\psi_{T0} - V_{yT0}\sin\psi_{T0} + V_{zT0}) \\ -0.8732(V_{xT0}\cos\psi_{T0} + V_{yT0}\sin\psi_{T0}) + 0.0876V_{zT0} \end{bmatrix}$$

$$H6_{04} = \begin{bmatrix} 0 \\ 0.4794(-V_{xT0}\sin\psi_{T0} + V_{yT0}\cos\psi_{T0}) - 0.0876(V_{xT0}\cos\psi_{T0} + V_{yT0}\sin\psi_{T0}) - 0.8732V_{zT0} \\ 0.8776(-V_{xT0}\sin\psi_{T0} + V_{yT0}\cos\psi_{T0}) + 0.0478(V_{xT0}\cos\psi_{T0} + V_{yT0}\sin\psi_{T0}) - 0.4770V_{zT0} \end{bmatrix}$$

REFERENCES

[1] J. P. Nalepka and J. L. Hinchman, "Automated aerial refueling: Extending the effectiveness of unmanned air vehicles," in *AIAA Modeling and Simulation Technologies Conference and Exhibit*, San Francisco, California, August 15-18 2005.

[2] S. M. Ross, M. Pachter, D. R. Jacques, B. A. Kish, and D. R. Millman, "Autonomous aerial refueling based on the tanker reference frame," in *Aerospace Conference, 2006 IEEE*, Big Sky, Montana, March 4-11 2006.

[3] A. L.Smith and D. L.Kunz, "Dynamic coupling of the kc-135 tanker and boom for modeling and simulation," in *AIAA Modeling and Simulation Technologies Conference and Exhibit*, Keystone, Colorado, August 21-24 2006.

[4] Y. Ochi and T. Kominami, "Flight control for autonomous aerial refueling via png and los angle control," in *AIAA Guidance, Navigation, and Control Conference and Exhibit*, San Francisco, California, August 15-18 2005.

[5] M. D. Tandale, R. Bowers, and J. Valasek, "Trajectory tracking controller for vision-based probe and drogue autonomous aerial refueling," *AIAA Journal of Guidance, Control and Dynamics*, vol. 29:4, pp. 846–857, Jul-Aug 2006.

[6] G. Campa, M. Fravolini, A. Ficola, M. Napolitano, B. Seanor, and M. Perhinschi, "Autonomous aerial refueling for uavs using a combined gps-machine vision guidance," in *AIAA Guidance, Navigation, and Control Conference and Exhibit*, Providence, RI, Aug 2004.

[7] M. Herrnberger, G. Sachs, F. Holzapfel, W. Tostmann, and E.Weixler, "Simulation analysis of autonomous aerial refueling procedures," in *AIAA Guidance, Navigation, and Control Conference and Exhibit*, San Francisco, California, August 15-18 2005.

[8] V. Stepanyan, E. Lavretsky, and N. Hovakimyan, "Aerial refueling autopilot design methodology: Application to f-16 aircraft model," in *AIAA Guidance, Navigation, and Control Conference and Exhibit*, Providence, RI, Aug 2004.

[9] K. Johnson and K. Awni, "A roll autopilot for autonomous air refueling," in *AIAA Guidance, Navigation, and Control Conference and Exhibit*, Monterey, CA, Aug 2002.

[10] S. Venkataramanan and A. Dogan, "Dynamic effects of trailing vortex with turbulence & time-varying inertia in aerial refueling," in *Proceedings of the AIAA Atmospheric Flight Mechanics Conference and Exhibit*, Providence, RI, Aug 2004, AIAA paper 2004-4945.

[11] ——, "A multiuav simulation for formation reconfiguration," in *Proceedings of the AIAA Modeling and Simulation Technologies Conference and Exhibit*, Providence, RI, Aug 2004, AIAA paper 2004-4800.

[12] A. Dogan and S. Venkataramanan, "Nonlinear control for reconfiguration of unmanned–aerial–vehicle formation," *AIAA Journal of Guidance, Control and Dynamics*, vol. 28:4, pp. 667–678, Jul–Aug 2005.

[13] A. Dogan, S. Venkataramanan, and W. Blake, "Modeling of aerodynamic coupling between aircraft in close proximity," *AIAA Journal of Aircraft*, vol. 42:4, pp. 941–955, Jul–Aug 2005.

[14] S. Venkataramanan and A. Dogan, "Modeling of aerodynamic coupling between aircraft in close proximities," in *Proceedings of the AIAA Atmospheric Flight Mechanics Conference and Exhibit*, Providence, RI, Aug 2004, AIAA paper 2004-5172.

[15] S. Venkataramanan, A. Dogan, and W. Blake, "Vortex effect modelling in aircraft formation flight," in *Proceedings of the AIAA Atmospheric Flight Mechanics Conference and Exhibit*, Austin, TX, Aug 2003, AIAA paper 2003-5385.

[16] S. Venkataramanan and A. Dogan, "Nonlinear control for reconfiguration of uav formation," in *Proceedings of the AIAA Guidance, Navigation, and Control Conference*, Austin, TX, Aug 2003, AIAA paper 2003-5725.

[17] S. Venkataramanan, *Dynamics and Control of Multiple UAVs Flying in Close Proximity.* Arlington, TX: M.S. Thesis, The University of Texas at Arlington, 2004.

BIOGRAPHICAL STATEMENT

EUNYOUNG KIM was born in Seoul, Korea, and majored in Food and Nutrition at Dongduck Women's University. After graduation she transferred to the U.S in 2000 and pursued a bachelor's degree in aerospace engineering with computer science as a double major at Iowa State University. After graduating from ISU in spring 2005, she joined the aerospace engineering graduate program at the University of Texas at Arlington in August 2005. While she worked on the Computer Aided Control Systems Design Lab with Dr. Atilla Dogan, she published a paper entitled "Control of a Receiver Aircraft Relative to the Tanker in Racetrack Maneuver" to the American Institute of Aeronautics and Astronautics (AIAA) in August 2006. After graduating from UTA she will pursue fulltime research in the aerospace field.